Final Technical Report

DOE Award number DE-SC0005429

Recipient: Carnegie Mellon University

Project title:

Accelerated corrosion of stainless steel in thiocyanate-containing solutions

Principal investigator:
Petrus Christiaan Pistorius

Date of Report: September 18, 2012

Disclaimer

This report was prepared as an account of work sponsored by an agency of the United States Government. Neither the United States Government nor any agency thereof, nor any of their employees, makes any warranty, express or implied, or assumes any legal liability or responsibility for the accuracy, completeness, or usefulness of any information, apparatus, product or process disclosed, or represents that its use would not infringe privately owned rights. Reference herein to any specific commercial product, process or service by trade name, trademark, manufacturer, or otherwise does not necessarily constitute or imply its endorsement, recommendation, or favoring by the United States Government or any agency thereof. The views and opinions of authors expressed herein to not necessarily state or reflect those of the United States Government or any agency thereof.

Executive Summary

It is known that reduced sulfur compounds (such as thiocyanate and thiosulfate) can accelerate active corrosion of austenitic stainless steel in acid solutions, but before we started this project the mechanism of acceleration was largely unclear**.** This work combined electrochemical measurements and analysis using scanning electron microscopy (SEM) and X-ray photo-electron spectroscopy (XPS), which provided a comprehensive understanding of the catalytic effect of reduced sulfur species on the active corrosion of stainless steel. Both the behavior of the pure elements and the steel were studied and the work focused on the interaction between the pure elements of the steel, which is the least understood area. Upon completion of this work, several aspects are now much clearer.

The main results from this work can be summarized as follows: The presence of low concentrations (around 0.1 mM) of thiocyanate or tetrathionate in dilute sulfuric acid greatly accelerates the anodic dissolution of chromium and nickel, but has an even stronger effect on stainless steels (iron-chromium-nickel alloys). Electrochemical measurements and surface analyses are in agreement with the suggestion that accelerated dissolution really results from suppressed passivation. Even well below the passivation potential, the electrochemical signature of passivation is evident in the electrode impedance; the electrode impedance shows clearly that this pre-passivation is suppressed in the presence of thiocyanate. For the stainless steels, remarkable changes in the morphology of the corroded metal surface and in the surface concentration of chromium support the suggestion that pre-passivation of stainless steels is suppressed because dissolution of chromium is accelerated. Surface analysis confirmed that adsorbed sulfur / sulfide forms on the metal surfaces upon exposure to solutions containing thiocyanate or thiosulfate. For pure nickel, and steels containing nickel (and residual copper), bulk sulfide (visible as a black corrosion product) forms during anodic dissolution. The sulfide is electronically conductive, and gives an increase of several orders of magnitude in the electrode capacitance; the sulfide also causes anodic activation to persist after the pure metals and steels were removed from the thiocyanate-containing electrolyte and transferred to a thiocyanate-free electrolyte.

The main practical implications of this work are that low concentrations of reduced sulfur compounds strongly affect anodic dissolution of stainless steels, and that selecting steels with elevated concentrations of chromium, nickel or molybdenum would serve to limit the anodic dissolution rate in the presence of reduced sulfur compounds.

Actual accomplishments compared with established goals and objectives

Goal	Actual accomplishment
Pure iron: Electrochemical measurements compared with literature model	Measurements completed and compared with Keddam model
Fe-Cr and Fe-Cr-Ni alloys: Electrochemical measurements (potentiostatic and impedance)	Measurements completed; all impedance data fitted; measurements on pure Fe, Cr and Ni added.
Data set on effects of thiocyanate concentration and mass transfer conditions on anodic dissolution rate	Detailed measurements completed for Type 304 (Fe-Cr-Ni) stainless steel; surveys completed to show trends for Type 316 and Type 430 steels
Test proposed fundamental mechanism of acceleration	Completed for Fe and Cr, Ni and Type 304 and 430 stainless steels. X-ray photoelectron spectroscopy used to measure predicted change in surface composition, for these metals (excluding Fe).

Project Activity Summary

The presence of reduced sulfur compounds in acidic solutions can make such solutions very aggressive to corrosion resistance of stainless steel. Several parts per million of reduced sulfur compounds can greatly increase the active dissolution rate of stainless steel, sometimes by almost one order of magnitude.

This study focused on the effect of thiocyanate on the dissolution rate of stainless steel (Type 430 and Type 304) in sulfuric acid. The dissolution behavior of pure components of stainless steel (Fe, Cr and Ni) was studied in the same environment for better understanding of alloy behavior. Effects of thiocyanate concentration and mass transfer conditions on anodic dissolution rate were also studied.

Hypotheses

Thiocyanate is expected to decompose to elemental sulfur on the metal surface during active dissolution of stainless steel. Adsorbed sulfur catalyzes the active dissolution of the metal and the desorption rate of adsorbed sulfur is not zero during the active dissolution of the metal. The catalytic effect of thiocyanate on Type 430 stainless steel is due to the increased dissolution rate of chromium, counteracting the formation of the Cr-O-Cr passivating network at the ledges. The mechanism of the catalytic effect of thiocyanate on Type 304 stainless steel is similar to what was found for Type 430 stainless steel, but nickel is beneficial to the corrosion resistance of Type 304 stainless steel, in that nickel lowers the percolation limit of chromium to passivate the surface.

Approach used

Potentiodynamic and potentiostatic measurement were performed to investigate the effect of thiocyanate on steady-state dissolution behavior of the electrode. Electrochemical impedance measurements were also applied to study the mechanisms of anodic dissolution. Impedance spectra were fitted using equivalent circuits to quantitatively understand the corrosion mechanism. The surface of corroded samples was characterized using SEM, AFM and XPS.

Departure from planned methodology

Measurements on pure Cr and pure Ni were added (in addition to measurements on pure iron) to better understand the behavior of stainless steels, and extensive X-ray photoelectron spectroscopy was performed to measure changes in surface composition. Both of these additional areas of study significantly increased our confidence in the conclusions. Notably, the thiocyanate accelerates the dissolution of the stainless steels to a greater extent than it does the dissolution of any of the main metals (Fe, Cr and Ni) in stainless steel.

Project details

Please see Wen Li's PhD thesis, included as the Appendix, for detailed discussion of the experimental approach and results.

Products developed under the award and technology transfer activities:

Publications:

Wen Li, PC Pistorius, "Effects of thiocyanate on anodic dissolution of iron, chromium and Type 430 stainless steel." Journal of The Electrochemical Society, C114-C122, Vol. 159, 2012

Wen Li, PC Pistorius, "Effects of thiocyanate on anodic dissolution of iron, chromium, nickel and Type 304 stainless steel. Part I. Electrochemical measurements and surface morphology." Journal of The Electrochemical Society, In Press (accepted August 23, 2012)

Wen Li, PC Pistorius, "Effects of thiocyanate on anodic dissolution of iron, chromium, nickel and Type 304 stainless steel. Part II. Surface analysis by XPS." Journal of The Electrochemical Society, In Press (accepted August 23, 2012)

PhD student Wen Li defended her thesis on August 30, 2012 and submitted the final thesis on September 13, 2012 (the thesis is included in this report as the Appendix) .

Conference Presentation: Wen Li made a presentation at the Electrochemical Society Fall 2011 meeting.

Collaboration fostered: As a direct result of Wen Li's participation in the Fall 2011 Electrochemical Society meeting, the Swagelok Center for Surface Analysis of Materials at Case Western Reserve University was identified as a suitable laboratory for X-ray photoelectron spectroscopy. Several days of XPS measurements were completed at the Swagelok Center; the opportunity for us to operate the instrument ourselves was particularly helpful.

Appendix: PhD thesis, Wen Li

Activation of stainless steel corrosion in acid solutions by thiocyanate

A thesis submitted in partial fulfillment of the requirements for the degree of:

Doctor of Philosophy

in

Department of Materials Science and Engineering

Wen Li

B.S., Materials Science and Engineering, Shanghai Jiao Tong University

M.S., Materials Science and Engineering, Carnegie Mellon University

Carnegie Mellon University

Pittsburgh, PA

August, 2012

Table of Contents

List of Figures

List of Tables

Acknowledgements

I wish to express the deepest gratitude, first and foremost, to my advisor, Professor Petrus Chris Pistorius. I have been extremely indebted and privileged to be mentored by such an intelligent and knowledgeable advisor. This thesis would not been possible without the patient guidance, unreserved support, encouragement and inspiration from Professor Pistorius. His enthusiasm, commitment to scientific rigor and dedication make me understand what a great scientist and researcher should be like and motivate me to keep moving towards being not only a better researcher but also being a better person.

I would also like to thank my committee members, Professor Jay Whitacre, Professor Robert A. Heard and Dr. John F. Grubb for their great suggestions and comments. Their insightful and critical feedbacks significantly improved my thesis work.

I gratefully acknowledge the Department of Energy for the financial support under Award Number DESC0005429.

I would like to especially thank Professor Rudolph G. Buchheit for his help and guidance in using Zview. I am also grateful to Wayne Jennings and Annette Marsolais for the help in XPS measurements in Case Western University. I would also like to thank Roy J. Matway for the help in performing chemical analysis of the steel sample.

I must thank Roxann Martin, Jeanna Pekarcik, Tom Nuhfer, Jason Wolf, Bill Pingitore and Adam Wise and all the staff members of MSE department. I owe special gratitude to my colleagues, seniors and friends for their support, help and suggestions (Dr. Lan Yin, Dr. Jingxi Zhu, Jia Li, Yiling Zhang, Hyeon Jeong Cho, Dr. Neerav Verma, Aswin Tejasukanama, Debdutta Roy, Jiwon Park, Kelvin Cheung, Dr. Ayesha Hashambhoy, Ben Anglin, Wei Wu and Brian Lin).

Finally, I would like to heartily thank Shen Shen, my parents, sister, brothers and cousins for their love and support. Special thanks goes to my little nephew for bringing my family and me lots of joy.

Abstract

This study focuses on the effect of thiocyanate on the dissolution rate of stainless steel (type 430 and type 304) in sulfuric acid. The dissolution behavior of pure components (Fe, Cr, Ni) is also studied in the same environment.

Potentiodynamic and potentiostatic measurement were performed to investigate the effect of thiocyanate on steady-state dissolution behavior of the electrode. Impedance measurements were applied to study the anodic dissolution mechanisms. Impedance spectra were fitted using equivalent circuits to quantitatively understand the corrosion mechanism. The surface of corroded samples was characterized using SEM, AFM and XPS.

The results show that the catalytic effect of thiocyanate on the dissolution rate of the alloy is more apparent than the effect on the dissolution of any pure element. Thiocyanate did change the anodic dissolution mechanism to some extent. However, the main origin of the catalytic effect is that all the dissolution steps are accelerated. The surface morphology of corroded samples was also changed by thiocyanate. Strong crystal facet etching of the electrode was observed with thiocyanate present, while grain boundary etching was more apparent in thiocyanate free solutions.

For Type 430 stainless steel, more prominent crystallographic etching and the strong effect of thiocyanate on dissolution indicate that thiocyanate suppresses the passivating effect of Cr-O-Cr networks on crystal ledges. The catalytic effect of thiocyanate on anodic dissolution of Type 304 stainless steel also appears to be primarily caused by the increased dissolution rate of chromium, counteracting the formation of the Cr-O-Cr passivating network at ledges. Nickel does contribute to the corrosion resistance of Type 304 stainless steel in the presence of thiocyanate, but its beneficial effect appears to be secondary to that of chromium.

Surface analysis of the Fe-20wt% Cr alloy and stainless steels (Types 430 and 304) confirmed that chromium enriched on the metal surface during anodic dissolution in thiocyanate-free solution and that the surface enrichment of chromium was smaller in thiocyanate-containing solution. Surface analysis also confirmed the formation of sulfide or adsorbed sulfur on the Fe-20wt% Cr alloy in thiocyanate-containing solution.

1. Introduction

It is known that stainless steel has good corrosion resistance and mechanical properties combined with a relatively low price, which makes it the preferred material for a wide range of applications. However, in some severe corrosive environments the corrosion resistance of stainless steel can be lost and corrosion failure can happen.

One example of such a corrosive environment is that caused by the presence of reduced sulfur compounds in the corrosion electrolyte. There are several reasons why environments containing reduced sulfur are worth studying. First of all, reduced sulfur compounds can be found in several industrial environments such as paper and pulp mill industry. Besides, reduced sulfur compounds can form by oxidation of sulfide, which is wide-spread in many environments. A very low concentration of reduced sulfur compounds (even several parts per million) in dilute acid solution causes a large increase of the corrosion rate[1].

However, the mechanism of the acceleration effect of reduced sulfur compound on the dissolution of stainless steel remains unclear, so a detailed study of the mechanism is required.

Adsorbed sulfur, and reduced sulfur compounds in acid solution, have been shown to have strong effects on the active dissolution of several pure metals (Fe, Ni, Cr) and alloys[2][3][4][5][6]. "Reduced sulfur compounds" here refer to dissolved sulfur-bearing anions, in which the oxidation state of sulfur is lower than in sulfate. Examples are sulfide, tetrathionate and thiocyanate. The reduced sulfur compounds can react with the surfaces of metals to form adsorbed sulfur[7][8][9][10][11].

Thiocyanate was chosen as the reduced sulfur compound to be studied because preliminary measurements showed its effects on Type 304 stainless steel in dilute sulfuric acid to be similar to that of thiosulfate (the other commonly studied reduced sulfur compound), but without the danger of disproportionation in solution (which would render uncertain the actual

concentration of the reduced sulfur compound in solution). Also, thiocyanate is employed in the electrochemical potentiostatic reactivation (EPR) test for sensitization[12][13], and hence the specific effects of thiocyanate are of interest, in addition to offering insight into the effects of reduced sulfur compounds generally. Thiocyanate produces adsorbed sulfur by the disproportionation reaction[11]:

$$SCN^- \rightarrow CN^- + S_{ads} \quad (1)$$

Elemental sulfur is predicted to be stable on the metal surface over a wide potential range. For example, the blue area in Figure 1 indicates the stable range of adsorbed sulfur on pure chromium surface. At more negative potentials sulfide is the stable product, and sulfate at more positive potentials[9]. The red arrows and lines indicate the potential range and pH values of interest in this research.

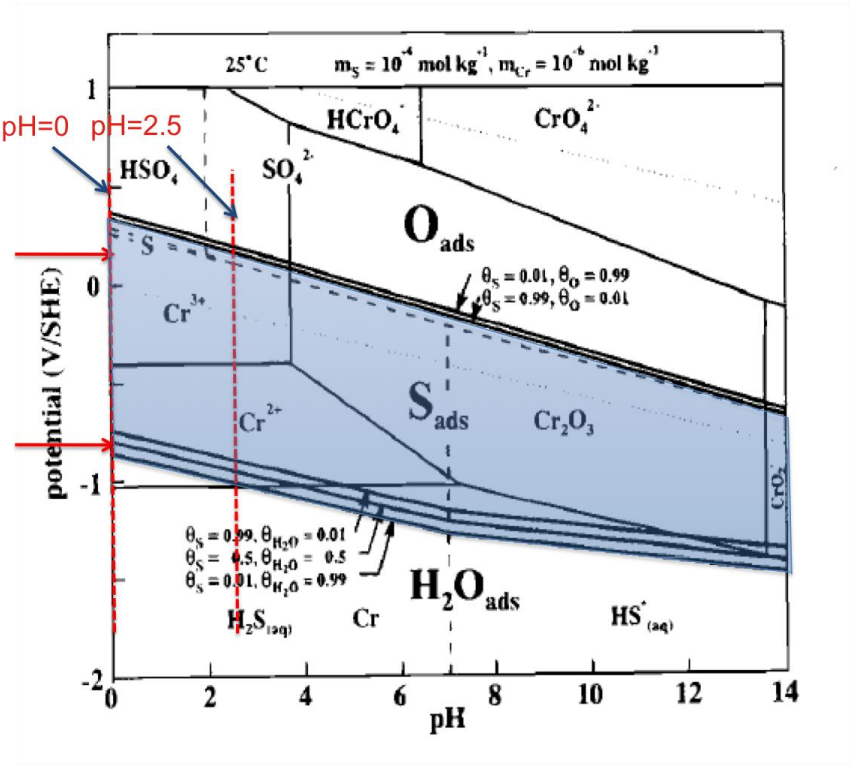

Figure 1. Equilibrium Potential-pH diagram for the system S_{ads}-Cr-H_2O at 25℃; lines marked −give stability range of adsorbed sulfur with relative surface coverage θ[9].

For acidic solutions containing thiocyanate, adsorbed sulfur is predicted to be the stable species at the metal surface in the potential range of active dissolution of the metals and alloys considered here[11]. Hence the mechanism by which reduced sulfur compounds in solution, and sulfur adsorbed onto the metal surface before exposure to the corrosive environment, affect dissolution is expected to be fundamentally the same. Surface analysis (by X-ray photoelectron spectroscopy) of electrodes after exposure to acidified sodium sulfate solution with thiocyanate at the active corrosion potential supported the assumption that elemental sulfur is stable on the metal surface. As shown in Figure 2, there are XPS peaks at 162eV and 169eV (sulfur 2p peaks) in the spectra of Fe20Cr exposed to sulfuric acid with thiocyanate. The peak with a binding energy around 162 eV is characteristic of adsorbed sulfur or sulfide, and the peak at 169 eV corresponds to sulfate. Surface analyses (by X-ray photoelectron spectroscopy) performed by previous workers also provide support for the suggestion that adsorbed sulfur forms on metals corroding in solutions containing thiosulfate[14] and in solutions containing sulfide[15] (although identification of adsorbed sulfur is ambiguous since its binding energy overlaps with that of bulk sulfide[16]).

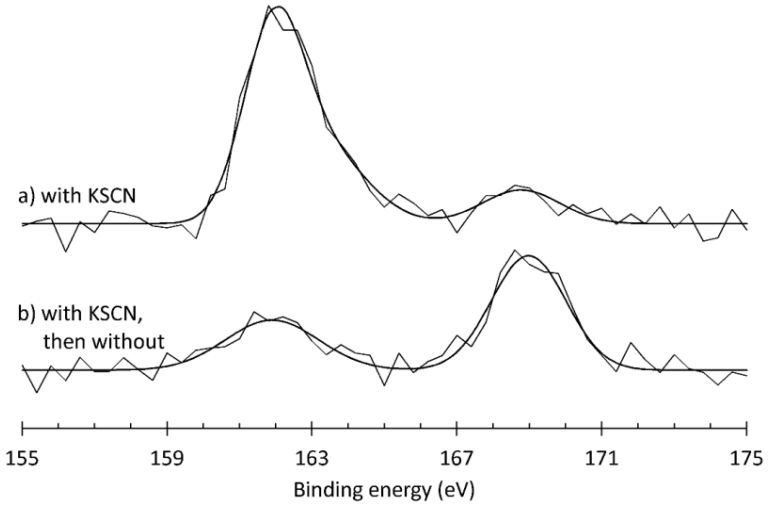

Figure 2. Sulfur 2p peak in XPS measurements on Fe20Cr alloy after dissolution in a) 1 M Na_2SO_4, 0.01 M H_2SO_4, 0.14mM KSCN, and b) KSCN-containing solution followed by transfer to KSCN-free solution; E=-0.41$V_{Ag/AgCl}$ (Smooth lines are fitted Gaussian peaks.)

The main envisaged difference between corrosion of metals with pre-adsorbed sulfur and metals corroding in solutions containing reduced sulfur compounds is that the latter can replenish sulfur which is lost from the surface during corrosion; the sulfur coverage of metal surfaces, onto which sulfur had been adsorbed before corrosion, was shown to decrease during corrosion[6]. Replenishment of adsorbed sulfur appears to be the likely reason for the observation that, in the presence of low concentrations of thiocyanate in solution, the current density during active dissolution is higher if the mass transfer coefficient to the electrode surface is higher; an example is shown in Figure 3. (These polarization curves were also measured in preliminary work for this project.)

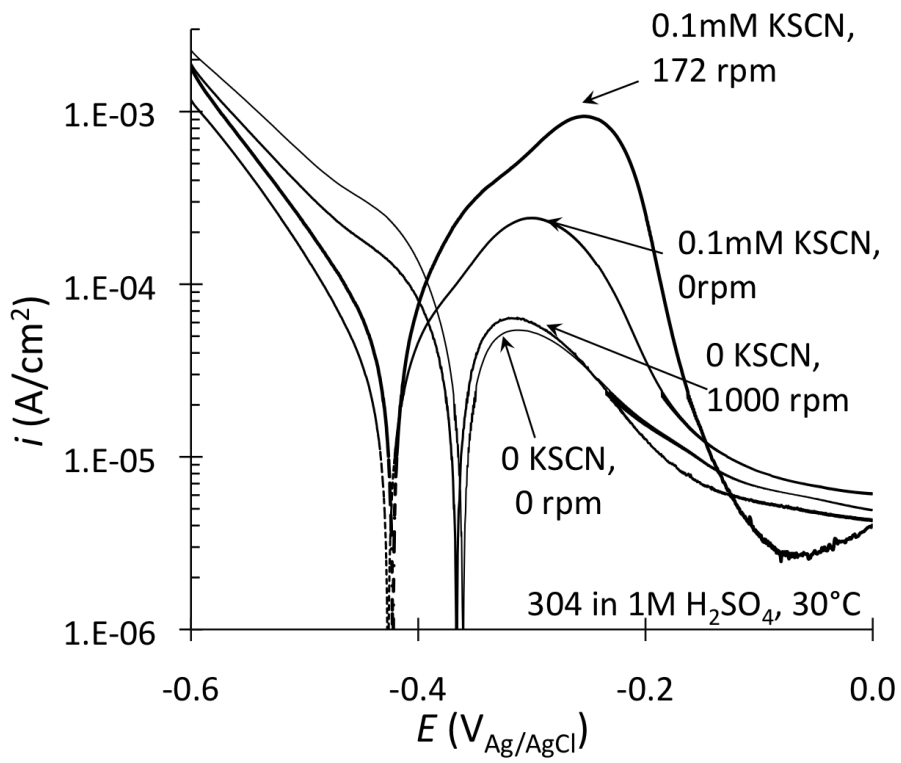

Figure 3. A small concentration of SCN^- (added as KSCN) in solution has a large effect on the anodic dissolution rate of Type 304 stainless steel in 1M H_2SO_4 at 30°C (potentiodynamic tests, scan rate 1 mV/s). The increase in anodic current density in the presence of SCN^- is larger if the disc electrode is rotated, whereas rotation has no effect in the absence of SCN^-.

Here, results are presented on the effect of thiocyanate on iron, chromium, nickel and Type 430 and 304 stainless steels; the effects of thiocyanate on type 304, 316, 444 and 434 are also presented to show the roles of mass transfer coefficient, thiocyanate concentration and alloy composition in the catalytic effect of thiocyanate.

In this research, thiocyanate was chosen as a source of sulfur rather than pre-adsorbed sulfur on the metal surface, to gave a continuous supply of sulfur. The mass transfer effect was eliminated using rotating electrode so the surface reaction was studied without interference of mass transfer effect.

Both the behavior of the pure elements and the steel were studied and the work was focused on the interaction between the pure elements of the steel, which is the least understood area.

This work combined the electrochemical measurements and surface analysis using SEM and XPS, which provided a comprehensive understanding of the catalytic effect of reduced sulfur species on the active corrosion of stainless steel.

2. Current Stage of Knowledge

As background to the project, the relevant information on active dissolution is briefly summarized in this section.

2.1 Increase of active dissolution rate of stainless steel in acid solutions by reduced sulfur species

2.1.1 Role of KSCN in Electrochemical Potentiodynamic Reactivation (EPR) Test

The Electrochemical Potentiodynamic Reactivation (EPR) Test is used to detect the degree of sensitization of austenitic stainless steels. When these steels are exposed to heat treatment (like welding) between 450°C and 870°C, chromium carbides can precipitate along grain boundaries, causing the grains next to chromium carbides to be depleted in Cr[12]. If the chromium content drops too low, those Cr-depleted zones are very easily corroded away first when exposed to aggressive environments, sometimes resulting in severe problems. One example is the intergranular stress corrosion cracking of welded piping, made of AISI 304 and 304L stainless steel, for boiling water nuclear reactor power plants[17]. The EPR test provides a nondestructive method to measure the sensitization at grain boundaries[13].

The EPR method consists of potentiodynamic polarization measurement. There are two types of the EPR test, the single-loop EPR test and the double-loop EPR test[12][13][18][19]. For the single-loop EPR test, a reactivation scan is applied from the passive region to the active region and a reactivation loop is generated during the scan, shown in Figure 4[19]. The area under the loop gives the amount of charge associated with the dissolution of Cr-depleted area. The charge density normalized by the area of grain boundaries shows the degree of sensitization[13]. The double-loop EPR test consists of a forward scan (from active region to

passive region) and a reverse scan (from passive region to active region) and an active loop and a reactivation loop are generated during the cyclic polarization measurement, shown in Figure 5[12]. The ratio of the peak current densities of the two loops (I_r/I_a) is used to indicate the degree of sensitization.

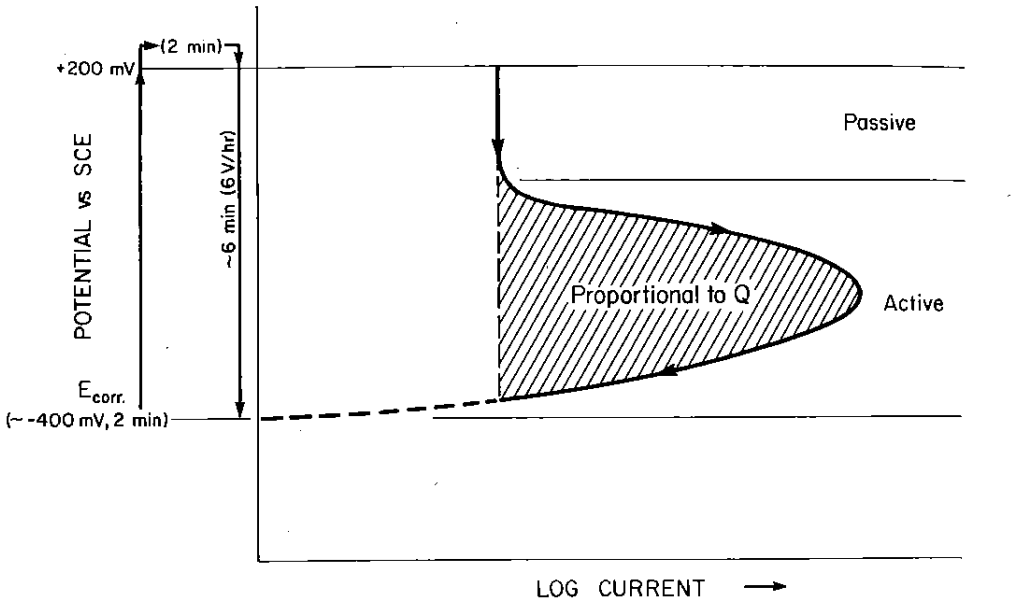

Figure 4. Schematic diagram for the single-loop EPR test of AISI 304 and 304L stainless steel[19].

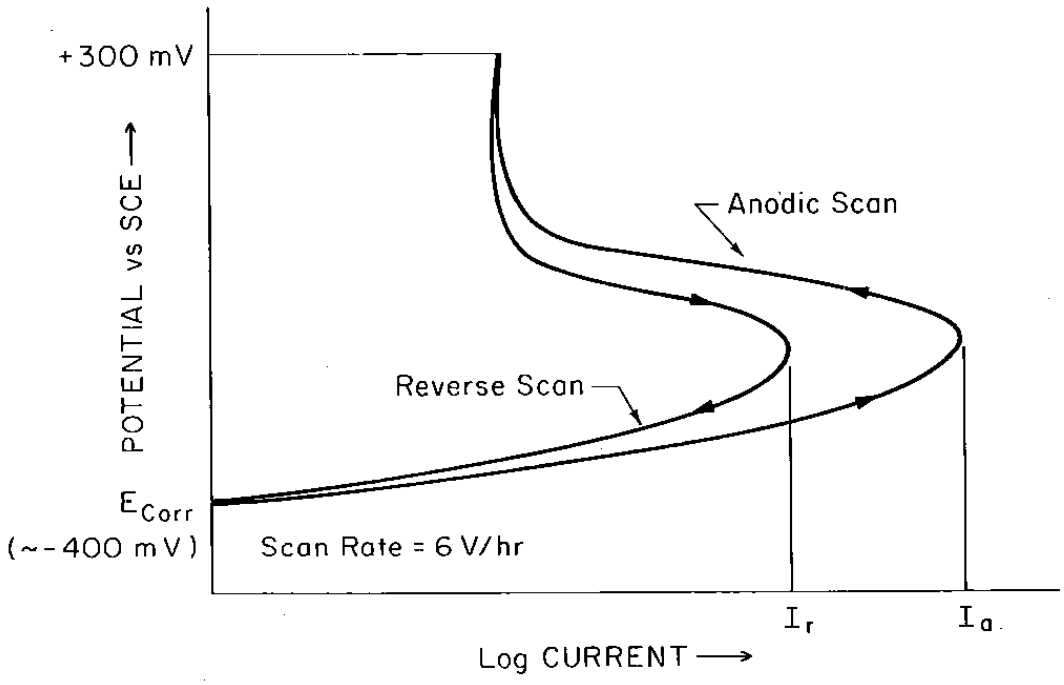

Figure 5. Schematic diagram of the double-loop EPR test for AISI 304 stainless steel [12].

The composition of the most commonly used solutions for the EPR test is 0.5M H_2SO_4 + 0.01M KSCN[13][20][21] and it varies slightly for different kinds of samples[22]. KSCN is stated to work as an activator or depassivator[12] because of the catalytic effect of KSCN on the dissolution of metals. During the double loop test, both the general corrosion during the forward scan and reactivated dissolution of Cr-depleted areas during the reverse scan are promoted by KSCN[12]. KSCN likely promotes dissolution of the passive film on Cr-depleted zones first and Cr-depleted areas along grain boundaries are reactivated preferentially[12]. Majidi and Streicher[12] did test the effect of thiocyanate concentration (from 0 to 50mM), but reported the results in terms of the reactivation current ratio rather than the actual current densities.

2.1.2 Effect of reduced sulfur compounds on the pitting corrosion of stainless steel

Thiosulfate ions can be found in fluids of many industrial systems, such as the paper and pulp industry. Pitting corrosion of paper machines, mainly made of type 304 and 316 stainless steel[23], in water with very low chloride concentration has been reported. This is believed to be caused by thiosulfate[24]. Newman and his coworkers[24] studied pitting of stainless steel by thiosulfate ions. They proposed that chloride is not necessary for thiosulfate pitting of 304 stainless steel and that pitting tends to occur when $\{[SO_4^{2-}]+[Cl^-]\}/[S_2O_3^{2-}]$ (molar ratio) is in the range of 10-30. However, thiosulfate pitting of type 316 stainless steel cannot happen without the assistance of chloride and pitting tends to happen at higher temperature and when chloride is the major anion in the solution.

Except for thiosulfate ions, other sulfur species can also affect pitting corrosion of stainless steel. The effects of several sulfur compounds on the pitting of type 304 stainless steel in chloride solutions have been studied by Newman and his coworkers[25]. It was shown that very low concentrations of $Na_2S_2O_3$ (0.01M-0.02M) can lower the pitting potential substantially and KSCN has similar but less strong effect. The pitting potential was also decreased when the concentration of H_2S increased. It was proposed that black metal sulfide covers on pits in thiosulfate, sulfide and tetrathionate-containing solutions help to form large pits, promoting pitting in sulfur-containing solutions.

2.1.3 Effect of reduced sulfur species on the stress corrosion cracking of sensitized stainless steels

Sensitized stainless steel is subject to stress corrosion cracking (SCC) in some environments because of the poor corrosion resistance of chromium depleted grain boundaries. One type of aggressive environment for SCC is solutions that contain sulfur species[26][27][28]. The presence of very low concentrations of thiosulfate in the solution makes type 304 stainless

steel highly susceptible to stress corrosion cracking[28]. A sufficient amount of sulfate ions added to dilute thiosulfate solutions can inhibit SCC[29].

2.2 Thermodynamic stability regions of reduced sulfur species in acid solutions on metal surface

It was proposed[25][24] that adsorbed sulfur is produced on the surface of stainless steel in solutions containing sulfur species; the adsorbed sulfur enhances active dissolution of stainless steel. So it is very important to predict the thermodynamic stability region of reduced sulfur on metal surface.

Marcus and his coworkers[7][8][9] constructed pH-potential diagrams for adsorbed sulfur on pure Fe, Cr and Ni surfaces in solutions containing sulfur species, which are shown in the following figures (Figure 6, Figure 7, Figure 8).

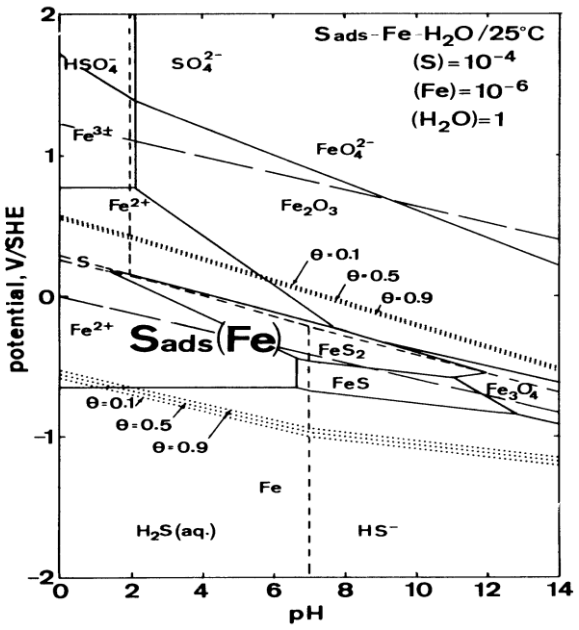

Figure 6. Equilibrium Potential-pH diagram for the system S_{ads}-Fe-H_2O at 25 ℃; lines marked ·····give stability range of adsorbed sulfur with relative surface coverage θ[8].

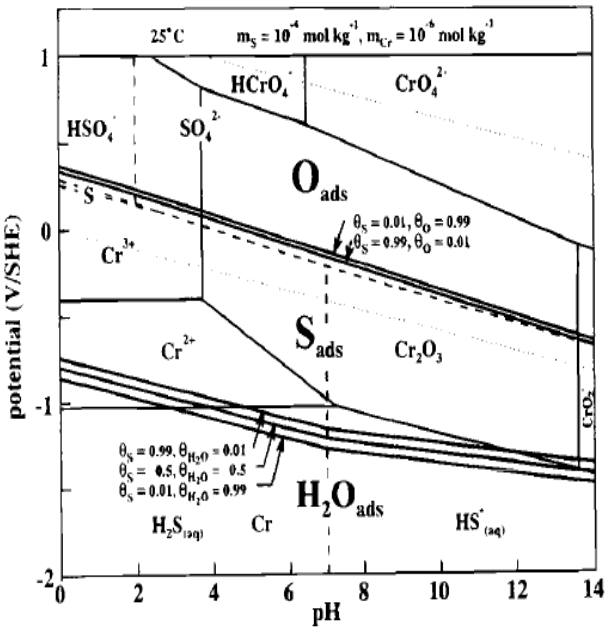

Figure 7. Equilibrium Potential-pH diagram for the system S_{ads}-Cr-H_2O at 25℃; lines marked –give stability range of adsorbed sulfur with relative surface coverage θ[9].

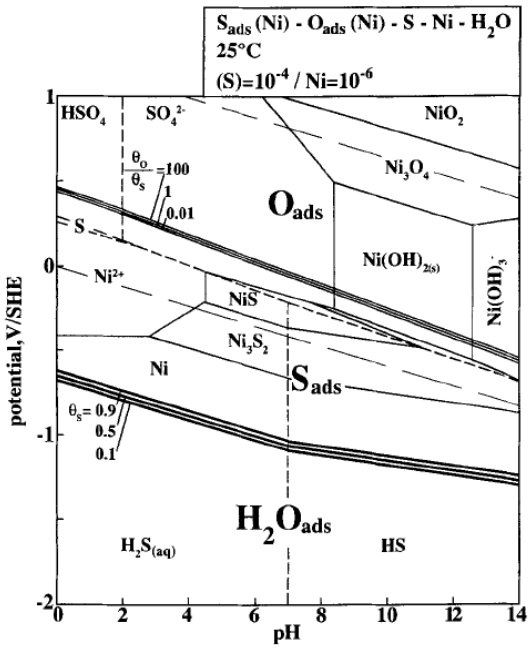

Figure 8. Equilibrium Potential-pH diagram for the system S_{ads}-Ni-H_2O at 25℃; lines marked – give stability range of adsorbed sulfur with relative surface coverage θ[7].

It can be seen that in acid solutions, adsorbed sulfur on Fe, Cr and Ni surfaces remains stable over a wide potential range, which spans the active corrosion potentials of Fe, Cr and Ni in acid solutions (as will be shown later in the Results section).

It was proposed that thiocyanate could decompose to elemental sulfur on the metal surface [11] according to the reaction $SCN^- \rightarrow CN^- + S_{ads}$. XPS analysis confirmed elemental sulfur could form by decomposition of thiosulfate on the metal surface[14]; the effect of thiocyanate is expected to be similar to thiosulfate, and this was confirmed by the XPS results such as those shown in Figure 2.

2.3 Catalytic effects of adsorbed sulfur on the active dissolution of stainless steel and its pure components

2.3.1 Effect of reduced sulfur species on pure Fe in acid solutions

In order to achieve a better understanding of the alloy behavior, it is necessary to understand the corrosion behavior of the pure components (Fe, Cr, Ni) in the same environment.

It is known that hydrogen sulfide can catalyze the dissolution of pure Fe in acid solutions[30][31][32]. With a small amount of H_2S in sulfuric acid, the anodic current density was increased by more than one order of magnitude, as shown in Figure 9[2].

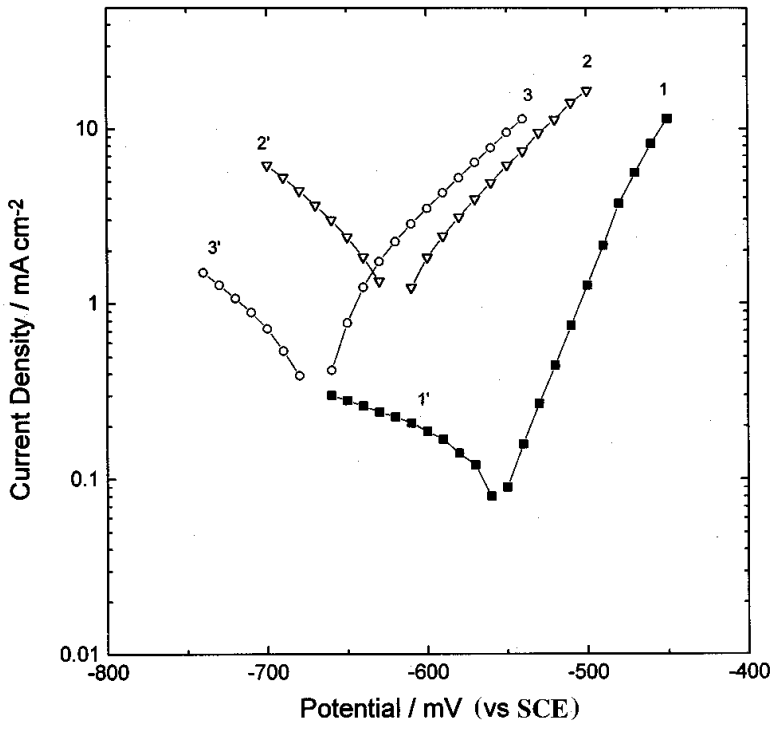

Figure 9. Polarization curves of iron in 0.2mol/L sulfuric acid with/ without H_2S at different pH values[2]; (■) without H_2S, pH=0.75; (Δ) with 0.4mmol/L H_2S, pH=0.75; (o) with 0.4mmol/L H_2S, pH=2.

Interestingly, H_2S can also inhibit the dissolution of Fe under specific conditions[33]. It was observed that H_2S acted as a strong inhibitor when its concentration was below 0.04mmol/L, pH of the solution was between 3 and 5 and the immersion time was over 2 hours[33].

2.3.2 Effect of reduced sulfur species on pure Cr in acid solutions

The corrosion behavior of Cr in sulfuric acid with H_2S was studied [4]. H_2S accelerates both cathodic reaction and anodic dissolution of Cr, as shown in the polarization curve in Figure 10[4]. The critical current density was increased by more than one order of magnitude with

1.5mmol/L H_2S present in the solution. No obvious shift of passivation potential was observed when H_2S is present.

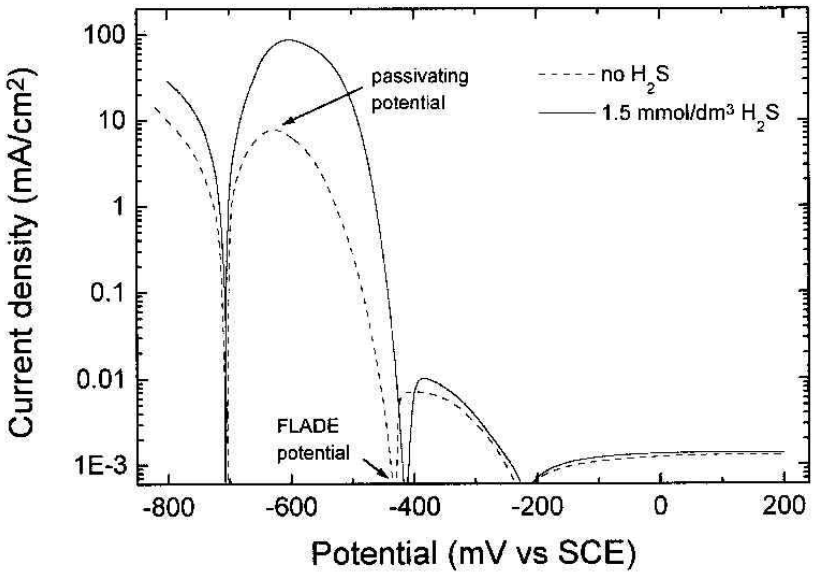

Figure 10. Potentiodynamic polarization curves of Cr in 0.5mol/L sulfuric acid with/without H_2S[4].

Both hydrogen evolution reaction rate and active current density increased as the concentration of H_2S increased, shown in Figure 11 for pH=2[4], although these results show the effect on the cathodic reaction rate to be weak.

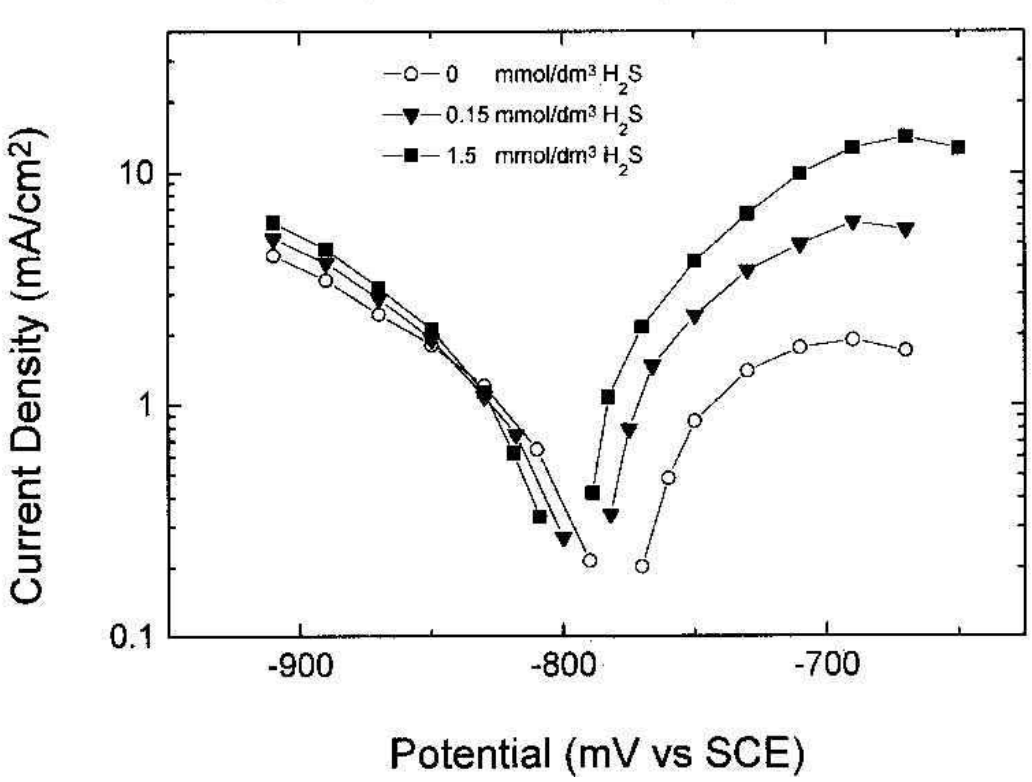

Figure 11. Potentiostatic polarization curves of Cr in 0.5mol/L Na_2SO_4/H_2SO_4 (pH=2) with various concentrations of H_2S[4].

2.3.3 Effect of reduced sulfur species on pure Ni in acid solutions

Marcus and his coworkers extensively investigated the effect of adsorbed sulfur on the dissolution and passivation of Ni and Ni alloys[34][35][5][36]. Elemental sulfur was adsorbed on the metal surface in a gaseous H_2-H_2S mixture prior to corrosion. With radiochemical methods, the coverage of sulfur on the metal surface could be measured[34]. It is shown in Figure 12 that a monolayer of adsorbed sulfur on Ni significantly accelerated the anodic dissolution of Ni and inhibited the passivation of Ni by extending the anodic dissolution potential range[34].

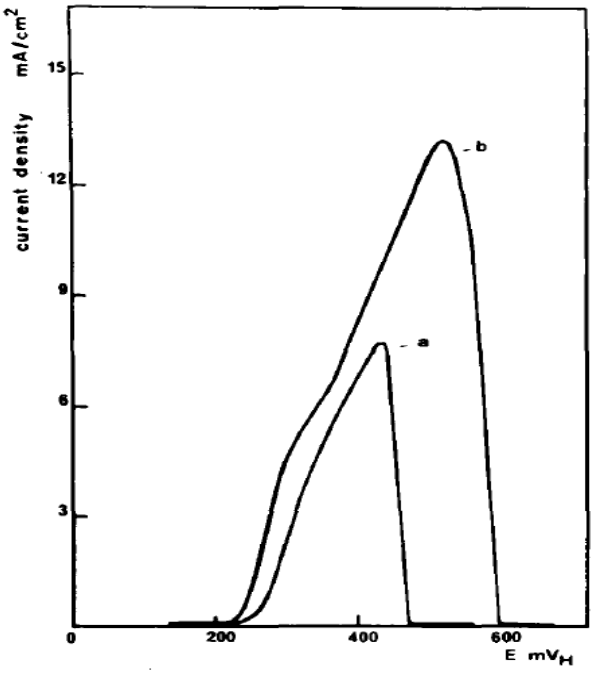

Figure 12. Polarization curves of pure Ni (110) in 0.1N sulfuric acid. a. Ni annealed in H_2; b, Ni + S adsorbed[34].

The effect of crystallographic orientation was also investigated[34]. As seen from table 1, the catalytic effect of adsorbed sulfur is most striking on Ni (100) planes compared with Ni (111) and Ni (110) planes, with a much larger increase in the critical current density.

Table 1. Critical current density and passivation potentials of Ni with various crystallographic orientations in sulfuric acid with/without adsorbed sulfur[34]

Orientation	Critical current density (No sulfur)	Critical current density (adsorbed S)	Passivation E (No S)	Passivation E (adsorbed S)
	mA (cm^2)	mA (cm^2)	mV (SHE)	mV (SHE)
(111)	5.4	7.6	396	450
(100)	5.7	115	420	440
(110)	8	13.25	430	530

2.4 Anodic dissolution mechanisms of stainless steel and pure components in acid solutions without sulfur species

Electrochemical Impedance results give insight into the reactions at the corroding metal surfaces, because the different reactions – and the associated reaction products – may be reflected in different circuit elements. For example, for the active dissolution of pure iron, Keddam et al. observed both pseudo-inductive and pseudo-capacitive behavior[37][38]. For anodic reactions, pseudo-inductive behavior is recognized by the current density continuing to increase following a positive potential step, by a positive phase angle, and by the reactance being proportional to frequency; in contrast pseudo-capacitive behavior is reflected in a current decay following a positive potential step, a negative phase angle, and inverse proportionality between reactance and frequency (Figure 13).

Observation of pseudo-capacitive or pseudo-inductive behavior was first related to reaction mechanisms by Gerischer and Mehl (for hydrogen evolution on mercury, silver and copper)[39]. For active dissolution of metals which can passivate, pseudo-inductive behavior is generally associated with formation – by an oxidation reaction – of an intermediate species which catalyzes dissolution; pseudo-capacitive behavior is generally associated with initial stages of passivation (and is distinguished from interfacial capacitance by the much larger capacitance and hence larger time constant associated with pseudo-capacitance)[37].

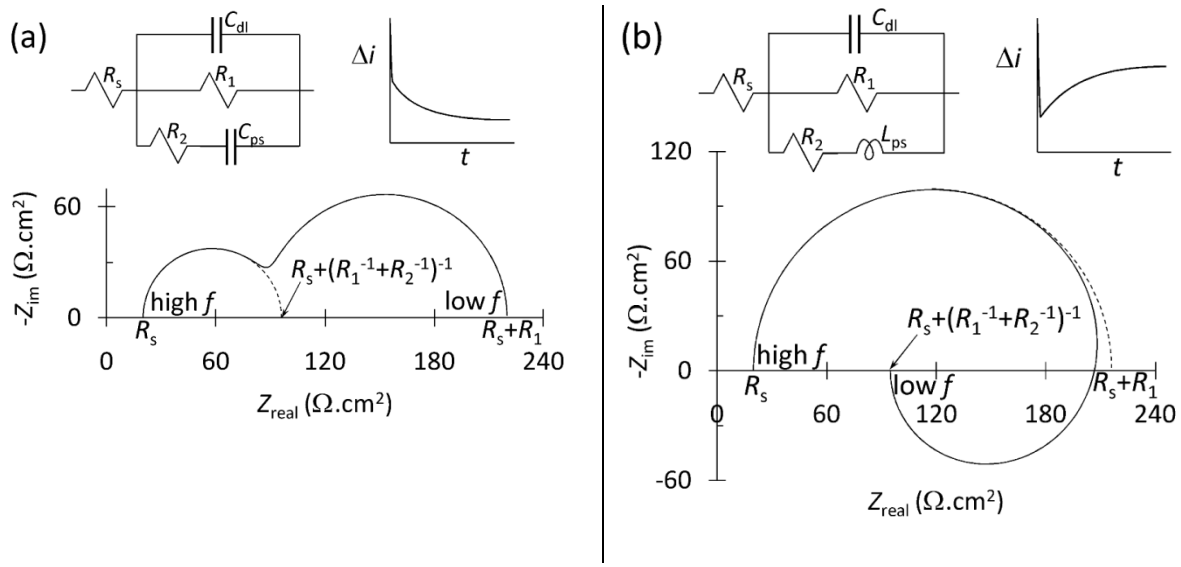

*Figure 13. Typical equivalent circuits for electrodes which display (a) pseudo-capacitive and (b) pseudo-inductive behavior, with the corresponding Nyquist diagrams and schematic current-time behavior upon a step change in potential in the positive direction. Nyquist diagrams are for R_s=20Ω.cm², R_1=200Ω.cm², R_2=120Ω.cm², C_{dl}=50μF/cm², C_{ps}=300 μF/cm² and L=1/(3*10⁻⁴) H.cm² (values chosen to be similar to some of the circuit elements found in this study)*

2.4.1 Anodic dissolution mechanism of pure Fe

Keddam et al. [37][38]illustrated the relationship between the mechanism of pure iron dissolution and the impedance of dissolving metals. A model[37] for pure iron dissolution was suggested by them, as illustrated in Figure 14. According to this mechanism, anodic dissolution of Fe to form Fe^{2+} in solution (denoted by $Fe[II]_{soln}$ in the reaction diagram) occurs via a number of adsorbed intermediates, namely two adsorbed monovalent iron species, and two adsorbed divalent iron species. Of these, $Fe\ (II)_{ad}$ is the passivating species. The rate of transformation of one species to another is described by the rate constant k_i, which depends exponentially on potential (Tafel relationship).

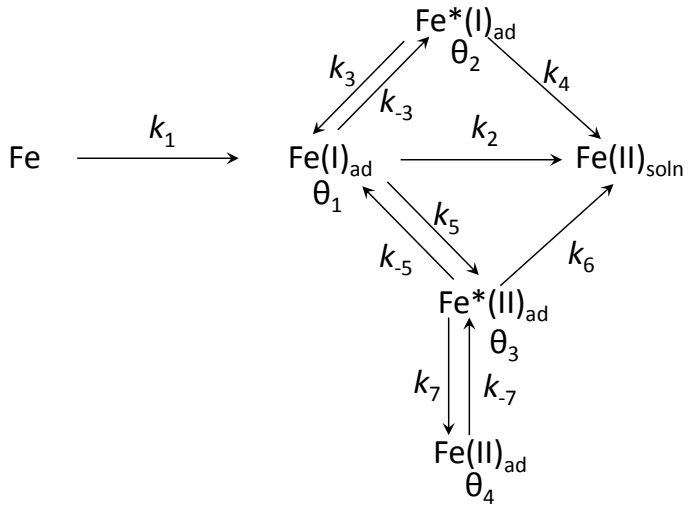

Figure 14. Proposed dissolution mechanism of pure iron in sulfate solutions[37]. The rate constants are given by k_i, and the surface coverage by adsorbed intermediates by θ_i.

2.4.2 Anodic dissolution mechanism of pure Cr

Using steady state and AC impedance techniques, Dobbelaar and de Wit studied the corrosion behavior of Cr in acid solutions and a reaction model was proposed[40][41]. The schematic illustration for the model of corrosion process is shown in Figure 15.

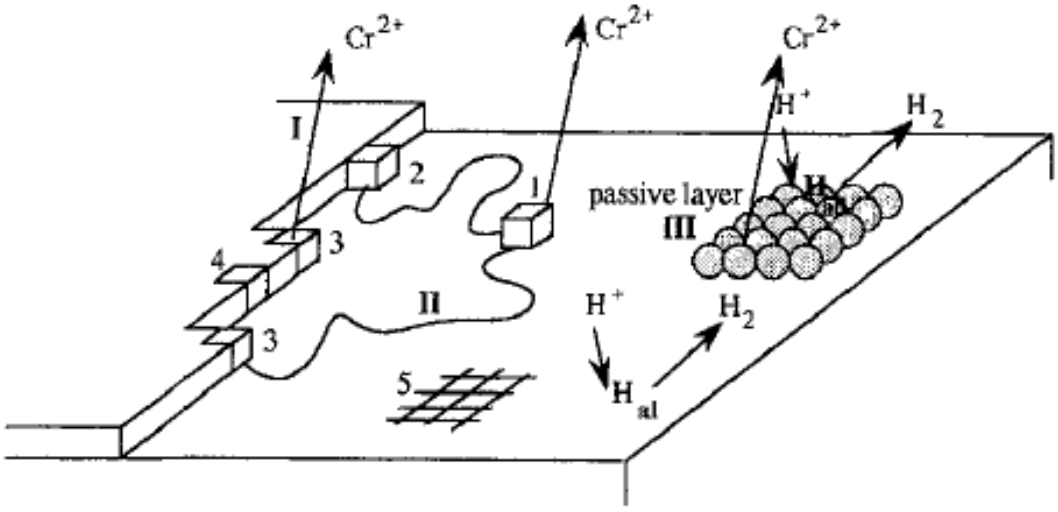

Figure 15. Schematic illustration of corrosion process at the chromium-electrolyte interface[41].

The active dissolution path of chromium shown in Fig. 13 can be interpreted using the following reaction equations [41],

Path I: $Cr \xrightarrow{k_1} Cr^{+,ad} + e^- \xrightarrow{k_2} Cr^{2+,sol} + e^-$

Path II: $Cr \xrightarrow{k_1} Cr^{+,ad} + e^- \xrightarrow[diffusion]{} Cr^{+}_{metal\ surface} \xrightarrow{k_2} Cr^{2+}_{sol} + e^-$ (2)

The passive film starts forming in the active dissolution region and chromium continues to dissolve under the passive film. The hydrogen evolution reaction occurs on both bare metal surface and passive film and the reaction rate is different from each other[41].

Based on the reaction model, an equivalent circuit was proposed[41] to fit the measured impedance data, shown in Figure 16.

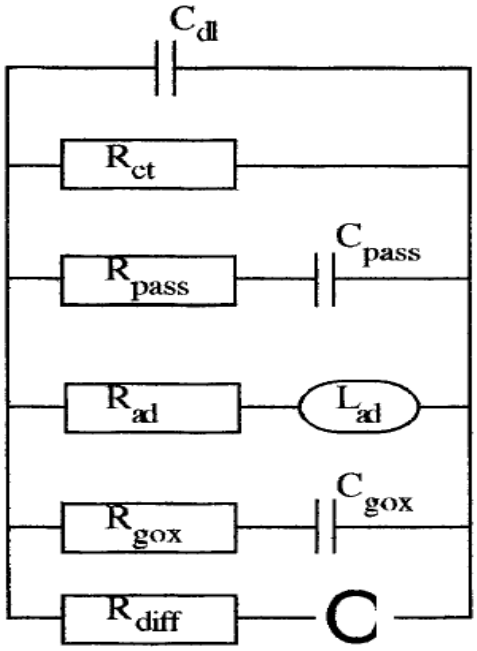

Figure 16. Equivalent circuit representing the reaction model used to fit measured impedance data. C_{dl}, double layer capacitance; R_{ct}, charge transfer resistance; R_{pass}, C_{pass}, resistance and capacitance associated with passivation; R_{ad}, L_{ad}, resistance and inductance due to the change of surface coverage of adsorbed catalytic species, Cr_{ad}^{+}; R_{gox}, C_{gox} represent the resistance and capacitance due to the change of the character of passive film; R_{diff} and O are the resistance and the finite boundary diffusion element associated with path II[41].

Equivalent circuits can be used to help estimate the time constant associated with one specific process. The mechanistic change of dissolution process can be recognized by the change of time constant of the process.

2.4.3 Anodic dissolution mechanism of pure Ni

Jouanneau, Keddam and Petit [42] studied the anodic behavior of Ni in several acidic solutions by applying DC and AC impedance techniques. A general model was proposed to explain active dissolution and passivity, shown in the following reaction steps. Dissolution of Ni proceeds through the first adsorbed intermediates and passivation occurs when the second layer adsorbs on the surface to block dissolution.

$$Ni + A^{-} \xrightarrow{k_1} Ni - A_{ad} + e$$

$$Ni - A_{ad} \xrightarrow{k_2} Ni - A_{ad}^{+} + e$$

$$Ni - A_{ad}^{+} \rightarrow Ni^{2+} + e \qquad (3)$$

The anodic dissolution mechanism of Ni in acid solution was also examined by Gregori and co-workers[43] using an electrochemical quartz crystal microbalance and electrochemical impedance spectroscopy techniques. They used a similar model to the above one, which involves several consecutive electron transfer reactions via adsorbed surface intermediates. An equivalent circuit was used to fit the impedance data, which helped to characterize the anodic dissolution.

Sato and Okamoto[44] also studied the kinetics of anodic dissolution of Ni in sulfuric acid and the effect of pH was investigated in detail. They came up with the following anodic dissolution model of Ni.

$$Ni + OH^- \rightarrow NiOH_{(ad)} + e$$

$$NiOH_{(ad)} \rightarrow NiOH^+ + e$$

$$NiOH^+ \rightarrow Ni^{2+} + OH^- \quad (4)$$

According to the model, OH^- plays a very important role in the dissolution of Ni. The activation energy of dissolution is lowered by forming adsorbed complex metal ion intermediates, which makes it easier for Ni to transfer from metal phase to solution[44].

2.4.4 Anodic dissolution mechanism of stainless steel

Stainless steel is known for its good corrosion resistance, which is mainly due to Cr in the steel. It is known that at least 12-13% Cr is needed to give the required corrosion resistance of stainless steel[45][46]. Passivity is imparted by chromium in acid solutions[45][47]. Passivity is relevant to active dissolution because passivation terminates active dissolution above the passivation potential, and also because available active dissolution models assume that initial stages of passivation are present on the actively dissolving surface. In one of these models, Newman, Sieradzki and coworkers[46][48][49] modeled the passivity of stainless steel in acid solutions based on percolation theory. Different dissolution probabilities were assigned to Fe atoms and Cr atoms. It was assumed that if a surface Cr atom has two or more nearest or next nearest neighbors, it would stay on the surface and contribute to passivity. For the case where the dissolution probability of Fe (q_{Fe})=1 and dissolution probability of Cr (q_{Cr})=0 (total selective dissolution of Fe) complete passivity is achieved when the Cr content is larger than 17%, which is the site percolation threshold for interaction up to second-nearest neighbors. When the ratio q_{Fe}/q_{Cr} decreases, passive to active transition was observed for Cr contents well above 17%. In this model, the transition from active to passive dissolution with increased potential is due to

changed dissolution probabilities. Specifically, the effect of potential on the dissolution rate of Cr is weaker than on that of Fe[48], hence q_{Cr}/q_{Fe} decreases as the potential increases. Davenport[50] and coworkers applied synchrotron X-ray microprobe measurement to confirm that the threshold of passivity for Fe-Cr alloys is around 17% in pH=4.5 buffer solutions, which is consistent with the percolation model.

Kirchheim[51] and his coworkers studied the corrosion behavior of several iron-chromium alloys in sulfuric acid using steady-state measurement and XPS analysis. The passivation potential decreases with an increase of Cr content in the alloy, shown in Figure 17. XPS analysis confirmed Cr enrichment in the active dissolution region and in the passive film, shown in Figure 18.

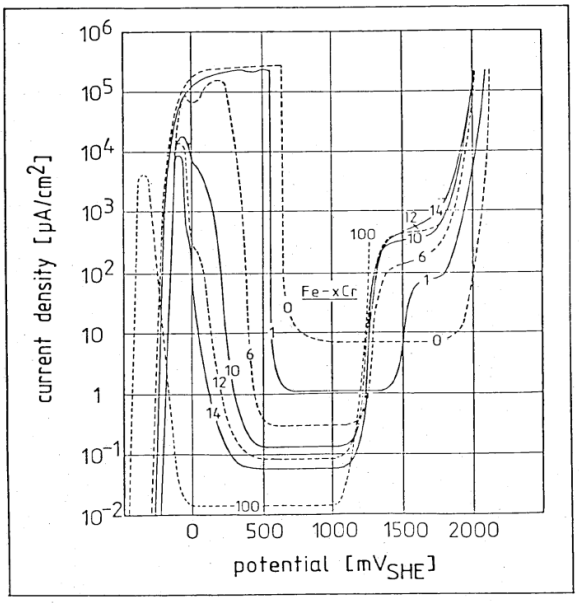

Figure 17. Steady-state current density of Fe-xCr alloys in 1N sulfuric acid at 25°C, x in weight percentage[51].

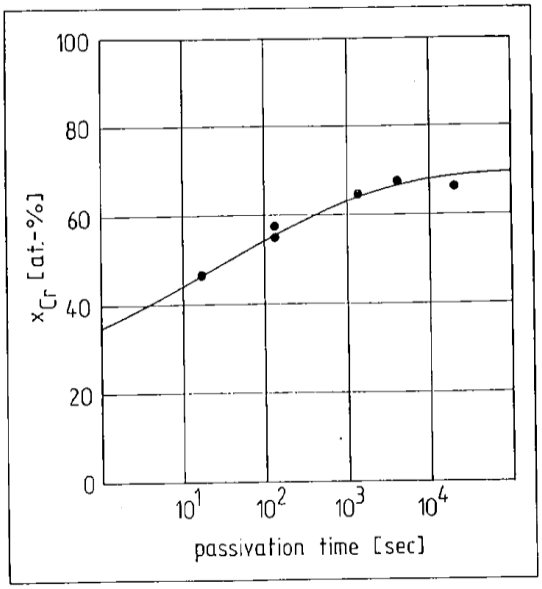

Figure 18. Average chromium content in passive film as a function of passivating time for Fe-18 at. % Cr in 1N sulfuric acid[51].

By applying electrochemistry impedance spectroscopy, Keddam and his coworkers[52][53] investigated the mechanism of active dissolution of Fe-Cr alloys and a model was proposed, shown in Figure 19. The essence of the model is that several reaction intermediates can form. The presence of adsorbed chromium intermediates, especially the passivating species $Cr(II)_{ad}$, lowers the dissolution rate of Fe.

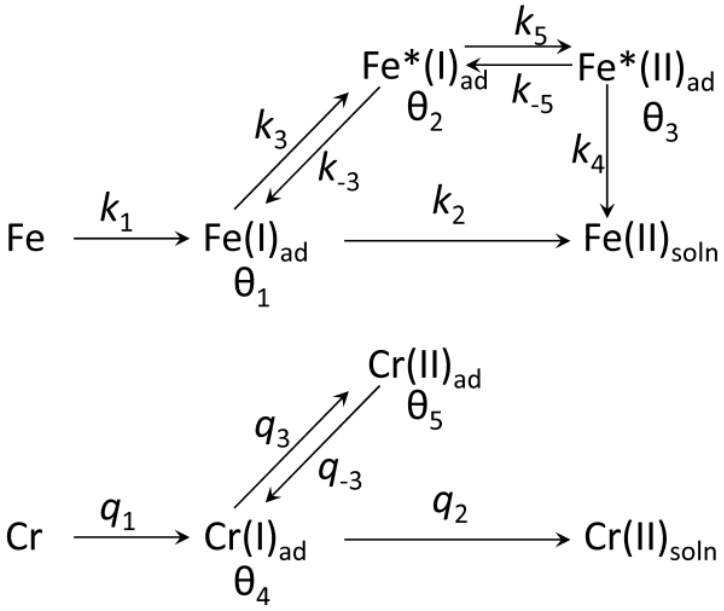

Figure 19. Reaction steps in active dissolution of Fe-Cr alloy according to Keddam's model[53].

Based on the Keddam et al. model and rate constants, the model was tested for steels containing 22% Cr and 17% Cr (detailed calculation is shown in Appendix 9.2.2). According to the calculations, the surface concentration of iron would be larger than 0.9999 at most potentials, which means that the surface is nearly pure iron. This conflicts with the experimental data observed by Knote and coworkers[54], which indicated Cr enrichment on the surface because of the preferential dissolution of Fe. Since the model fails to predict a reasonable Cr content on the surface, the model does not capture the quantitative nature of Fe-Cr interaction well. However, the qualitative features of the model might still be helpful in understanding the dissolution mechanism of stainless steel.

2.5 Anodic dissolution mechanisms of stainless steel and pure components in acid solutions with sulfur species present

2.5.1 Anodic dissolution mechanism of Fe in sulfur species containing solutions

The mechanisms of the catalytic effect of H_2S on dissolution of Fe were studied by Iofa and coworkers[30]. It was proposed by them that the mechanism of H_2S catalysis is due to the formation of a surface catalyst (Fe $(HS^-)_a$)[30]. The mechanisms are shown in the following steps[30]

$$H_2S + H_2O = H_3O^+ + HS^-$$

$$Fe + HS^- = Fe(HS^-)_a$$

$$Fe(HS^-)_a \rightarrow Fe(HS)_a + e$$

$$Fe(HS)_a \rightarrow FeHS^+ + e$$

$$FeHS^+ + H_3O^+ \rightarrow Fe^{2+} + H_2S + H_2O \quad (5)$$

It was proposed by Sury[32] that the catalytic effect of sulfide may be also be due to the lowered Me-Me bond strength or destabilized Me_{ad} by enhanced H absorption into the metallic lattice.

The inhibiting effect of H_2S under certain conditions (H_2S concentration< 0.04mmol/L, pH3-5 and long immersion time>2hrs) was explained by the formation of a protective FeS film on the surface[33]. When the FeS film is destroyed, the catalytic effect of H_2S returns, as shown in Figure 20[33].

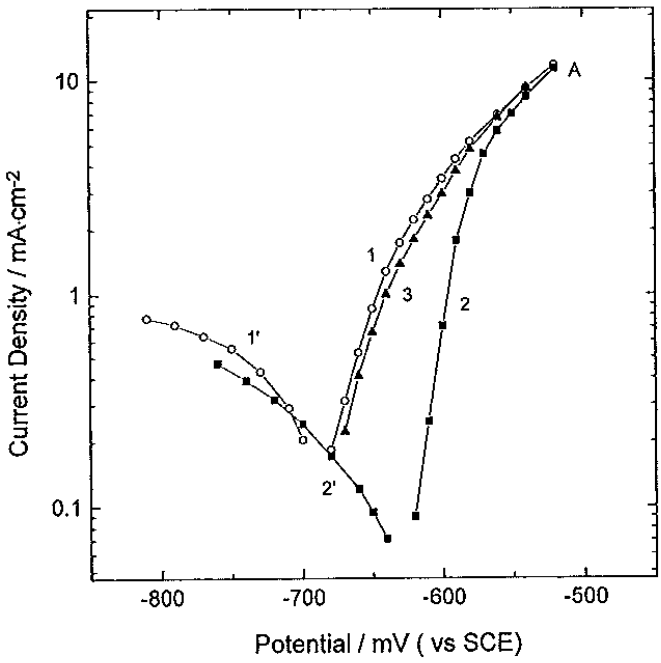

Figure 20. Polarization curves of iron in 0.5mol/L sulfuric acid + 0.02mol/L H_2S, pH=3[33]. 1. Immersed for 5mins; 2. Immersed for 3hrs. 3. After immersion for 3hrs, the electrode was polarized at point A for 1min, and then a reverse scan was applied.

2.5.2 Anodic dissolution mechanism of Cr in sulfur species containing solutions.

The mechanisms of anodic dissolution of Cr in acid solutions containing H_2S were investigated using electrochemical impedance[4]. The mechanism proposed is similar to the anodic dissolution mechanism of iron in acid solution containing H_2S. Dissolution of Cr occurs via two catalytic adsorbed intermediates, $(CrHS^-)_{ad}$ and $(CrHS)_{ad}$, when H_2S is present, shown in the following reaction steps[4].

$$Cr + H_2S + H_2O = (CrHS^-)_{ad} + H_3O^+$$
$$Cr + H_2S + H_2O = (CrHS)_{ad} + H_3O^+ + e^-$$
$$(CrHS^-)_{ad} = (CrHS)_{ad} + e^-$$
$$(CrHS)_{ad} = CrSH^+ + e^-$$
$$CrSH^+ + H^+ = Cr^{2+} + H_2O \quad (6)$$

2.5.3 Anodic dissolution mechanism of Ni in sulfur species containing solutions

A mechanism for the catalytic effect of adsorbed sulfur on the dissolution of Ni was suggested by Marcus[55]. It was proposed that, due to the strong interaction between nickel atoms and adsorbed sulfur, nickel-nickel bonds are weakened. Hence the activation energy for dissolution of metal is decreased, as shown in Figure 21[55].

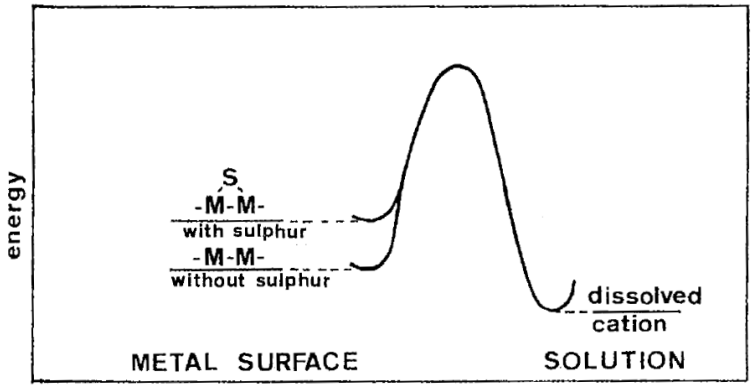

Figure 21. Weakening of the metal-metal bond by adsorbed sulfur and acceleration of dissolution[55]

Another factor mentioned is that adsorbed sulfur changes the electric field of the surface by creating a surface dipole, which facilitates metal passing through the interface into solution[34].

By applying *in situ* scanning tunneling microscopy (STM) dissolution of sulfur-modified Ni electrodes was observed directly and a model of Ni dissolution was proposed[3]. It was observed that dissolution of Ni primarily occurred at step edges, accompanied by movement of

S atoms from the upper terrace to the lower terrace[3]. The structure model is shown below (Figure 22); dissolution of nickel atoms *a* and *b* is accompanied by movement of a sulfur atom from the upper terrace to the lower terrace. In this way sulfur stays adsorbed on the surface while metal dissolution continues.

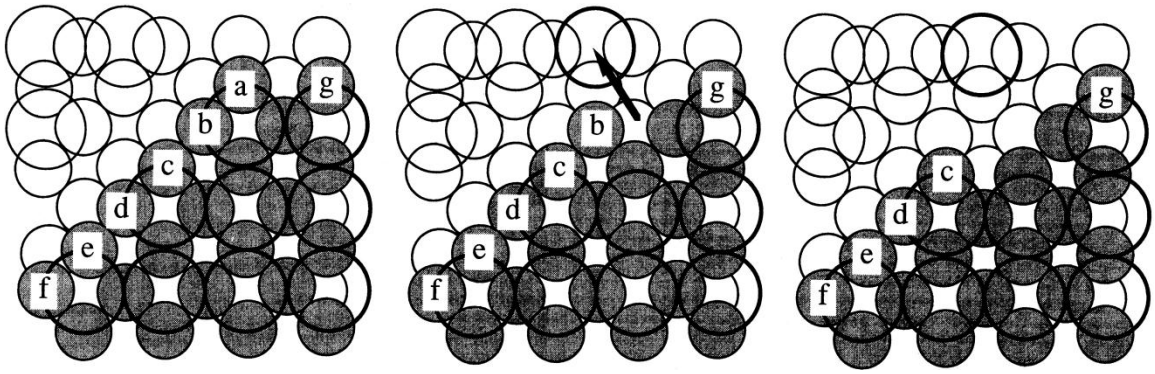

Figure 22. Schematic illustration of the anodic dissolution process at a ledge in a sulfur-covered (100) nickel plane. Smaller circles are nickel atoms (darker circles are in the upper terrace), and larger circles are adsorbed sulfur atoms[3].

2.5.4 Anodic dissolution mechanism of stainless steel in sulfur species containing solutions

For pitting of stainless steel in thiosulfate solutions, it was proposed by Newman and coworkers[24][25] that thiosulfate is not stable in acid solutions and generates elemental sulfur or sulfide ions by disproportionation. Dissolution in the acidic environment of pits is activated by sulfur or sulfide ions and repassivation of the metal surface is also retarded by sulfur or sulfide ions[24][25][26]. Within certain concentration and potential ranges, pitting corrosion remains active with continuous delivery of sulfur to the pit by thiosulfate[24]. It was also confirmed by XPS analysis[14] that thiosulfate reduced to sulfur or sulfide on the bare metal surface but it did not reduce on the passive metal surface.

The mechanism proposed for the effect of thiosulfate on stress corrosion cracking is similar to the mechanism of the effect of thiosulfate on pitting corrosion of stainless steels.

Sulfur is generated by disproportionation of thiosulfate at the crack tip to assist the active dissolution of the crack and inhibit repassivation of the crack tip[27][28].

3. Objective

The objectives of the current research work are to investigate the effect of thiocyanate on the anodic dissolution behavior of Type 304 stainless steel in acid solutions and to study the mechanisms of the catalytic effect of thiocyanate on the anodic dissolution of stainless steels. Specific objectives are as follows:

(1) Investigate the effect of thiocyanate on the anodic dissolution behavior of pure elements (Fe, Cr and Ni) of stainless steel in acid solutions.

(2) Study the mechanisms of the effect of thiocyanate on pure elements.

(3) Investigate the effect of thiocyanate on a simpler stainless steel, Type 430 stainless steel (Fe-Cr alloy), and relate this to the behavior of pure elements.

(4) Study the effect of thiocyanate on the anodic dissolution of Type 304 stainless steel. Use the knowledge of behavior of pure elements and the simpler alloy system to understand the mechanisms of the thiocyanate effect.

4. Hypothesis

1. Thiocyanate is expected to decompose to elemental sulfur on the metal surface during active dissolution of stainless steel. Adsorbed sulfur catalyzes the active dissolution of the metal and the desorption rate of adsorbed sulfur is not zero during the active dissolution of the metal.

2. The catalytic effect of thiocyanate on 430 stainless steel is due to the increased dissolution rate of chromium, counteracting the formation of the Cr-O-Cr passivating network at the ledges.

3. The mechanism of the catalytic effect of thiocyanate on 304 stainless steel is similar to what was found for 430 stainless steel, but nickel is beneficial to the corrosion resistance of 304 stainless steel, in that nickel lowers the percolation limit of chromium to passivate the surface.

5. Methodology

5.1 Materials

The corrosion behavior of pure Fe, Cr, Ni and type 430 & 304 stainless steel was studied in dilute sulfuric acid and acidified sodium sulfate with/without KSCN. The pure metal electrodes were prepared from polycrystalline electrolytic metal; the chemical compositions of Types 430 & 304 stainless steel are given in Table 2&3 and the microstructures of the steels are shown in Figure 23. Rods with an approximately square cross-section (side length 2-3 mm) were cut with a diamond saw, and sealed (with epoxy resin) into acrylic rods (diameter 12.5 mm) to prepare rotating electrodes with areas of approximately 0.05 cm^2. The exposed area of the Type 304 stainless steel electrode was approximately 0.3cm^2. The relatively small electrode area was used to minimize IR effects.

Table 2: Composition of Type 430 stainless steel

Element	Mass %
Cr	16.75
Mn	0.46
Si	0.32
Ni	0.20
Cu	0.085
Mo	0.034
C	0.043
N	0.042
P	0.025
S	0.003

Table 3: Composition of Type 304 stainless steel

Element	Mass%
Cr	18.46
Ni	7.94
Mn	1.66
Cu	0.38
Si	0.26
N	0.089
C	0.024
S	0.019

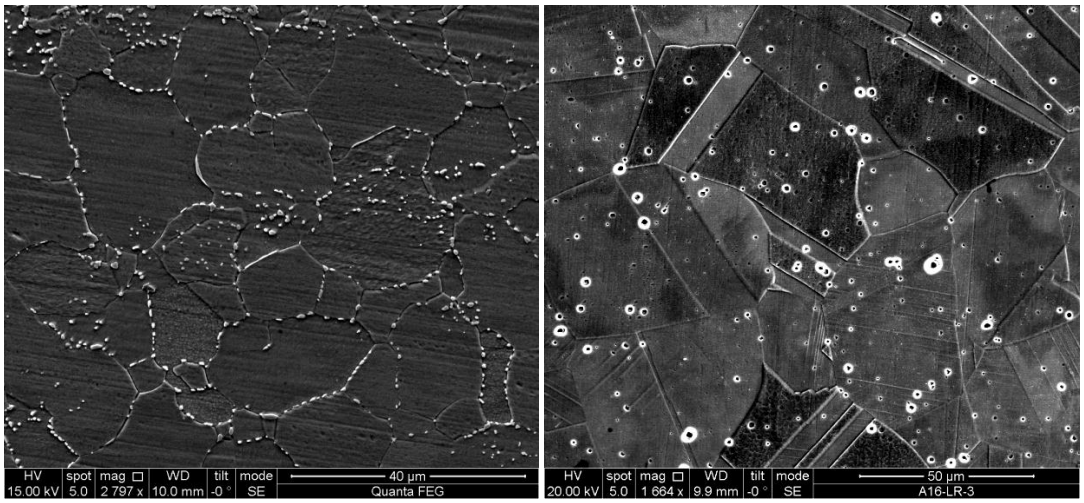

Figure 23. Microstructure of Types 430 (left) & 304 (right) stainless steels (scanning electron microscopy; secondary electron images); etchant used for 430 stainless steel was Kalling's no. 2 solution and was oxalic acid electrolytic for 304 stainless steel[56]. White dots in Type 430 image are chromium-rich carbies; white dots in Type 304 image are etch pits.

The samples used for XPS measurement were different in shape from the samples used for electrochemical measurements. The steel electrodes (chemical compositions in Table 4) were cut from cold-rolled sheet into strips approximately 0.5 mm thick, 1-2 cm wide and 2-3 cm long; the immersed length was approximately 1 cm. Microstructures of the steels are shown in Figure 24. Chromium and nickel electrodes, with similar dimensions to the steel sheet electrodes, were cut from electrolytic metal using a diamond saw. Residual elements, notably

copper (and nickel in Type 430 stainless steel) were found to affect the development of sulfide product. To eliminate the effect of such residual elements, vacuum arc melting was used to prepare a high-purity Fe-20 weight % Cr alloy (Fe20Cr) from electrolytic metal.

Table 4. Compositions of Type 430 and Type 304 stainless steels for XPS measurements (mass percentages; balance Fe)

Element	Type 430	Type 304
Cr	16.7	18.3
Mn	0.46	1.09
Si	0.4	0.48
Ni	0.16	8.41
Cu	0.12	0.56
C	0.049	0.056
N	0.033	0.067
Mo	0.024	0.37
S	0.002	<0.002

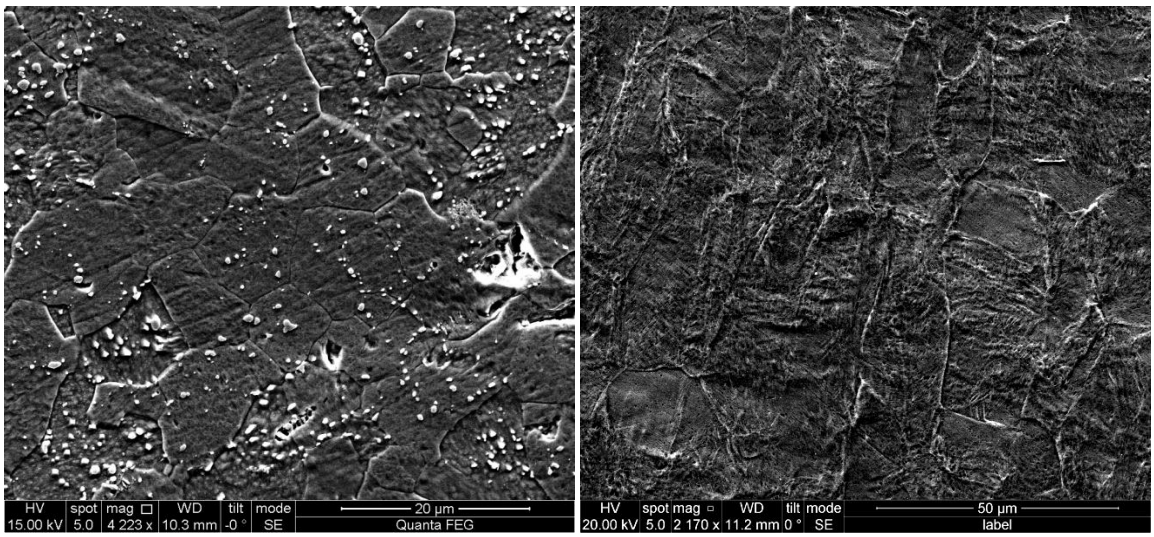

Figure 24. Microstructure of Types 430 (left) and 304 (right) stainless steels used for XPS measurements (scanning electron microscopy; secondary electron images). White dots in Type 430 image are carbides; etchant used for 430 stainless steel was Kalling's no. 2 solution and was oxalic acid electrolytic for 304 stainless steel[56].

The electrolytes (containing 0.01 M H_2SO_4 and 1M Na_2SO_4 with *p*H=2.5 or 1 M H_2SO_4 with pH=0; zero or 14 mg/dm^3 [0.14 mM] KSCN; volume 0.35 dm^3) were prepared using analytical-grade reagents and deionized water.

5.2 Experiment setup

A Gamry Reference 3000 Potentiostat was used to perform electrochemical measurements, including steady-state measurements and AC impedance measurements.

A three-electrode system was used during the measurement. The working electrode was rotated by an electrode rotator (Gamry RDE 710 Rotating Electrode). A mercury contact was used for the rotating electrode to lower the noise coming from the contact system (see Appendix). Two graphite rods served as counter electrode. A KCl-saturated Ag/AgCl reference electrode (E=0.20 V_{SHE}) was used and all the potentials are given with respect to this reference electrode. A length of platinum wire was used for capacitive coupling of the reference electrode to lower the noise of impedance data at high frequencies[57]. A glass cell with double wall was used and connected to a water bath to keep the cell temperature constant.

Potentiodynamic curves of 430 stainless steel at 1M Na_2SO_4 + 0.01M H_2SO_4 with reference electrode connected via a sodium sulfate salt bridge and with reference electrode in the test electrolyte are shown in Figure 25. It can be seen that the polarization curves measured with/without salt bridge are very similar to each other. There is no indication that the reference electrode filling solution affected the results.

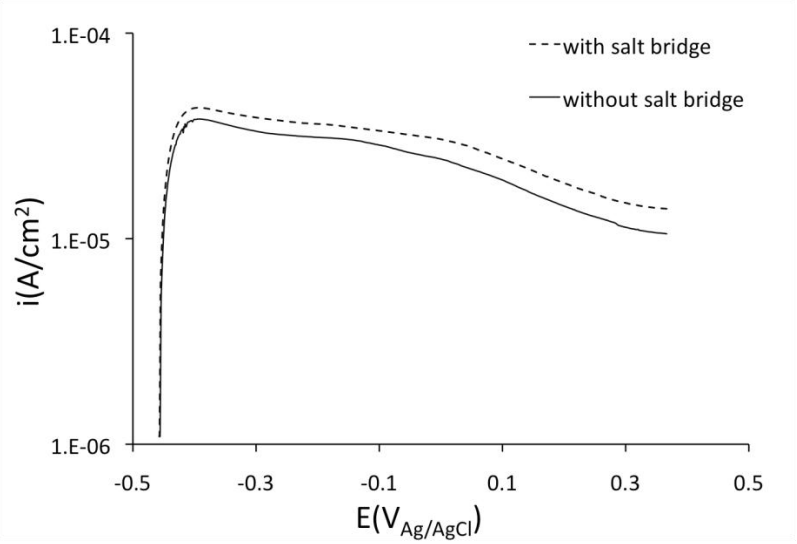

Figure 25. Potentiodynamic polarization curves of 430 stainless steel 1M Na_2SO_4 + 0.01M H_2SO_4 measured with reference electrode connected via salt bridge and with reference electrode in the test electrolyte; scan rate 1mV/s

It was shown (Figure 26) that the polarization curves of 430 stainless steel in thiocyanate-containing solutions measured with two different counter electrode are nearly the same, which indicated that possible impurities in the graphite electrode did not affect the measurements.

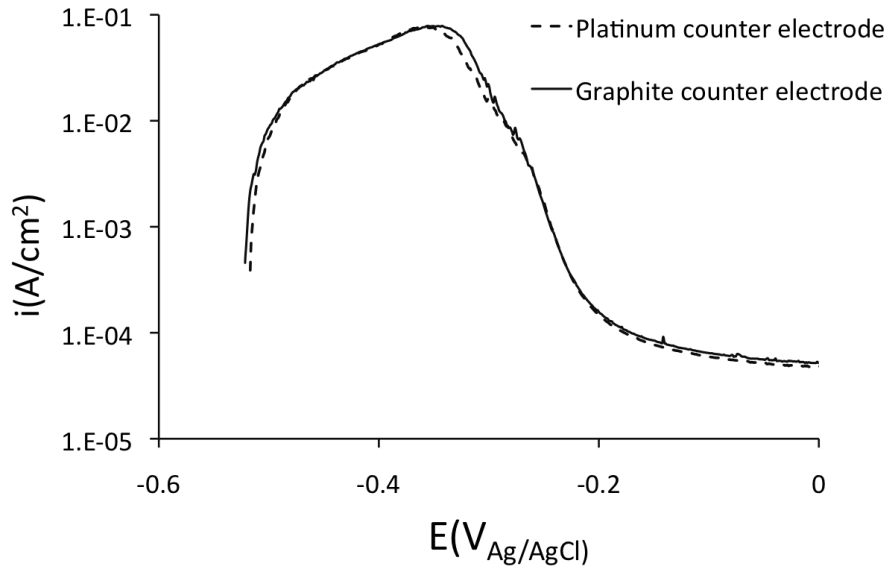

Figure 26. Potentiodynamic polarization curves of 430 stainless steel in 1M H_2SO_4 + 0.14mM KSCN measured with two different counter electrodes: platinum and graphite; scan rate 1mV/s

5.3 Experiment procedure

Electrode surfaces were wet ground on silicon carbide paper (600 grit) before measurements. The electrolyte was deoxygenated by bubbling pure N_2 for half an hour prior to measurements and during the measurement. The flow rate of N_2 was 10ml/second. The temperature of the electrolyte was kept at 25°C. Some measurements were also performed at 35°C. The rotation speed of working electrode was 1000rpm during measurement, unless stated otherwise.

As shown in Figure 27, there is no obvious difference in the polarization curves of 430 stainless steel for two different surface preparations, which suggested that surface finish did not affect the result much.

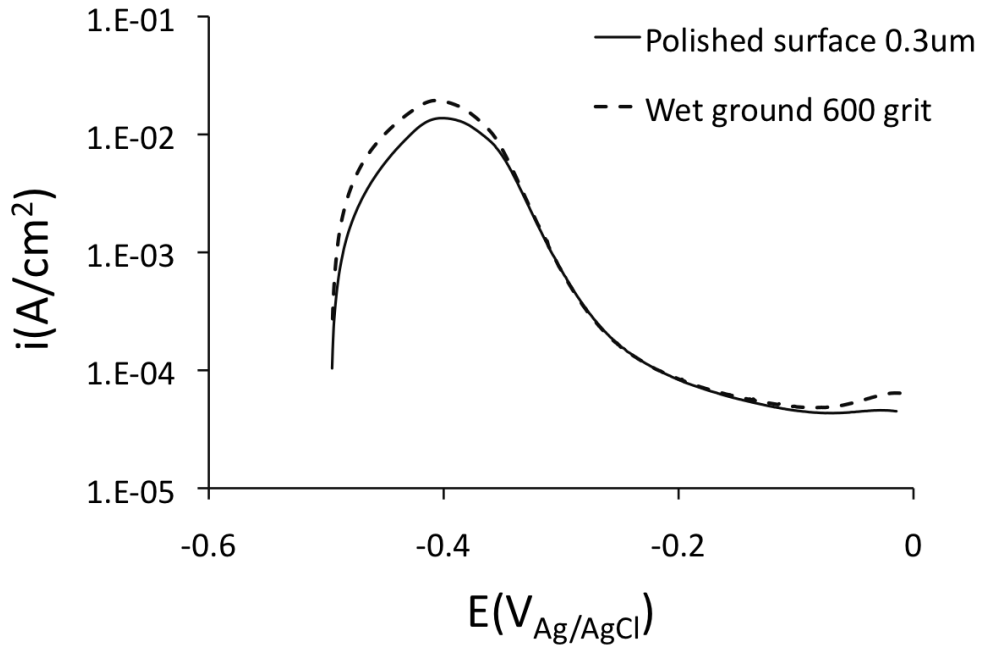

Figure 27. Potentiodynamic polarization curves of 430 stainless steel with different surface finishes (diamond polished surface vs. 600 grit wet ground surface) in 1 M H_2SO_4; scan rate 1mV/s

The general procedure for electrochemical measurements was as follows. First a potentiostatic scan was performed to measure the polarization curve of anodic dissolution with/without KSCN. Starting from a lower potential the electrode was kept at the potential for at least 5 min to allow the current to stabilize. Then the electrode was stepped to a higher potential, waiting until the current stabilized, repeating the process to obtain a complete steady-state polarization curve of the sample. The effect of KSCN on the steady state dissolution behavior of metals was obtained by comparing the steady state polarization curves of metal with/without KSCN. The size of potential steps ranged from 10mV to 50mV. Measured potentials were corrected for IR errors, by using the measured current density and solution resistance (from impedance measurement).

AC impedance measurements were then performed at selected potentials. The potentials for impedance measurements were selected based on the following principles:

1. The potential should be in the active range.
2. The potential should not be too close to the open circuit potential to avoid interference by the cathodic reaction.
3. The corrosion current density at the chosen potential should not be too high, since this would make the impedance results noisy, also corrosion product might precipitate on the surface at high current density.
4. The current density at the chosen potential can reach steady state in a reasonable time.

Prior to the impedance measurement, the electrode was held at the same potential as the impedance measurement for sufficient time to stabilize the current. If the sample surface did not reach steady state, sometimes the impedance result obtained was not reasonable. For example, the impedance curve shown in Figure 28 was measured while the DC current was still decreasing. A tail in the low frequency region was obtained. That is because the charge transfer resistance was increasing during the measurement and hence the diameter of the capacitive

loop was increasing. So the true diameter of the steady state capacitive loop would be larger than measured and the tail should be part of the inductive loop at the low frequency, shown in Figure 29.

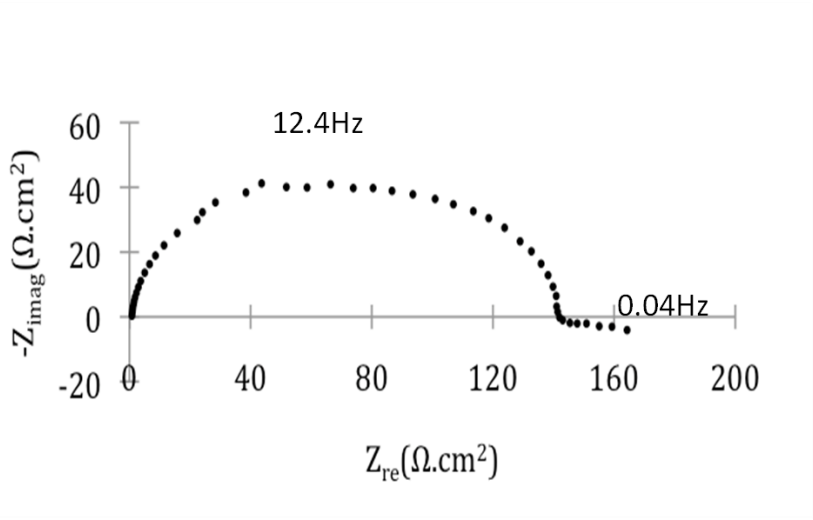

Figure 28. Impedance curve obtained at E=-0.75V of Cr in sulfuric acid at pH 2.5 when the current density was not stable yet; holding time=300s.

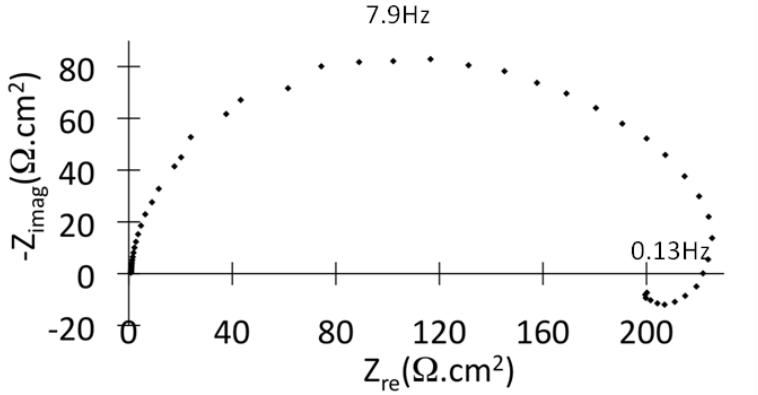

Figure 29. Impedance curve obtained at E=-0.75V of Cr in sulfuric acid at pH2.5 after current stabilized; holding time=1500s.

Additional information about dissolution mechanisms, which is not evident in steady state measurements, can be obtained from impedance spectra[37]. By comparing the impedance

spectra obtained with/without KSCN, it can be deduced how KSCN affects the dissolution mechanism of metals.

Equivalent circuits were used to fit impedance spectra using Zview™ software (Scribner Associates). The parameters of each element of the equivalent circuit were estimated by finding the best fit of impedance curves. Equivalent circuits can help to get better understanding of the mechanistic character of the dissolution process. Physical meanings were assigned to each circuit element and the parameter of the element can help to understand the dissolution process quantitatively, such as the estimation of time constants of reaction steps. In most cases, constant-phase elements (CPEs)[58], rather than pure capacitors or inductors, were used to fit the reactive circuit elements. The impedance of such a constant-phase element is defined as follows:

$$Z = \frac{1}{A(i\omega)^{\alpha}} = \frac{1}{A\omega^{\alpha}}\exp\left(-\frac{\pi}{2}\alpha i\right) \tag{7}$$

Hence the size of the impedance of a CPE is $1/(A\omega^{\alpha})$ and its phase angle is (-90α) degrees; a pure capacitor corresponds to α=1, and a pure inductor to α=-1. In general, $|\alpha|$ was smaller than 1, which implies that, in addition to a pure reactive component, the CPE impedance also included a frequency-dependent real component. For comparison with ideal circuit elements, the impedance at a given frequency was calculated (equation [8); the real component was taken to correspond to a frequency-dependent series resistance, and the imaginary component to a reactive component (capacitor or inductor) with an "effective" size which also depends on frequency.

$$Z_{re} = \frac{1}{A\omega^{\alpha}}\cos\left(-\frac{\pi}{2}\alpha\right) = R_{series}$$
$$Z_{im} = \frac{1}{A\omega^{\alpha}}\sin\left(-\frac{\pi}{2}\alpha\right) \tag{8}$$

The effective capacitance or inductance is then given by:

$$C_{eff} = -\frac{A\omega^{(\alpha-1)}}{\sin\left(-\frac{\pi}{2}\alpha\right)}$$

$$L_{eff} = \frac{\sin\left(-\frac{\pi}{2}\alpha\right)}{A\omega^{(\alpha+1)}} \qquad (9)$$

Estimates of the error of the impedance results are as follows:

Experimental error:

Each impedance measurement was repeated at least once and if was is not reproducible the measurement was repeated several times until a reproducible result was obtained. In general the experimental results were very reproducible, for example, as shown in Figure 30.

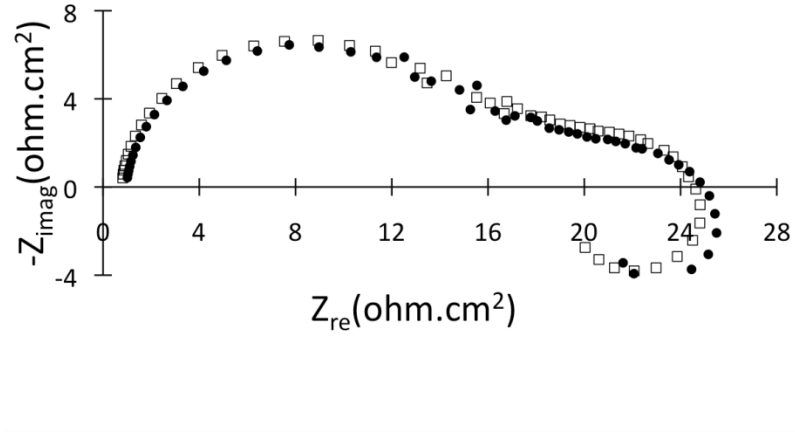

Figure 30. Impedance results of pure chromium at 1M Na_2SO_4 + 0.01M H_2SO_4 with two repeats; E=-0.75$V_{Ag/AgCl}$

Fitting error: The Fitting error of most parameters was within 10% of the size of the parameter; a few were around 20%. According to the Zview help file, "the error estimates are calculated by testing several solutions near the best fit. For example, if the best value for a particular resistor

is 100 Ohms, the value is increased until the goodness of fit starts to decrease. If 98 and 102 Ohms produces a very similar goodness of fit, but 97 and 103 Ohms produces a poorer fit, the error is reported as 2 Ohms."

Scanning Electron Microscopy and Atomic Force Microscopy were applied to characterize the surface morphology of corroded samples. The surface morphology of corroded surfaces can provide useful information about the dissolution process. Microanalysis by energy-dispersive spectroscopy (EDS) was used to analyze the composition of corrosion product. While EDS can give no information on products that are only a few atomic layers thick, EDS was useful in indentifying corrosion debris (such as carbides on the surface of corroded type 430 stainless steel).

Surface analysis (X-ray photoelectron spectroscopy) was performed on pure chromium and nickel, a high-purity Fe-20wt% Cr alloy and Type 430 and Type 304 stainless steel to test mechanisms proposed on the basis of electrochemical measurements.

6. Results and Discussion

6.1 Mass transfer and alloy effects

6.1.1 Role of mass transfer in the catalytic effect of thiocyanate

As mentioned in the Introduction, the anodic current density of the electrode was increased by increasing the mass transfer coefficient to the electrode surface. The role of mass transfer rate was examined by measuring the anodic current densities at various rotation speeds of the electrode, as shown in Figure 31.

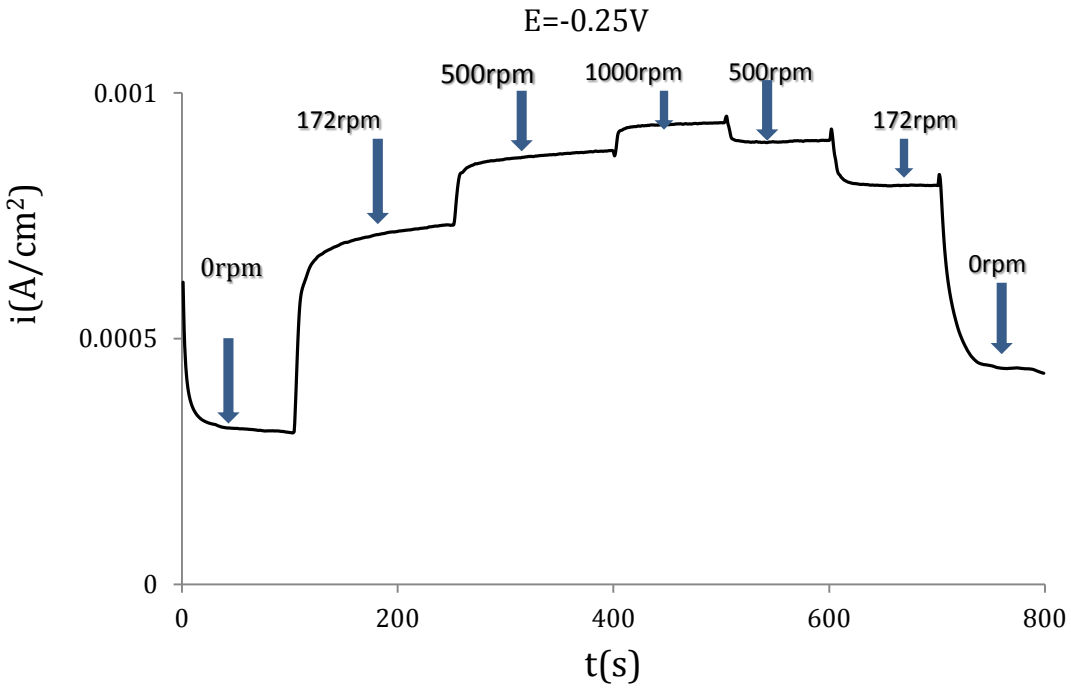

Figure 31. Potentiostatic polarization curve of type 304 stainless steel in 1M H_2SO_4 and 0.086mM SCN^- at different rotation speeds; E=-0.25$V_{Ag/AgCl}$; T=25°C;

During the measurement the potential was kept constant in the active loop and the rotation speed of electrode was adjusted to change the mass transfer rate. The results show that at

different mass transfer rates the current density is different and the current density has a fast response to a change of rotation speed of electrode. At the same rotation speed the current density became stable over time. The relationship between steady-state current density and rotation rate can be seen from Figure 32. A similar effect of mass transfer conditions on the anodic dissolution rate was also observed by Horowitz in the case of carbon steel dissolution in phosphate buffer solution with tetrathionate and thiosulfate[59]. The anodic dissolution rate of carbon steel was accelerated by tetrathionate and thiosulfate and the anodic peak current density was proportional to the mass transfer rate[59].

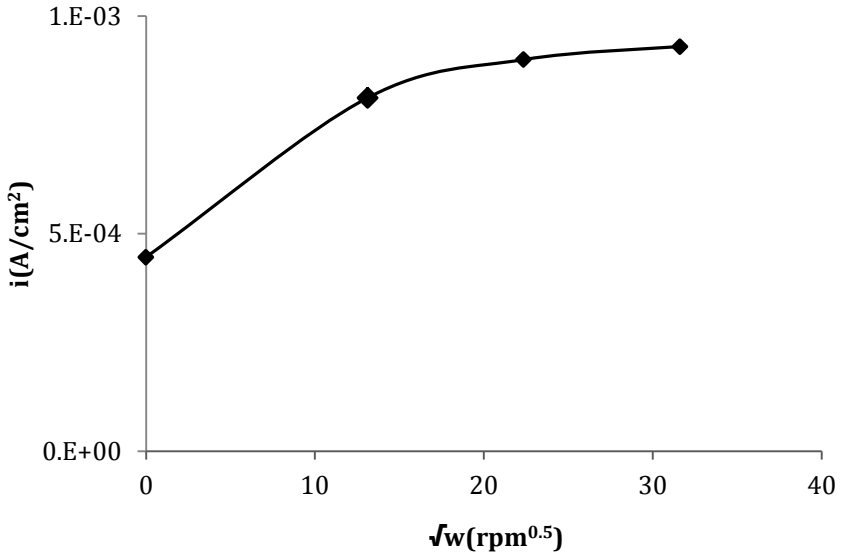

Figure 32. Relationship between steady state current density of type 304 stainless steel and rotation speed of the electrode in 1M H_2SO_4 and 0.086mM SCN^-; E=-0.25$V_{Ag/AgCl}$.

As mentioned before, it is proposed that the elemental sulfur remains on the surface during the active dissolution of metal, even if a large amount of metal has been dissolved away[3]. If this is the case, then once there is enough sulfur on the metal surface the sulfur will remain there and keep catalyzing dissolution of metals. Further transportation of thiocyanate to the metal surface would not change the dissolution rate. However, this cannot explain what we

found here, namely that the mass transfer rate does increase the anodic current density. One probable explanation suggested by Betts and Newman [60] is that the sulfur desorption rate from the metal surface is not zero and a continuous supply of sulfur is needed to the metal surface to sustain the effect of sulfur on dissolution.

In contrast, the mass transfer coefficient did not affect anodic current density of the electrode in thiocyanate-free sulfuric acid solutions. As shown in Figure 33, there is no obvious change of the anodic current densities of type 304 stainless steel when the rotation speed of the electrode was adjusted from 0 rpm to 1672 rpm.

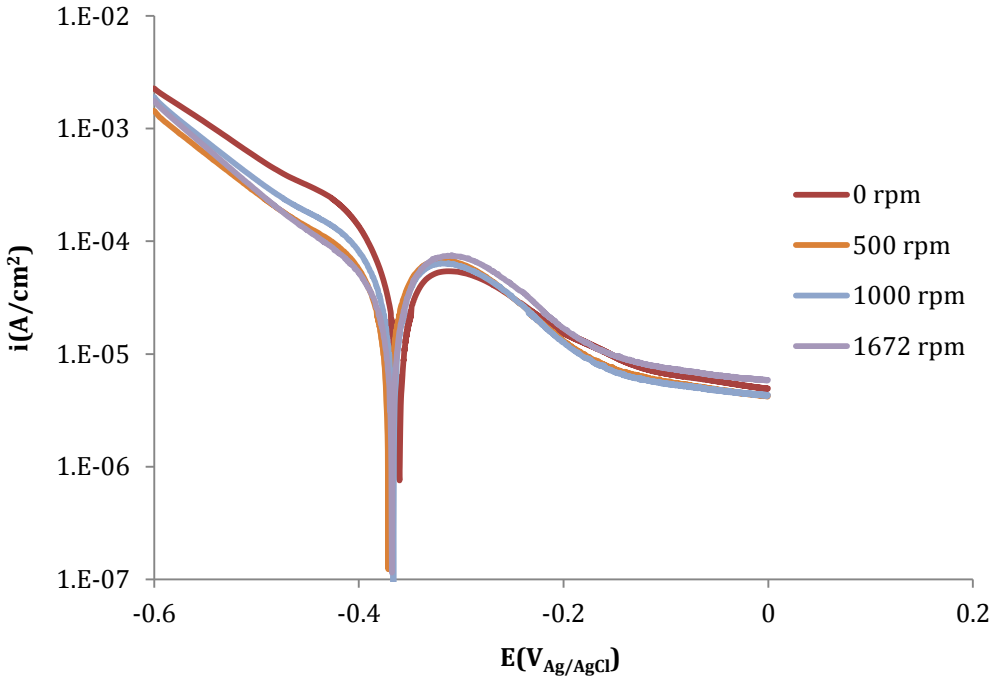

Figure 33. Effect of mass transfer rate on the polarization curve of type 304 stainless steel in deaerated 1M H_2SO_4 without thiocyanate at 35 ℃; scan rate was 1mV/s.

The Reynolds numbers of the rotating disc electrode at different rotating speeds were calculated to estimate the boundary condition.

$$\mathrm{Re} = \omega r^2 / \nu$$
$$r = 0.0032\,m,\ \nu = 1\times10^{-6}\,m^2/s \qquad (10)$$

Re is Reynolds number; r is the radius of the electrode; ν is the kinematic viscosity

For rotating speeds 172rpm, 500rpm, 1000rpm and 1672rpm, the Reynolds numbers are as follows: 190, 552, 1106 and 1838. It was noted[61][62] that the flow over the rotating disc is laminar when Reynolds number is less than 4.5×10^4. The Reynolds numbers of the rotating electrodes used here were much smaller than 4.5×10^4 so the flow over the rotating electrodes was laminar.

The observed effect of mass transfer conditions on the anodic dissolution rate is qualitatively in agreement with the suggestion that transport of thiocyanate to the dissolving surface serves to replace adsorbed sulfur that is lost during dissolution. However, the dissolution rate is not a linear function of the square root of the rotation rate (Figure 33), showing that the increase in dissolution rate by thiocyanate is not fully mass transfer controlled. Quantitative comparison of the thiocyanate transport rate to the surface also indicates mixed control. For freely corroding Type 304 and Type 316 stainless steel in 0.05 M H_2SO_4, the rate of removal of sulfur from the electrode surface was shown as 0.3 ng/cm^{2}min for Type 304, and 0.8 ng/cm^{2}min for Type 316, for the first 30 minutes of exposure to the solution [6]. If replenishment of adsorbed sulfur is fully controlled by thiocyanate transport, the thiocyanate concentration at the electrode surface is much smaller than the bulk concentration; the thiocyanate flux to the surface is then given by $J=kC_{bulk}$, where J is the flux, k the mass transfer constant, and C_{bulk} the bulk concentration of thiocyanate. Using the relationship for a rotating disc electrode ($Sh = 0.6205Re^{0.5}Sc^{0.33}$)[63], where Sh is the Sherwood number, Re the Reynolds number, and Sc the Schmidt number, the mass transfer constant is calculated to be 2.6×10^{-5} m/s for a rotation rate of 172 rpm, corresponding to a thiocyanate flux of 2.3×10^{-6} mol/m^{2}s (bulk concentration of 5 mg SCN^- per dm^3), or 436 ng/cm^{2}min of sulfur. This is more than 3 orders of magnitude as large as the rates of sulfur loss reported by Elbiache and Marcus[6]. Possible reasons for the difference include mixed control of dissolution (not just

limited by thiocyanate mass transfer), and a higher anodic dissolution rate in the present work (resulting from polarizing the electrode to a potential more positive than the corrosion potential, but still in the active loop, and the higher acid concentration of 1 M H_2SO_4 compared with 0.05 M H_2SO_4 for the measurements reported by Elbiache and Marcus).

The effect of the higher dissolution rate on the sulfur removal rate can be estimated for the case of type 316 steel, using the approach of Elbiache & Marcus. In their approach, sulfur is removed during dissolution through the effect of molybdenum at the dissolving surface; if no sulfur replenishment occurs, the fraction coverage of sulfur remaining after one atom layer of alloy has been removed is given by:

$$\theta(n+1) = \theta(n) - \left\{ [\theta(n)]^2 (C_{Mo})^m \right\} \tag{11}$$

where θ is the fractional surface coverage by sulfur, C_{Mo} is the mole fraction of molybdenum at the alloy surface, m is a kinetic constant (found by Elbiache & Marcus to be approximately 1), and n is the number of atomic layers of steel removed by dissolution.

The rate of decrease of surface coverage is hence given by

$$\frac{d\theta}{dt} = -\theta^2 (C_{Mo})^m \frac{dn}{dt} \tag{12}$$

where dn/dt is the rate of corrosion, expressed as the number of atomic layers removed per unit time (which is proportional to the anodic current density).

This analysis assumes that only molybdenum causes sulfur removal from the surface. The measured effect of mass transfer on the anodic current density (Figure 32) is for Type 304, so cannot be compared directly. However, taking the anodic dissolution rate of Type 316 to be 0.2 times that of Type 304 allows an approximate comparison to be made. Based on the unit cell size of austenite of 3.6Å and an average charge of dissolved cations of 2.2, the relationship between the rate of removal of (100) planes and the current density is as follows:

$$dn/dt = 1.8 \times 10^3 \, i, \tag{13}$$

where dn/dt is in layers per second, and i is in A/cm^2.

Table 5 compares the limiting rate of sulfur transport (as SCN^-) to the electrode surface, and the estimated rate of sulfur removal by dissolution. The values for sulfur removal were based on complete coverage of sulfur (θ=1, corresponding to 40 ng sulfur per cm^2). The results confirm that the estimated thiocyanate flux to the surface is much larger than the sulfur desorption rate; the conclusion is that the desorption data of Elbiache & Marcus cannot be used to explain the thiocyanate mass transfer effect quantitatively.

Table 5. Comparison of limiting rate of thiocyanate transport to the electrode surface (J_S) with the estimated rate of removal of sulfur by dissolution ($d\theta_S/dt$), for Type 316

ω (rpm)	k (m/s)	i (A/cm^2)	J_S (ng S/cm^{2}min)	$d\theta_S/dt$ (ng S/cm^{2}min)
172	2.6E-05	1.4E-04	436	8.1
500	4.5E-05	1.7E-04	743	9.9
1000	6.3E-05	1.9E-04	1051	11.0

6.1.2 Role of concentrations of thiocyanate in its catalytic effect

The presence of very low concentrations of thiocyanate can greatly increase the anodic dissolution current of stainless steel, as shown in the Introduction. Also, by increasing the concentration of thiocyanate, the anodic current density of stainless steel was increased, which can be seen from Figure 34 and Figure 35.

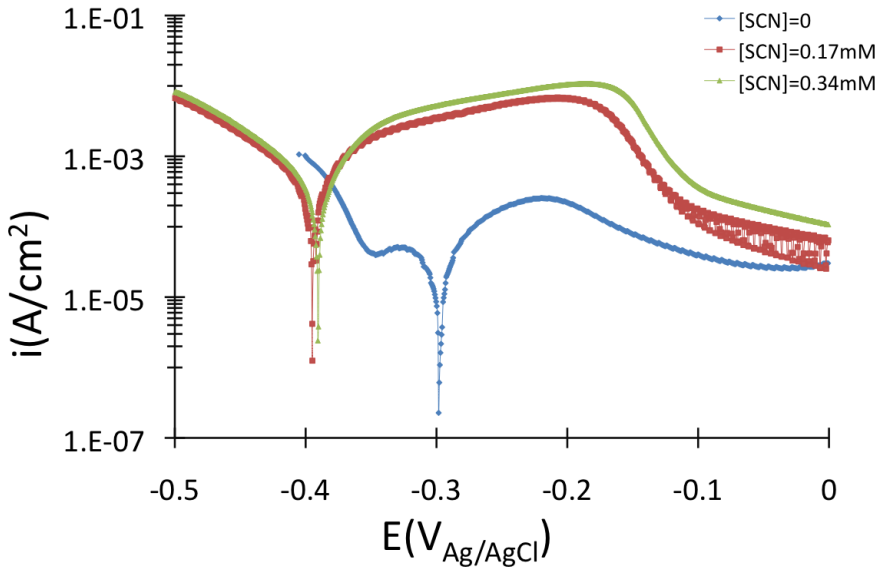

Figure 34. Potentiodynamic polarization curves of type 304 stainless steel in deaerated 1M H_2SO_4 at 35℃ with different concentrations of thiocyanate; a static electrode was used during the measurements; scan rate was 1mV/s.

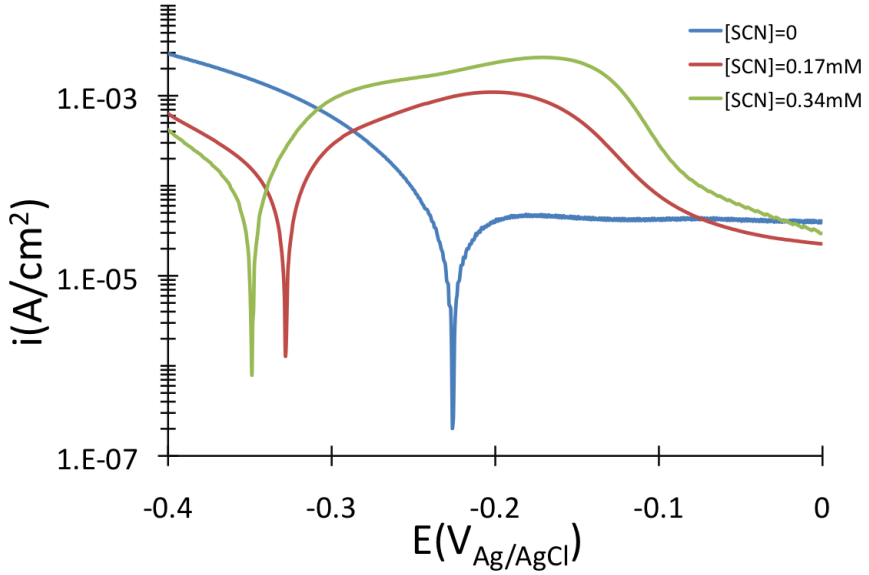

Figure 35. Polarization curves of type 316 stainless steel in deaerated 1M H_2SO_4 at 35℃ with different concentrations of thiocyanate; a static electrode was used during the measurements; scan rate was 1mV/s.

As discussed previously, thiocyanate decomposed to elemental sulfur adsorbed on the metal surface. At the same time desorption rate of sulfur was not zero. The effect of thiocyanate concentration is qualitatively consistent with an effect of mass transfer conditions on the rate at which thiocyanate is transported to the electrode surface to replenish adsorbed sulfur. The stronger effect of thiocyanate concentration for Type 316 (Figure 35) is consistent with the higher sulfur desorption rate from Mo-containing steels[6].

6.1.3 Role of alloy composition in the catalytic effect of thiocyanate

In general, the anodic dissolution rate of stainless steels is increased by thiocyanate. However, the catalytic effect of thiocyanate is different on different types of stainless steels with different compositions.

As seen in Figure 36, the dissolution rate of 316 stainless steel is much lower than the dissolution rate of 304 stainless steel in thiocyanate-free sulfuric acid, which is because of the inhibiting effect of molybdenum on the active dissolution rate of the alloy. It was suggested by Newman[64] that Mo most likely accumulates at the kink and step sites during the active dissolution, giving a significant inhibiting effect at a very low surface coverage of molybdenum. In thiocyanate-containing sulfuric acid, it is shown that the critical current density of type 304 is much higher than type 316 stainless steel at the same concentration of thiocyanate. When $[SCN^-]$=0.01g/L, the critical current density of 304 stainless steel is almost one order of magnitude higher than for type 316 stainless steel. However, the ratio of the critical current density in the presence of thiocyanate to that in the absence of thiocyanate (which defines the accelerating effect of thiocyanate) is nearly the same for types 304 and 316 stainless steel.

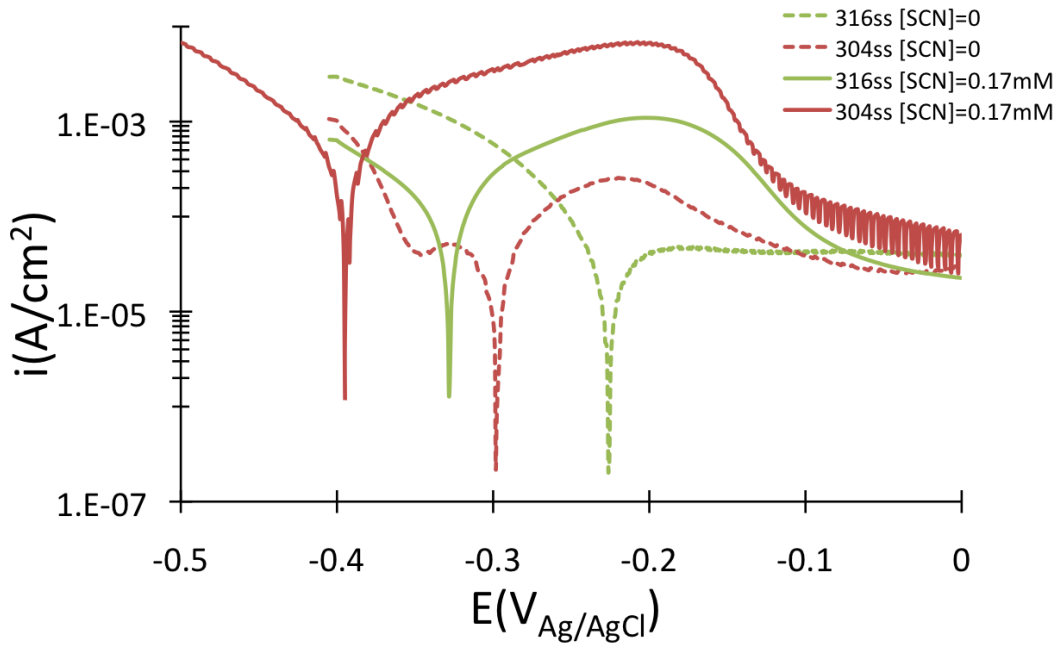

Figure 36. Potentiodynamic polarization curves of type 304ss and type 316ss in 1M sulfuric acid with different concentrations of thiocyanate; scan rate was 1mV/s.

Similar results were obtained from a set of ferritic stainless steels (type 430, 434 and 444). The compositions of types 444 and 434 stainless steel are shown in Table 6. Stainless steel with a lower molybdenum content has a higher active dissolution rate whether thiocyanate is present or not, as shown in Figure 37. However the relative accelerating effect of thiocyanate was not necessarily lowered by molybdenum, which can be more directly seen from Figure 38.

Table 6. Compositions of Type 434 and 444 stainless steel (mass percentages)

Element	Type 434	Type 444
Cr	16.44	17.58
Mo	1.037	1.9
Mn	0.496	0.35
Si	0.386	0.44
Ni	0.146	0.23
Ti	0.004	0.2
Cb	0.027	0.169
Cu	0.076	0.09
V	0.066	0.066
N	0.062	0.0114
C	0.054	0.0096
P	0.021	0.022
Al	0.0012	0.009
Sn	0.012	0.009
B	0.0001	0.006
S	0.0012	0.0005

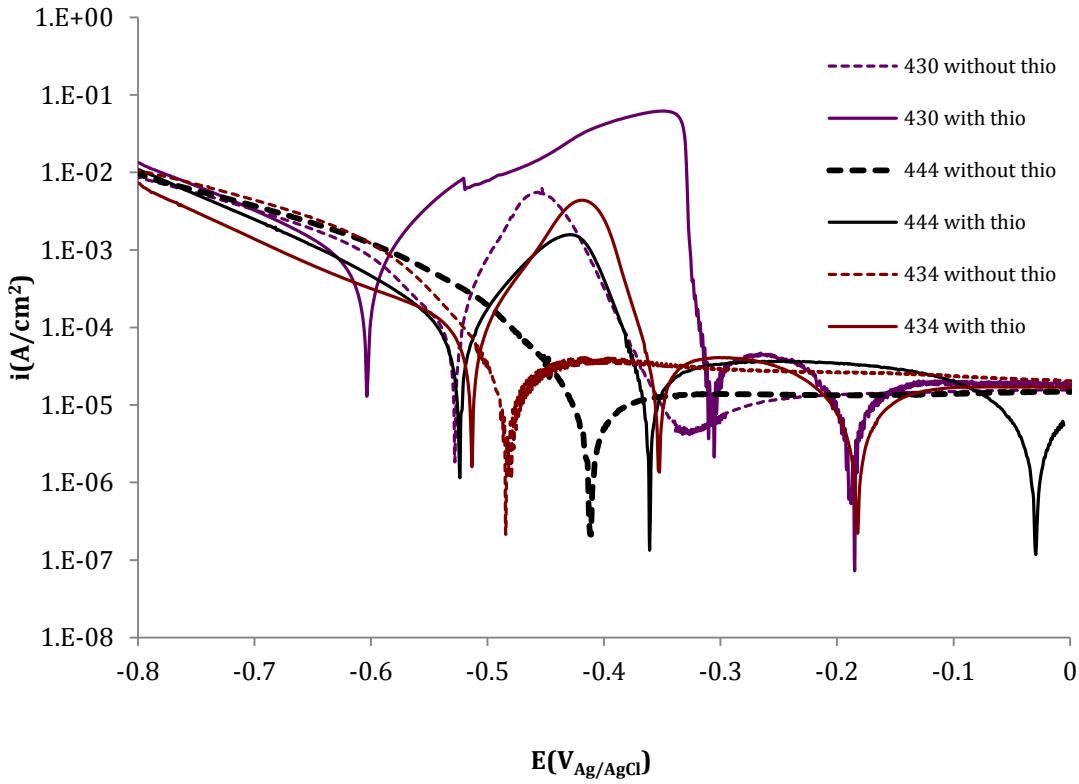

Figure 37. Potentiodynamic polarization curves of 430, 434 and 444 stainless steel in sulfuric acid with/without thiocyanate at pH2.5; scan rate was 1mV/s.

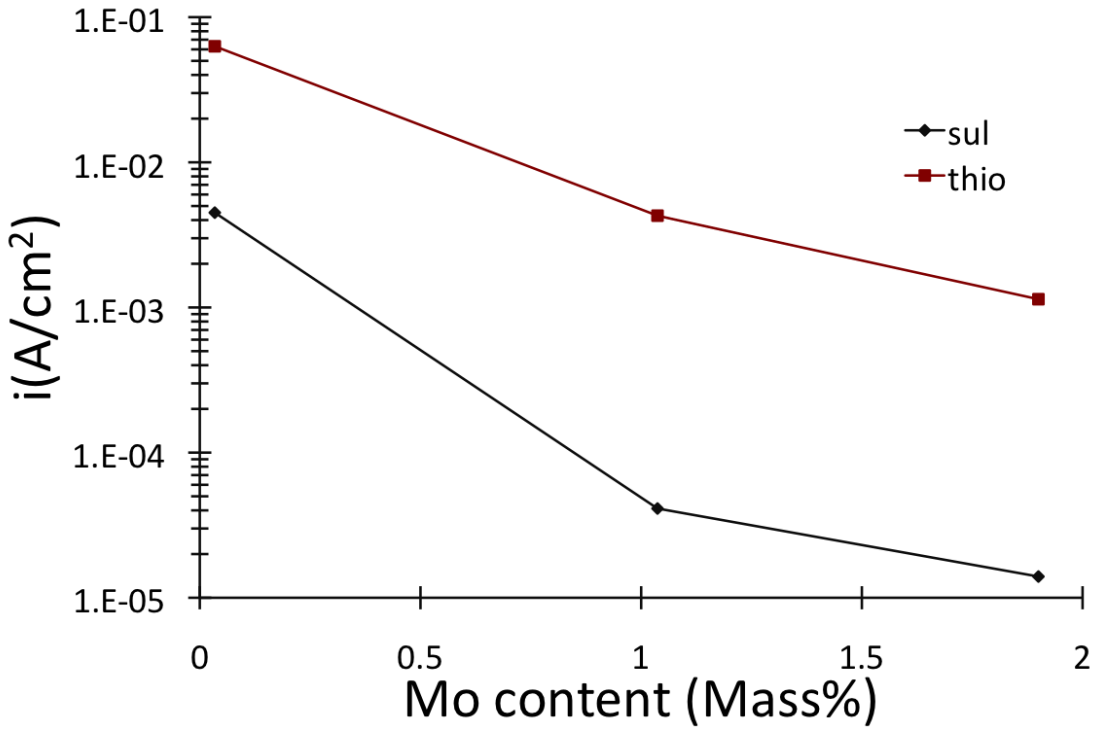

Figure 38. The relationship between the critical current density of ~17% Cr ferritic stainless steels and molybdenum content. The electrolyte was Na_2SO_4 +H_2SO_4 with/without thiocyanate at pH2.5.

It was shown by Marcus and co-workers[35] that the desorption rate of sulfur from the metal surface increases in the presence of Mo and it was also confirmed by Betts and Newman [60] that Mo would decrease the residence time of sulfur on metal surface (so a higher concentration of sulfur is needed to achieve the same catalytic effect). However, the experimental results presented here do not fully support this argument. If it were the case, one would expect a smaller relative catalytic effect of thiocyanate on steels with a higher content of Mo.

6.2 The effect of thiocyanate on type 430 stainless steel and its pure components (Fe, Cr)

6.2.1 Steady State Results

The potentiostatic polarization results for pure iron, pure chromium and Type 430 stainless steel (Figure 39) show that the presence of KSCN had little effect on the anodic dissolution rate of pure iron, increased the dissolution rate of chromium by approximately one order of magnitude, and had an even stronger effect on Type 430. The result for chromium is similar to previous work, which showed that a small concentration of H_2S accelerated anodic dissolution (and hydrogen evolution; not studied in this work) of chromium in sulfuric acid [4].

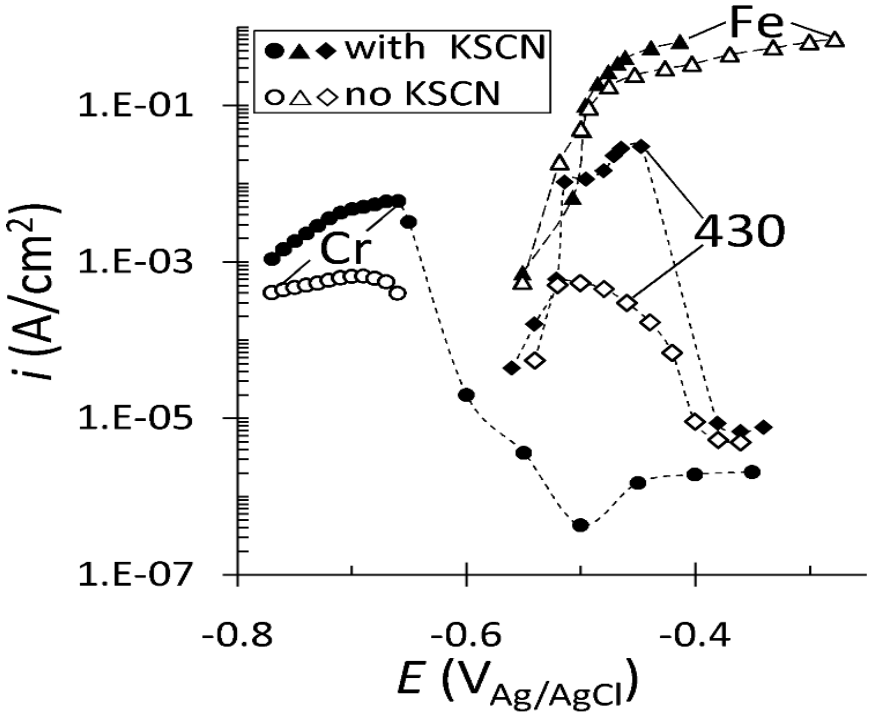

Figure 39. Potentiostatic polarization curves of pure Cr, pure Fe and Type 430 stainless steel in deaerated 1 M Na_2SO_4, 0.01 M H_2SO_4 (pH=2.5) at 25°C. Open symbols: electrolyte without KSCN; filled symbols: electrolyte containing KSCN (0.14mM).

For pure iron, there is evidence of precipitation of a salt film on the metal surface at the highest potentials: as Figure 39 shows, the current density was weakly dependent on potential at the highest potentials and current densities; for measurements on iron in the KSCN-free solution, it was also found that the ohmic resistance was larger than expected (by about 0.3 $\Omega.cm^2$) for potentials higher than -0.42 $V_{Ag/AgCl}$, after allowing for the increased solution resistance arising from dissolution of the electrode. This difference was not observed in the KSCN-containing solution, indicating a possible effect of adsorbed sulfur in preventing nucleation of the salt film. Evidence for a salt film forming on the dissolving Fe surface is even more obvious for measurements in 1M Na_2SO_4 adjusted to pH=5. Figure 40 shows the current-time curves as the potential was stepped, for Fe in Na_2SO_4 adjusted to pH=5. The sample was kept at one potential for 300s and the current was recorded during the time. Then the potential was stepped to a more positive value and the current was recorded. It can be seen (circled area in the figure) that the current dropped dramatically to a minimum from the peak, which indicated a salt film precipitating on the metal surface. Then the current recovered to a lower maximum and was controlled by diffusion, which is evidence of a steady state salt film formed on the Fe surface. This current density transient (marked by the circle) is consistent to the current transient observed when salt layer precipitated on 304 stainless steel in NaCl solution[65] and is also similar to the current transient when there was salt forming on pure Fe in 1N Na_2SO_4 during polarization[66].

To support this conclusion, the limiting current needed for saturation of $FeSO_4$ in the solution at the electrode surface was estimated using the following equations[63]:

For rotating disc electrode,

$$Sh = 0.6205\mathrm{Re}^{0.5}\, Sc^{0.33}$$
$$\mathrm{Re} = rv/\nu$$
$$Sc = \nu/D$$
$$Sh = Kr/D \qquad (14)$$

Sh, Sherwood number; *Sc*, Schmidt number; Re, Reynolds number; D, diffusivity of relevant species; ν, Kinematic viscosity of water; r, radius of metal surface; v, relevant viscosity; K, mass transfer coefficient; F, Faraday constant; ΔC, concentration difference;

Values of parameters: D=1×10^{-9} m^2/s, r=0.001m, ν=1×10^{-6} m^2/s, F=96485 C/mol,

$\Delta C=(C_{saturated})_{FeSO4}-(C_{bulk})_{FeSO4}$=1571.7mol/m^3[67].

The recessed depth of the electrode was included in the total resistance to mass transfer, d_{rec} =0.22mm with KSCN; $d_{eff}=d_{rec}+D/K$; $K_{eff}=D/d_{eff}$ =4.24×10^{-6} m/s;

This gives the limiting current density i_L =0.1286A/cm^2; $I_L = i\,A$ = 4.04mA.

It can be seen from Figure 40 that the peak current was higher than 4mA before the sharp current decrease (circled area); this is in line with the suggestion that the solution was supersaturated with $FeSO_4$ at the electrode surface before the salt film precipitated.

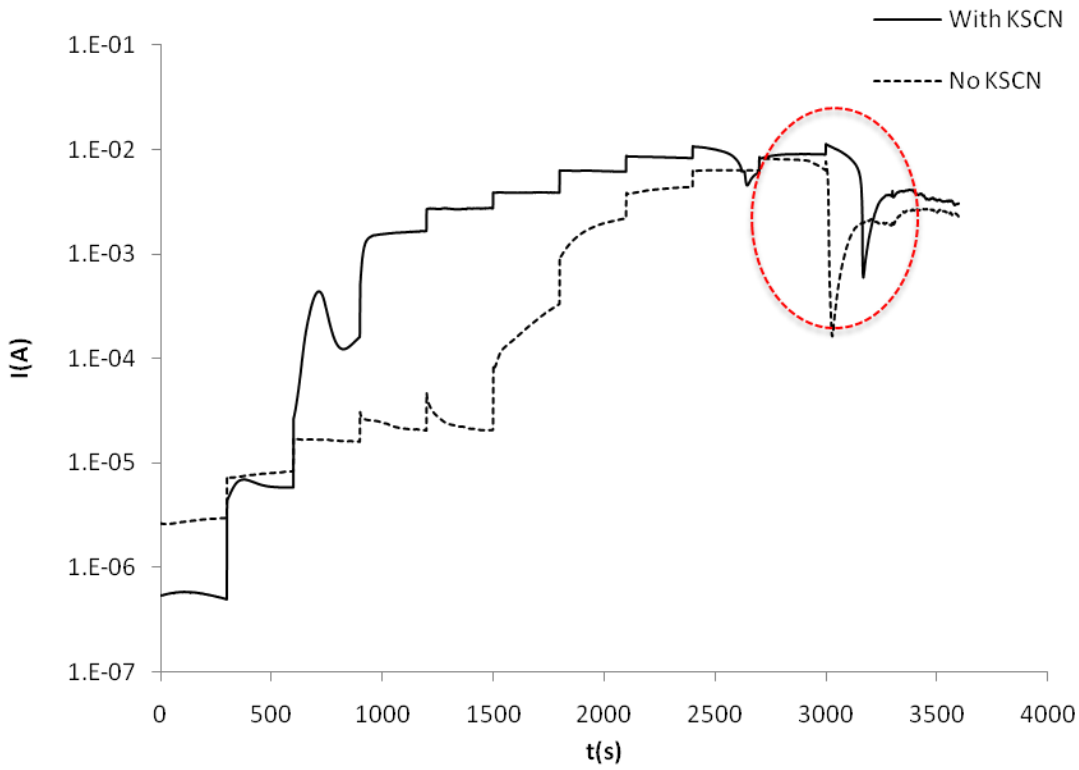

Figure 40. Current versus time at various stepped potentials, for Fe in Na_2SO_4 + H_2SO_4 with different concentrations of thiocyanate (0, 0.14mM) at pH5; E, -0.71V~0.2V (No KSCN), -0.65V~0.2V (with KSCN). Current transients showing salt film formation circled.

As has been observed for other stainless steels, the anodic behavior of even this relatively simple steel is no simple combination of the anodic response of its constituent elements: interaction between the elements affects the polarization behavior of the steel. This is even more apparent in the presence of thiocyanate: the ratio by which the anodic current density of Type 430 is higher in the presence of thiocyanate (relative to the SCN^--free case) is much larger than for either of the pure elements; it appears that thiocyanate diminishes the interaction between chromium and iron at the surface of Type 430, rendering the behavior of the steel more like that of iron.

The dissolution and passivation of Fe-Cr alloys in KSCN-free dilute sulfuric acid have been well studied[68][52][48][69][70]. Prominent features are a slight shift of polarization curves towards negative potentials with increasing bulk chromium contents, and progressive changes in passivation behavior for alloy contents up to 17 at.% chromium (which level corresponds to the second-neighbor Cr percolation limit[48]). Primary passivation in Fe-Cr alloys was ascribed to suppression of dissolution at ledges by formation of Cr-O-Cr networks[68][70]. In this work, the large effect of thiocyanate on dissolution of Type 430 stainless steel was observed in the active loop *before* the onset of passivation. However, as demonstrated by Keddam et al. [37](and confirmed in this work, as discussed below) the electrode impedance in this potential range shows evidence of initial stages of passivation. Hence the effect of thiocyanate may simply be to increase the dissolution rate of chromium (making the dissolution of iron less specific[48]) and counteracting the formation of passivating Cr-O-Cr networks. A difference in the appearance of the etched surface (as discussed in the next section), for dissolution of Type 430 stainless steel in KSCN-containing and KSCN-free solutions, is in line with suppression of passivation of ledges by KSCN.

6.2.2 Morphology of corroded surface

Etched electrodes surface were characterized using SEM and AFM to investigate the effect of thiocyanate on the surface morphology. Electrodes were held at the same potential but for different times to ensure that the anodic charge passed was the same for the solutions with and without thiocyanate. Figure 41 gives one example of the current and charge passed through the surface of an Fe electrode.

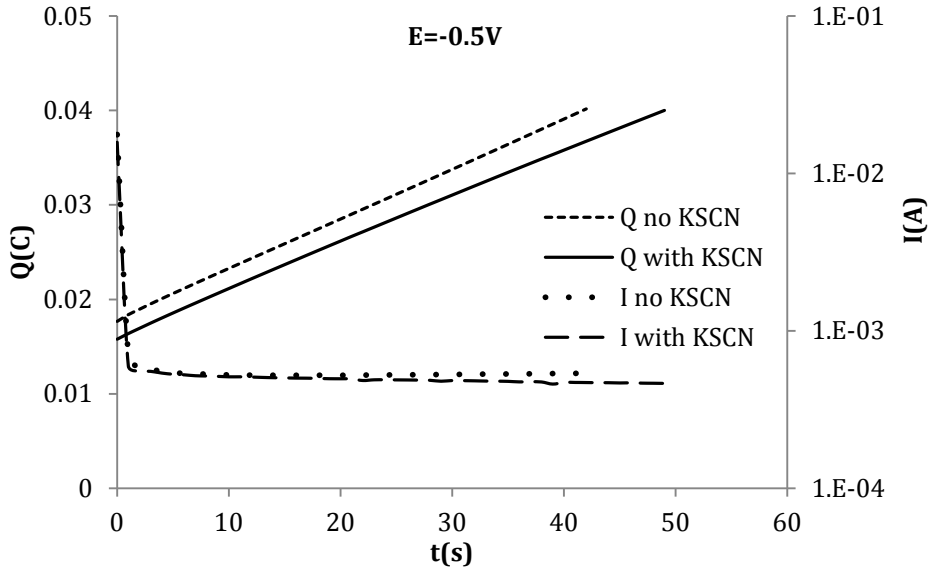

Figure 41. Total charge and current passed through Fe surface in Na_2SO_4 solution adjusted to pH2.5, with/without KSCN, E=-0.5V.

6.2.2.1 Scanning Electron Microscopy images

For pure iron, the lack of a strong effect of thiocyanate on the current density is paralleled by the absence of any large change in the appearance of the corroded surface (Figure 42). Crystallographic etching, characteristic of slower dissolution on terraces than at edges, was observed in both cases; the grain boundary etching was more obvious for the thiocyanate-free solution.

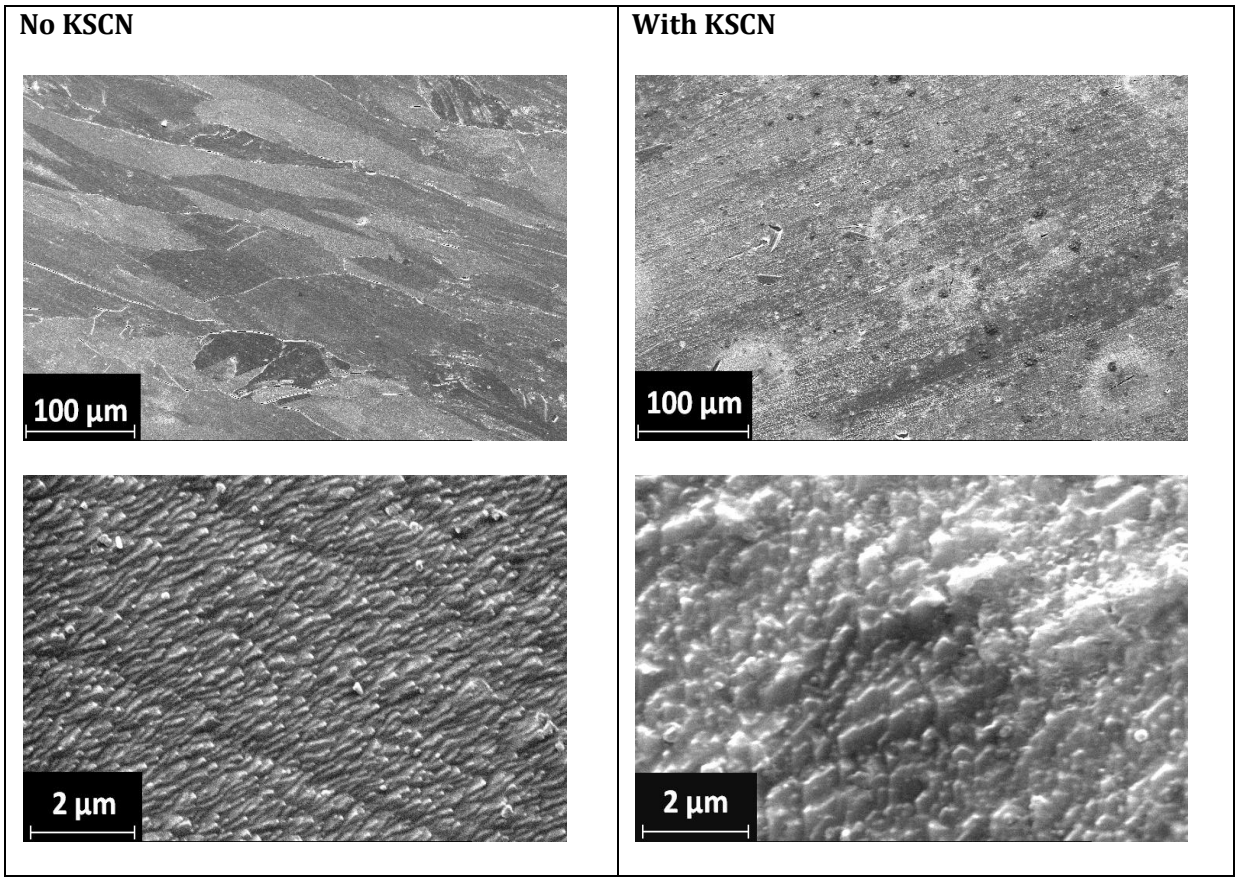

Figure 42. Fe: etched electrode surfaces after potentiostatic polarization in deaerated 1 M Na_2SO_4, 0.01 M H_2SO_4 (pH=2.5) at 25°C, for solutions without (left) and with (right) KSCN ($E=-0.5V_{Ag/AgCl}$; anodic charge passed 1.3 C/cm^2). Scanning electron micrographs (secondary electron images), at lower magnification (upper images) and higher magnification (lower images).

For chromium, stronger grain boundary etching was also observed for the electrode after dissolution in the solution without thiocyanate (Figure 43); crystallographic etching was more evident for the thiocyanate-containing solution. This may reflect an effect of adsorbed sulfur similar to that noted by Ando et al. [3] for dissolution of sulfur-modified nickel; in that case, *in situ* atomic force microscopy indicated that dissolution at the step edges involved movement of

adsorbed sulfur atoms from the upper (receding) terrace to the lower terrace as the step edge receded.

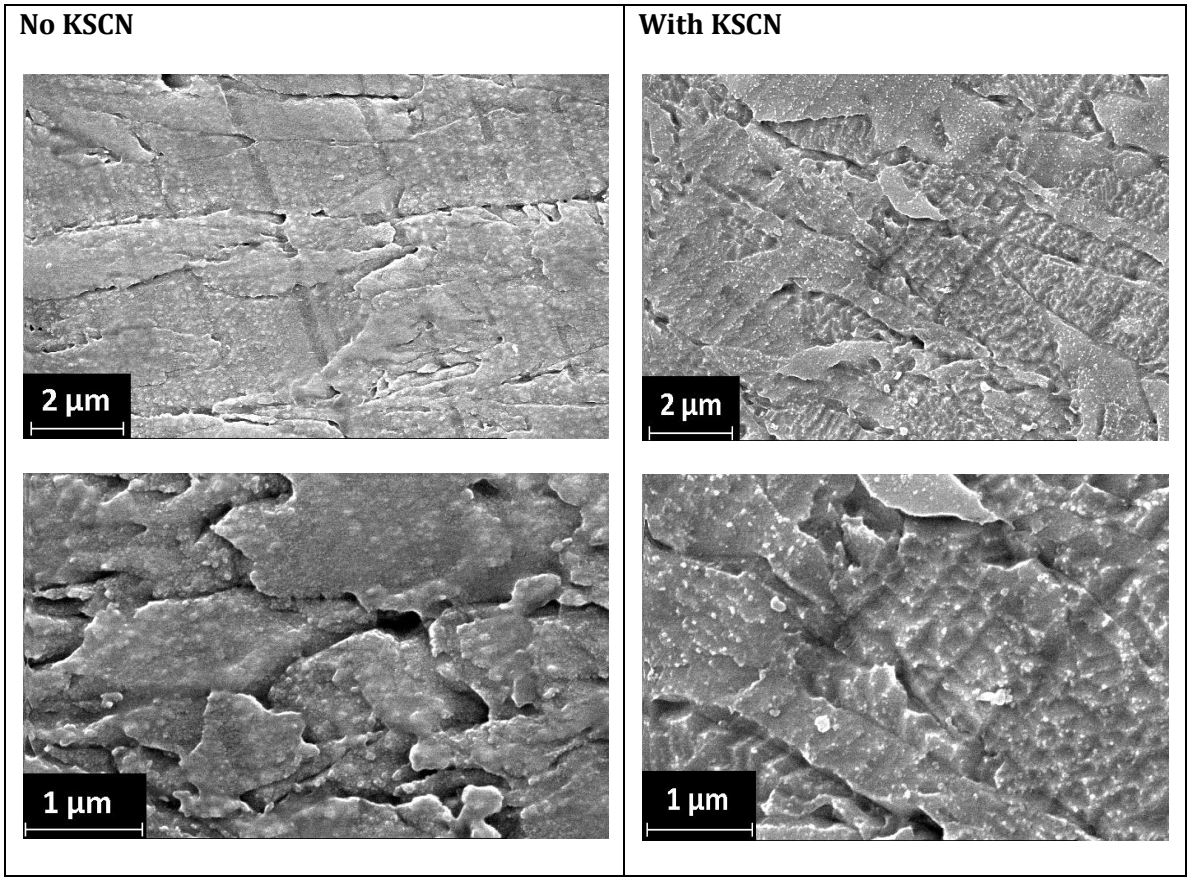

Figure 43. Cr: etched electrode surfaces after potentiostatic polarization in deaerated 1 M Na_2SO_4, 0.01 M H_2SO_4 (pH=2.5) at 25°C, for solutions without (left) and with (right) KSCN ($E=-0.75V_{Ag/AgCl}$; anodic charge passed 0.33 C/cm^2). Scanning electron micrographs (secondary electron images), at lower magnification (upper images) and higher magnification (lower images).

This difference in etching response was much more evident for the Type 430 stainless steel (Figure 44), with very strong etching of crystal facets in the thiocyanate-containing solution, but none in the thiocyanate-free solution. (The particulate debris on the etched surfaces was identified - based on energy dispersive X-ray microanalysis - as carbides, probably $Cr_{17}Fe_6C_6$)

Note that the anodic charge passed for the Type 430 electrodes (shown in Figure 44) was much larger than for iron and chromium (Figures 42 and 43); the charge is that passed in the thiocyanate-containing solution during the holding time of 3600 s which was employed before all impedance measurements on Type 430 (see Table 7). The potential at which the Type 430 electrodes of Figure 44 were held (-0.5 $V_{Ag/AgCl}$) was the lowest potential at which a large difference in dissolution behavior (with and without KSCN) was found (see Figure 39). As noted in the previous section, the large difference in the etching response is consistent with loss of Cr-O-Cr passivation of ledges in the KSCN-containing solution.

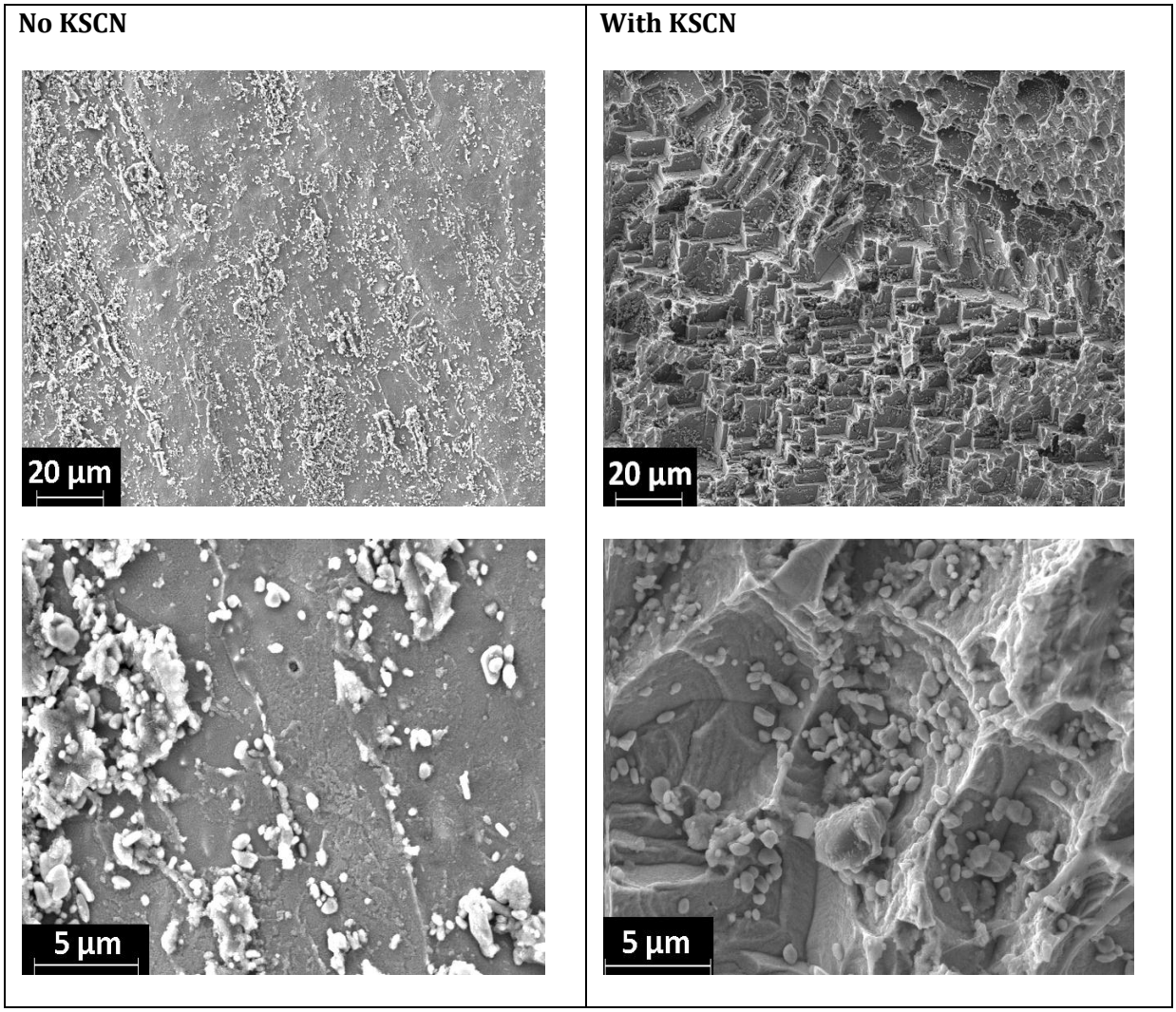

Figure 44. Type 430 stainless steel: etched electrode surfaces after potentiostatic polarization in deaerated 1 M Na_2SO_4, 0.01 M H_2SO_4 (pH=2.5) at 25°C, for solutions without (left) and with (right) KSCN (E=-0.5$V_{Ag/AgCl}$; anodic charge passed 31 C/cm^2 [with KSCN] and 43 C/cm^2 [no KSCN]). Scanning electron micrographs (secondary electron images), at lower magnification (upper images) and higher magnification (lower images).

6.2.2.2. Atomic Force Microscopy images

AFM images and height profiles of etched Fe surfaces after dissolution in pH=2.5 sulfate solutions with/without KSCN are shown in Figure 45. From the height profile, the depth of features on Fe corroded with and without KSCN are very similar (20nm~40nm). The surface finish (presence of scratches) did affect the AFM measurement results.

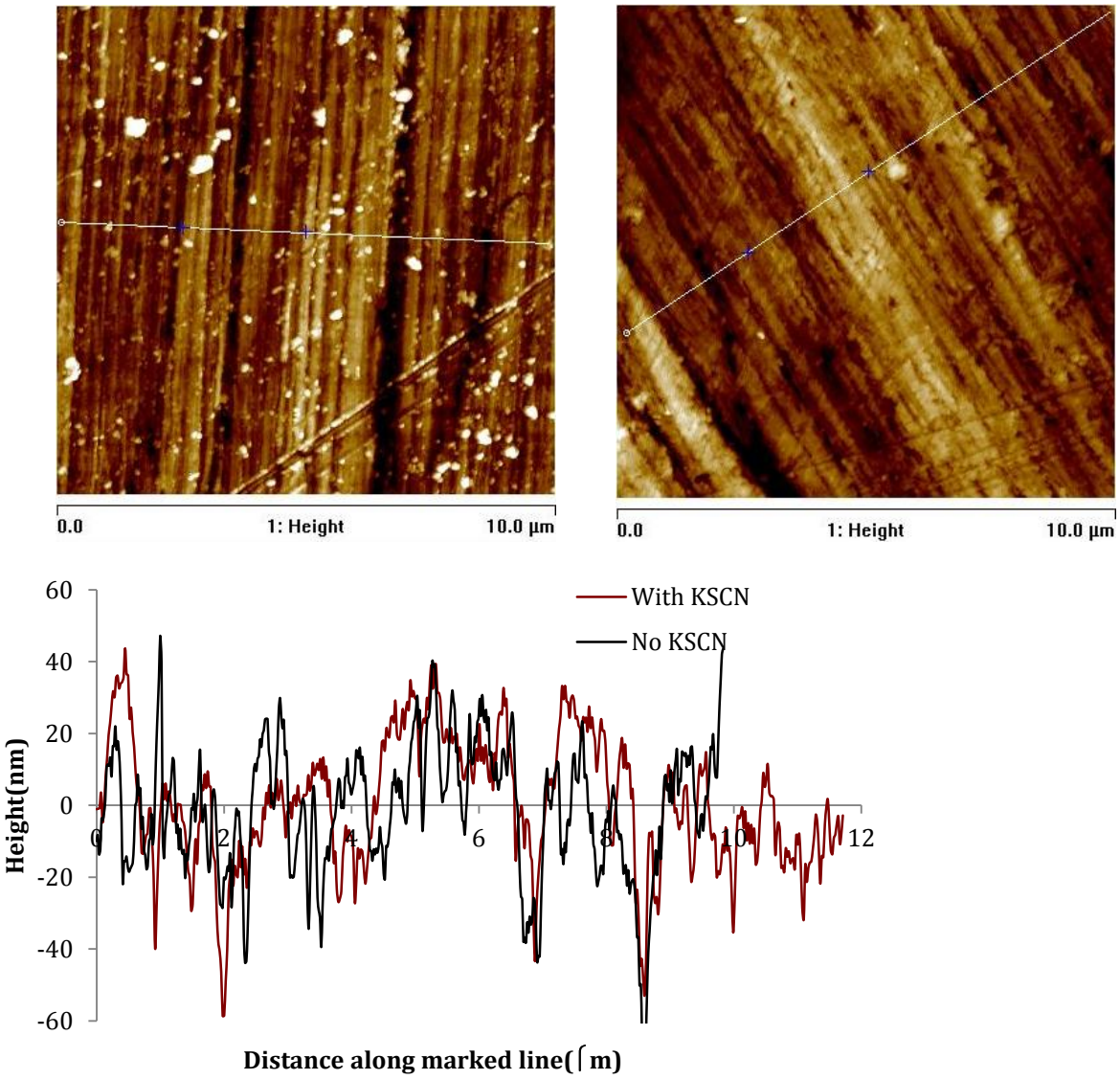

Figure 45. AFM images and height profile of corroded Fe surface (1.3C/cm² charge passed) in 1M Na_2SO_4+H_2SO_4 (pH=2.5) with 0.14mM (right side)/without (left) KSCN.

Similar measurements for Cr corroded in *p*H=2.5 sulfate solution with/without thiocyanate (0.33 C/cm^2 charge passed) are shown in Figure 46. From the height profile it can be seen that there are many small bumps on the surface and the size of the bumps is in the range 20nm to 30nm when thiocyanate is absent in the solution. When thiocyanate is present the surface was mainly etched along the ledges and the depth of the ledges is around 40nm-50nm.

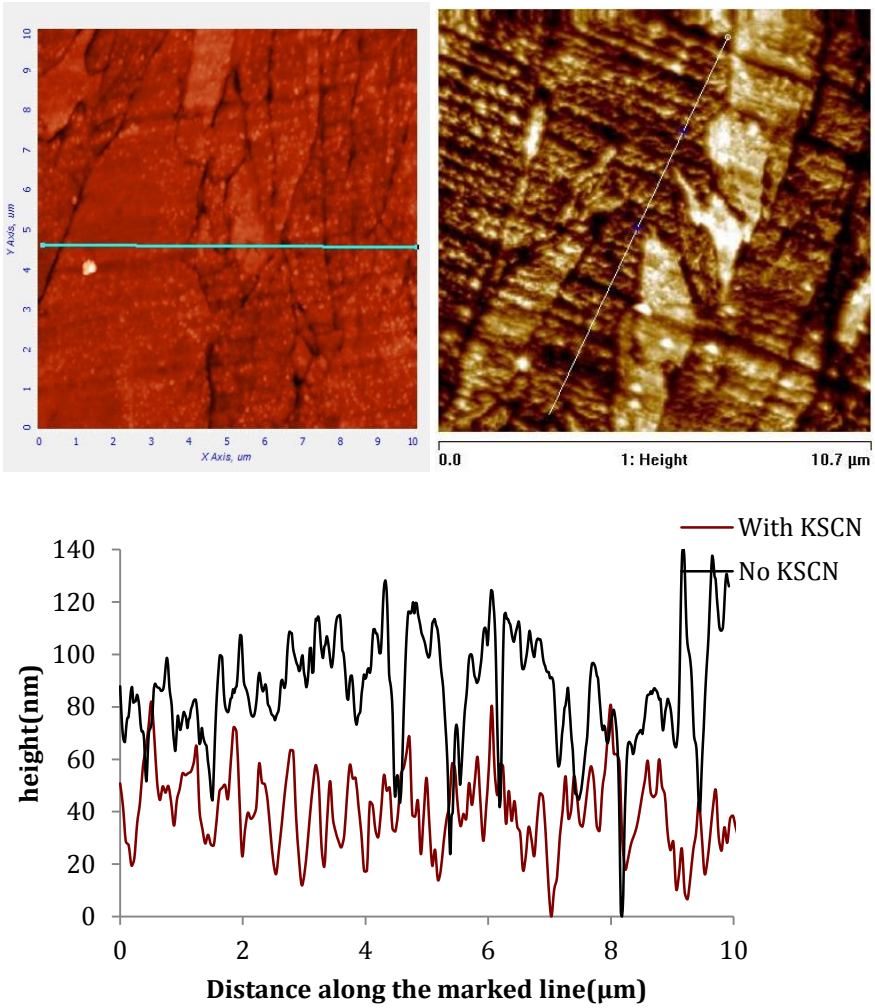

Figure 46. AFM images and height profile of corroded Cr surface (0.33 C/cm^2 charge passed) in 1M Na_2SO_4+H_2SO_4 (pH=2.5) with 0.14mM (right side)/without (left) KSCN.

AFM images of corroded Type 430ss surface (0.41 C/cm^2 charge passed) and height profile are shown in Figure 47. It can be seen the depth of etched surface is similar to each

other in sulfuric acid with/without KSCN. The surface roughness is much smaller than that shown in Figure 44, simply because much less charge was passed through the surface for these samples.

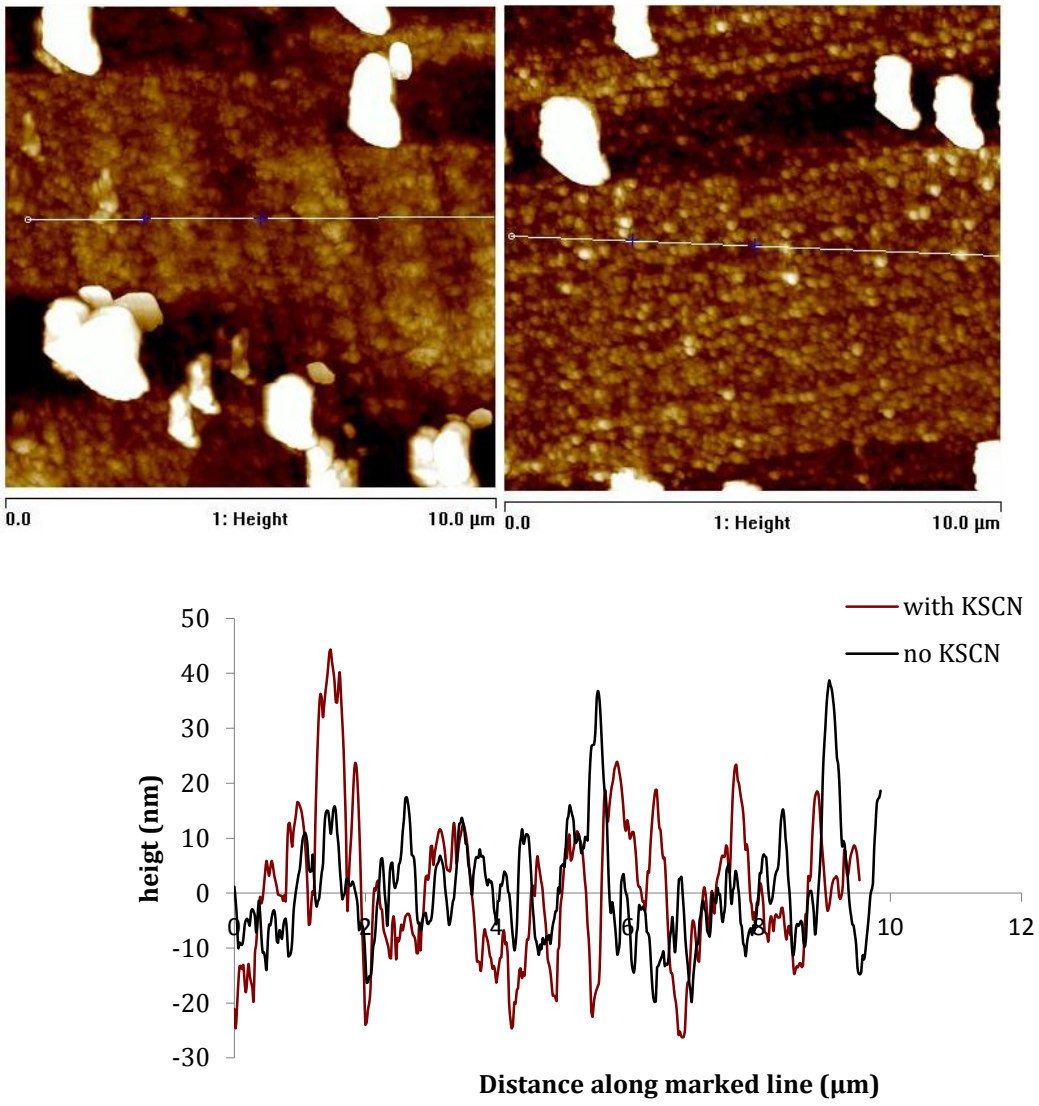

Figure 47. AFM images and height profile of corroded 430 stainless steel surface (0.41 C/cm² charge passed) in 1M Na_2SO_4+H_2SO_4 (pH=2.5) with 0.14mM (right side)/without (left) KSCN.

6.2.3 Electrode Impedance

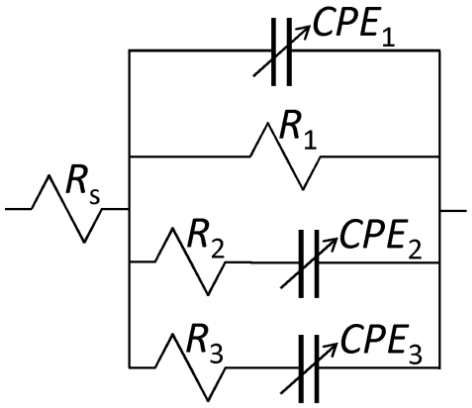

Figure 48. Equivalent circuit used when fitting impedance results. "CPE" indicates constant-phase elements, which could be either inductive or capacitive in nature.

The impedance results were fitted to the equivalent circuit shown in Figure 48, which is similar to that used by Dobbelaar and de Wit to fit the impedance behavior of pure chromium[41]. As this figure indicates, the equivalent circuit contained the solution resistance, interfacial (double layer) capacitance, a charge transfer resistance, and up to two series combinations of a resistance and a constant-phase element (which could be capacitive or inductive in nature). In general, R_2 and CPE_2 were associated with pseudo-inductive behavior (negative value of α) and R_3 and CPE_3 with pseudo-capacitive behavior (positive value of α; the single exception to this is Fe in KSCN-free solution at -0.5 $V_{Ag/AgCl}$, see the first entry in the table of results, Table 7). The impedance results (data points) and fitted behavior (lines) are shown in Figures 49-51, for the three materials, and fitted values are summarized in Table 7 (where an entry in the table is blank, that circuit element was not required to fit the data). Selected

frequencies are noted on the impedance curves; these are at the top (or bottom) of semi-circles corresponding to capacitive (or inductive) behavior.

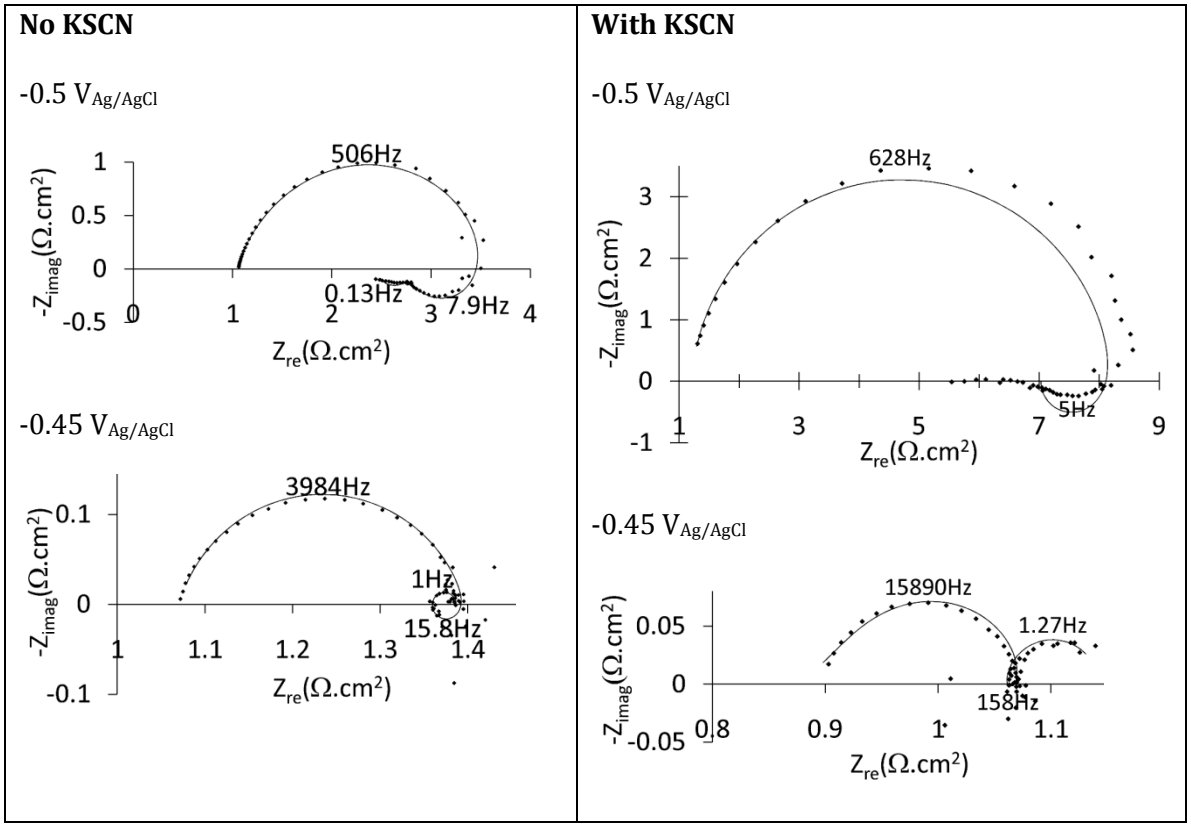

Figure 49. Fe: impedance results in deaerated 1 M Na_2SO_4, 0.01 M H_2SO_4 (pH=2.5) at 25°C, for solutions without (left) and with (right) KSCN; potentials as indicated on figures. Symbols: measured data; lines: fitted equivalent circuits.

In a few cases (examples are the results for Fe in solution with KSCN at -0.5 $V_{Ag/AgCl}$, Figure 49, and for Cr in solution with KSCN at -0.67 $V_{Ag/AgCl}$, Figure 50) the impedance results showed some evidence that the electrode surface had not fully reached steady state before the impedance was measured, despite extended holding times; changes in current density with time (upon applying potential steps) did show large differences in the time required to reach steady state (see Figure 52 for examples). However, the few instances of failure to reach steady

state do not appear to affect the overall trends of the electrode impedance. (Holding times before impedance measurements were started are noted in Table 7.)

It is worth noting that the results for Fe in the KSCN-solution are similar to those reported by Keddam et al[37][38]. For pure iron, the small difference in potentiostatic behavior (in solutions with and without KSCN) is paralleled by little difference in impedance (Figure 49). For the lower potential, the impedance is somewhat larger for the KSCN-containing solution (echoing the lower current density); in both cases pseudo-inductive behavior shows the presence of a catalytic intermediate reaction product on the electrode surface, whereas pseudo-capacitive behavior reflects early stages of passivation at the higher potential[37][38], again for both solutions.

For pure chromium (Figure 50), pseudo-capacitive behavior was evident at all three potentials studied, including the negative-resistance region beyond the passivation potential (E=-0.67 $V_{Ag/AgCl}$); in addition, pseudo-inductive behavior was observed at the more negative potentials. While the impedance is much lower in the presence of thiocyanate, the shapes of the impedance plots are similar, reflecting similar reaction steps. It hence appears that the presence of thiocyanate does not have any specific effect on the dissolution mechanism, but simply increases the rates of the dissolution steps. The frequencies noted on the impedance plots do show the longer time constants associated with the processes on the chromium electrode in the absence of thiocyanate, as also evident in the current-time examples in Figure 52.

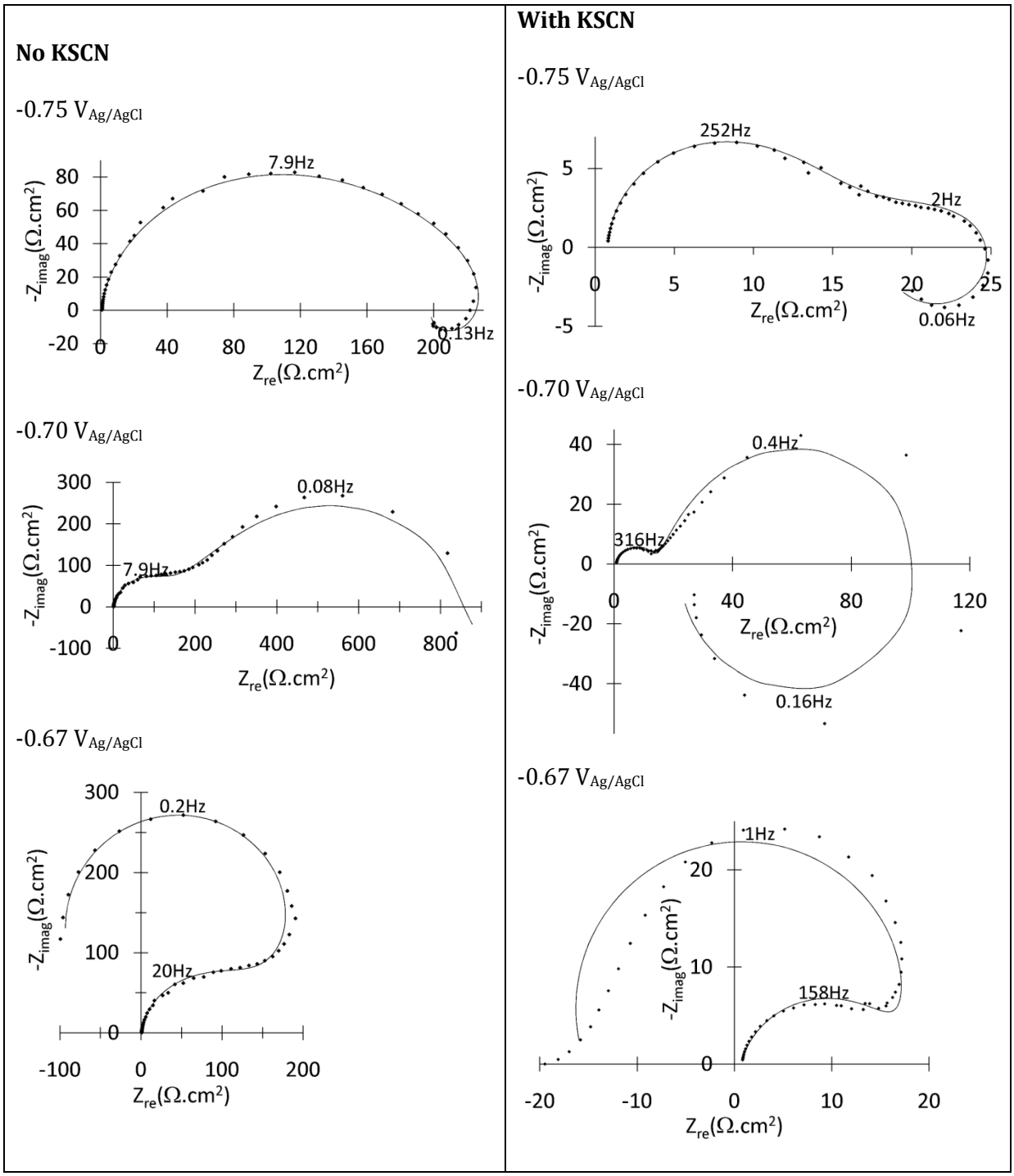

Figure 50. Cr: impedance results in deaerated 1 M Na_2SO_4, 0.01 M H_2SO_4 (pH=2.5) at 25°C, for solutions without (left) and with (right) KSCN; potentials as indicated on figures. Symbols: measured data; lines: fitted equivalent circuits.

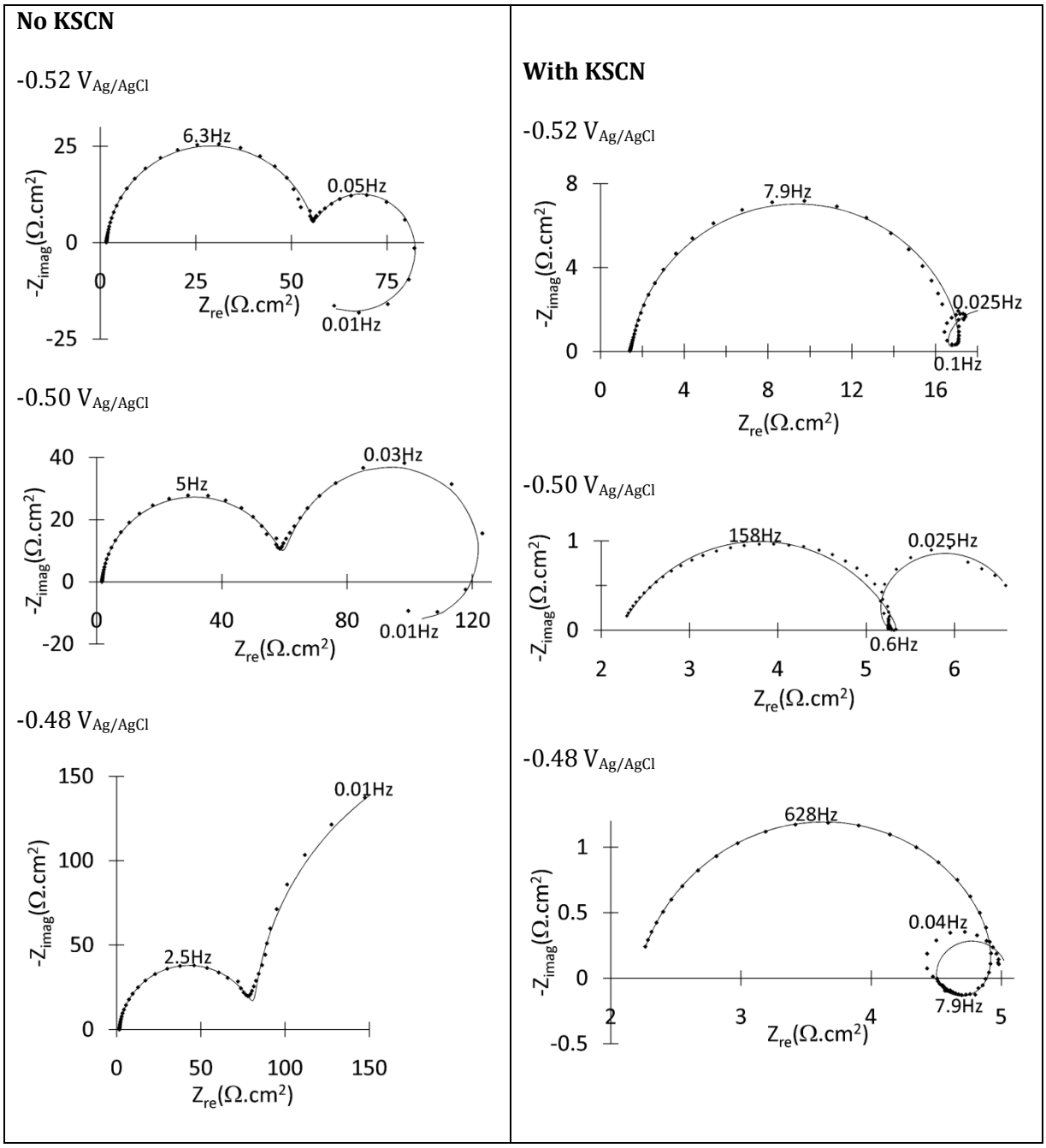

Figure 51. Type 430: impedance results in deaerated 1 M Na_2SO_4, 0.01 M H_2SO_4 (pH=2.5) at 25°C, for solutions without (left) and with (right) KSCN; potentials as indicated on figures. Symbols: measured data; lines: fitted equivalent circuits.

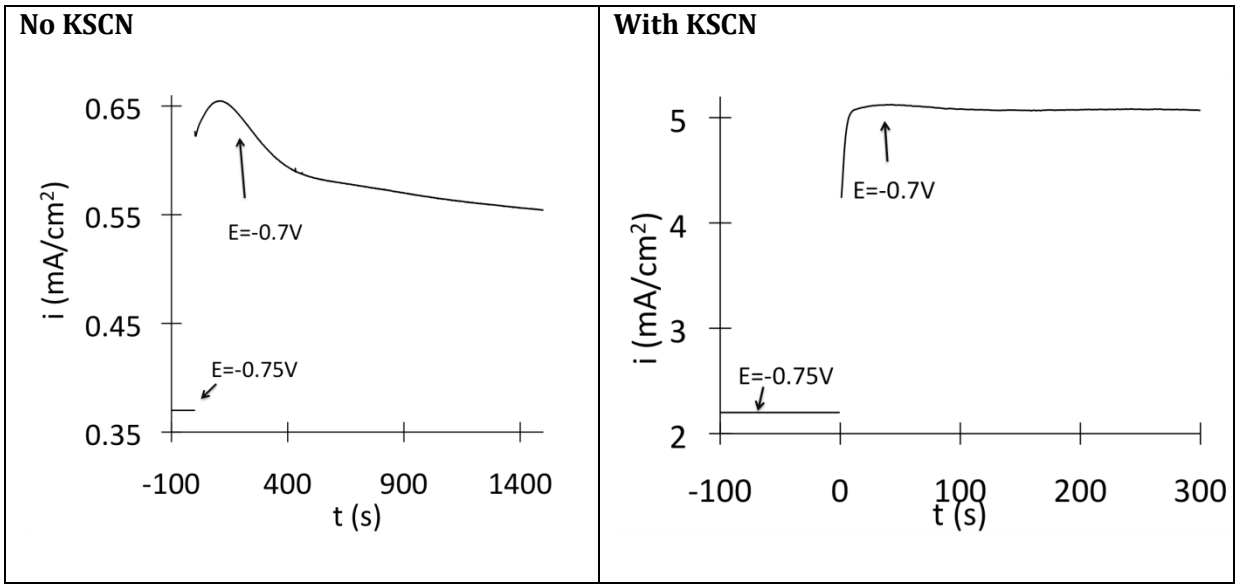

Figure 52. Current-time curves for chromium in 1 M Na_2SO_4, 0.01 M H_2SO_4 (pH=2.5) at 25°C, as examples of differences in the time required to reach steady state; result for solution without KSCN at left, and with KSCN at right. The potential was stepped from -0.75 $V_{Ag/AgCl}$ to -0.70 $V_{Ag/AgCl}$ at time zero (current densities before the potential step were 0.37 mA/cm² for the solution without KSCN, and 2.2 mA/cm² for the solution with KSCN). (Time and current density scales are different.)

In the case of Type 430 (Figure 51), the same circuit elements (reflecting both pseudo-capacitive and pseudo-inductive behavior) were found at the two more negative potentials considered (with and without thiocyanate), with the much lower impedance in the presence of thiocyanate evident. However, at the most positive potential, strong pseudo-capacitive behavior (indicative of the start of passivation) was evident for the KSCN-free solution, whereas in the KSCN-containing solution only weak pseudo-capacitive behavior was found, and pseudo-inductive behavior persisted. This does suggest a change in the dissolution mechanism, in contrast with what was found for the pure metals. It is also noticeable in Figure 51 that the time constant of the part of the circuit associated with pseudo-inductive behavior was

significantly larger for Type 430 electrodes in the KSCN-free solution (for the two potentials where pseudo-inductive behavior is observed in both the KSCN-free and KSCN-containing solutions). That is, the increase in current density associated with formation of a presumed catalytic intermediate product would take a longer time to be observed in the KSCN-free solution

Table 7. Fitted equivalent circuit element values of impedance result for Fe, Cr and type 430 stainless steel in sulfuric acid with/without thiocyanate at pH=2.5.

Matl	KSCN	E	t_{hold}	R_s	R_1	CPE_1		R_2	CPE_2		R_3	CPE_3	
		($V_{Ag/AgCl}$)	(s)	($\Omega.cm^2$)	($\Omega.cm^2$)	A ($F/cm^2s^{1-\alpha}$)	α (-)	($\Omega.cm^2$)	A ($F/cm^2s^{1-\alpha}$)	α (-)	($\Omega.cm^2$)	A ($F/cm^2s^{1-\alpha}$)	α (-)
Fe	Absent	-0.50	100	1.04	2.74	5.8E-04	0.798	8.21	8.5E-02	-0.948	4.51	5.5E+00	-0.777
		-0.45	100	1.07	0.37	7.3E-04	0.821	2.24	4.3E+01	-1	2.76	4.1E-02	1
	Present	-0.50	100	1.21	7.31	5.0E-05	0.943	34.0	1.7E+00	-1			
		-0.45	100	0.90	0.28	1.8E-04	0.9	1.81	5.6E+02	-1	0.46	2.2E-01	0.95
Cr	Absent	-0.75	1500	0.83	265	6.6E-05	0.961	835	1.3E-03	-1	127	4.1E-04	0.486
		-0.70	1500	0.80		8.2E-05	0.937	77.0	2.3E-04	-1	130	3.2E-03	0.507
		-0.67	1200	0.82	-11.8	6.9E-05	0.945				10.7	8.5E-01	0.285
	Present	-0.75	100	0.83	33.7	3.3E-05	1	43.0	8.4E-03	-1	11.0	1.2E-02	0.268
		-0.70	100	0.68		1.2E-04	0.873	21.5	1.6E-02	-1	13.8	1.1E-02	0.735
		-0.67	100	0.65	-15.9	1.7E-04	0.843				8.22	2.9E-02	0.782
430ss	Absent	-0.52	3600	1.55	125	5.2E-04	0.943	75.9	8.7E-04	-1	98.0	3.6E-02	1
		-0.50	3600	1.65		6.9E-04	0.951	86.5	1.2E-03	-1	59.0	6.3E-02	0.975
		-0.48	3600	1.61	429	8.3E-04	0.947				102	4.5E-02	1
	Present	-0.52	3600	1.42	20.7	1.7E-03	0.919	232	5.2E-03	-1	69.9	1.4E-01	1
		-0.50	3600	2.21		1.9E-03	0.715	4.54	1.2E-01	-1	3.16	8.7E-01	1
		-0.48	3600	2.20	4.03	2.4E-04	0.876	9.78	1.4E+00	-0.65	10.8	3.0E-01	1

Direct comparison of the fitted circuit values in Table 7 is complicated by frequency dispersion (that is, the presence of constant phase elements with values of $|\alpha|$ significantly smaller than 1). As one form of comparison, Figure 53 gives the effective capacitance of CPE_3 (calculated with equation 9) and the total real part of the resistance in that branch of the circuit (that is, the sum of R_3 and the real part of CPE_3, calculated with equation 8), for those cases where pseudo-capacitive behavior was observed. (In each case, the frequency used in the

calculation was that at the maximum of the semi-circle associated with pseudo-capacitive behavior.) The reason for focusing on the pseudo-capacitive behavior is that this is associated with the early stages of passivation; given that one proposed mechanism of the effect of thiocyanate is that it impedes passivation, an effect of thiocyanate on this pseudo-capacitive behavior is expected. As the results in Figure 53 show, with a single exception (Cr at the highest potential tested, -0.67 $V_{Ag/AgCl}$) the same trend was found, namely that in the presence of thiocyanate the series resistance in the pseudo-capacitive leg was smaller and the pseudo-capacitance was larger (with the result that in general – except for Cr – the frequency at the apex of the pseudo-capacitive semicircle was similar in solutions with and without thiocyanate at a given potential, as inspection of Figures 49 and 51 also shows). The implication of the larger pseudo-capacitance is that, upon an increase in potential, the transient charge associated with growth of precursors of the passive film would be larger in the presence of thiocyanate. This is qualitatively in agreement with the suggested effect of thiocyanate, namely that it suppresses passivation: that is, more dissolution occurs before partial passivation of the electrode surface is achieved, which is what was shown previously for dissolution of nickel - see Figure 54[71].

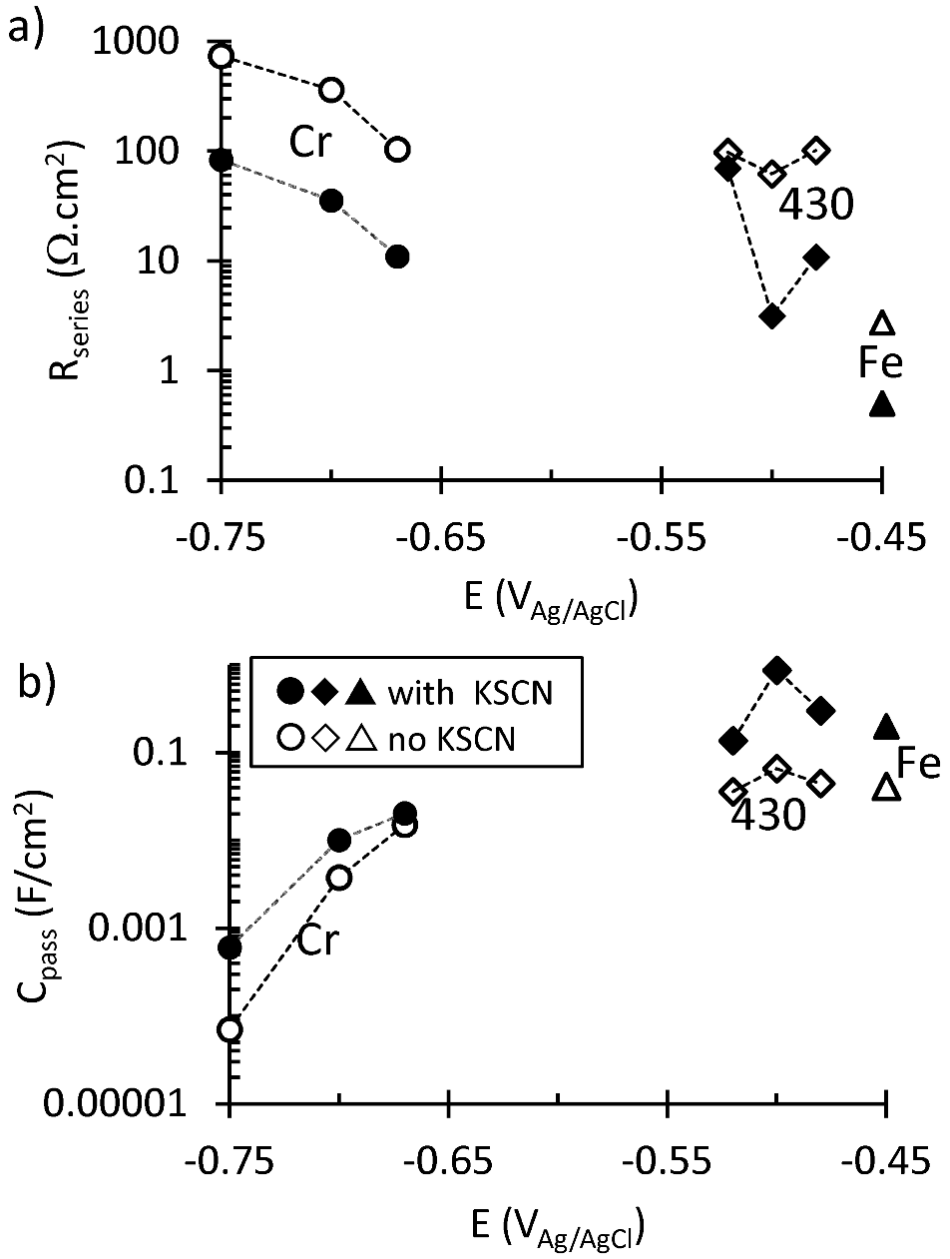

Figure 53. Fitted impedance values associated with pseudo-capacitive part of circuit (R_3-CPE_3 combination), for Fe, Cr and Type 430. The effective series resistance (a) and the effective pseudo-capacitance (b) are shown, both evaluated at the frequency corresponding to the apex of the semicircle associated with pseudo-capacitive behavior.

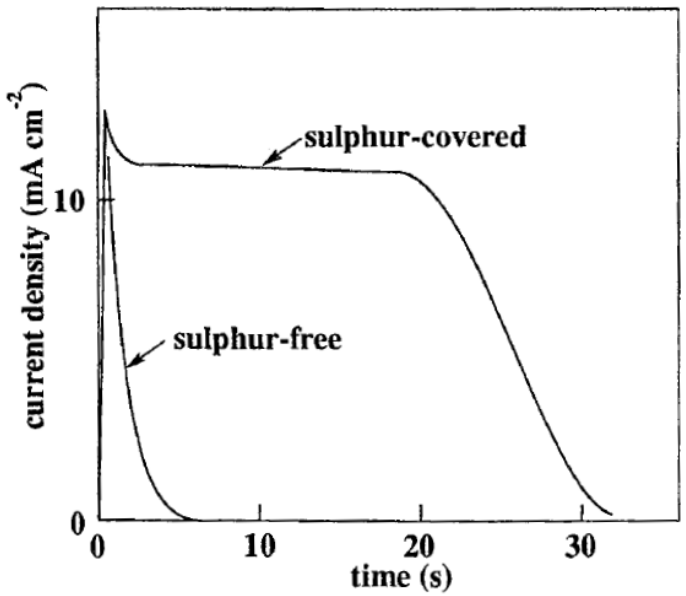

Figure 54. The effect of adsorbed sulfur on the passivation of Ni in 0.05M sulfuric acid; E=0.54V$_{SHE}$[71].

6.3 The effect of thiocyanate on type 304 stainless steel and its pure components (Fe, Cr, Ni)

In the previous section the effect of thiocyanate on the dissolution of ferritic Type 430 stainless steel in acidified (*p*H=2.5) sodium sulfate was reported. For service in dilute sulfuric acid, nickel-containing stainless steels are of greater practical importance than ferritic steels, hence this work was extended to Type 304 stainless steel in 1M SO_4^{2-} solutions, at both *p*H=2.5 (for comparison with the measurements on Type 430 stainless steel) and at the practically more relevant *p*H=0.

The proposed effect of thiocyanate on 430 stainless steel is that dissolution of chromium from the surface is accelerated, which hampers the early stages of passivation and hence increases the critical current density. This work sought to test whether this mechanism also holds for 304 stainless steel and whether accelerated dissolution of chromium would be sufficient to explain the effect of thiocyanate on active dissolution of Type 304 stainless steel.

6.3.1 Steady State Results

Potentiostatic polarization results for *p*H=2.5 show that, while dissolution of pure nickel is accelerated in the presence of thiocyanate at this *p*H, there is little effect on the active dissolution of Type 304 stainless steel (Figure 55). In contrast, as shown earlier (Figure 39) dissolution of Type 430 stainless steel is strong accelerated by the thiocyanate at *p*H=2.5. Clearly, the presence of nickel diminishes the active dissolution rate of the austenitic (Type 304) stainless steel, whether thiocyanate is present or not. Although there is up to 2% more Cr in 304 stainless steel than 430 stainless steel, the critical current density of the steel (in 1 M sulfuric acid) is not affected strongly by the content of Cr when the Cr content in the steel is above 10%[51].

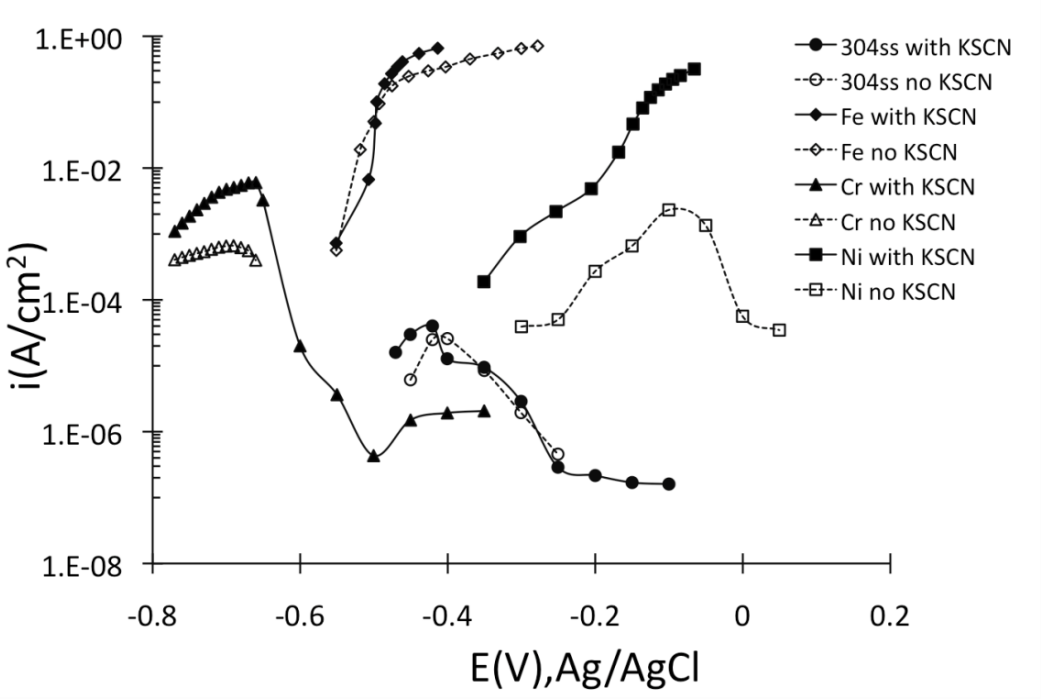

Figure 55. Potentiostatic polarization curves of pure Cr, pure Fe, pure Ni and Type 304 stainless steel in deaerated 1 M Na_2SO_4, 0.01 M H_2SO_4 (pH=2.5) at 25°C. Open symbols: electrolyte without KSCN; filled symbols: electrolyte containing KSCN (0.14mM).

However, this is not an effect of nickel alone; it arises from the joint action of nickel and chromium, as shown by the results for *p*H=0 (Figure 56). At *p*H=0, the active dissolution rate (polarization behavior) of *nickel* in the presence of thiocyanate is very similar to that at *p*H=2.5, yet unlike at *p*H=2.5, at *p*H=0 the presence of thiocyanate strongly accelerates the dissolution rate of *Type 304 stainless steel* (giving an increase in critical current density of more than two orders of magnitude). The important difference between the solutions with these two *p*H values appears to be in the proximity of the passivation potential of pure chromium to the active loop of the steel: at *p*H=0, the difference between the passivation potential of pure chromium and measurable start of the active loop of Type 304 stainless steel is smaller than at *p*H=2.5. It is worth noting that the effect of *p*H on the passive potential range of chromium, as found in this

work, is similar to what was obtained by Dražić *et al.*,[72] namely that the passivation potential is more positive at the lower *p*H.

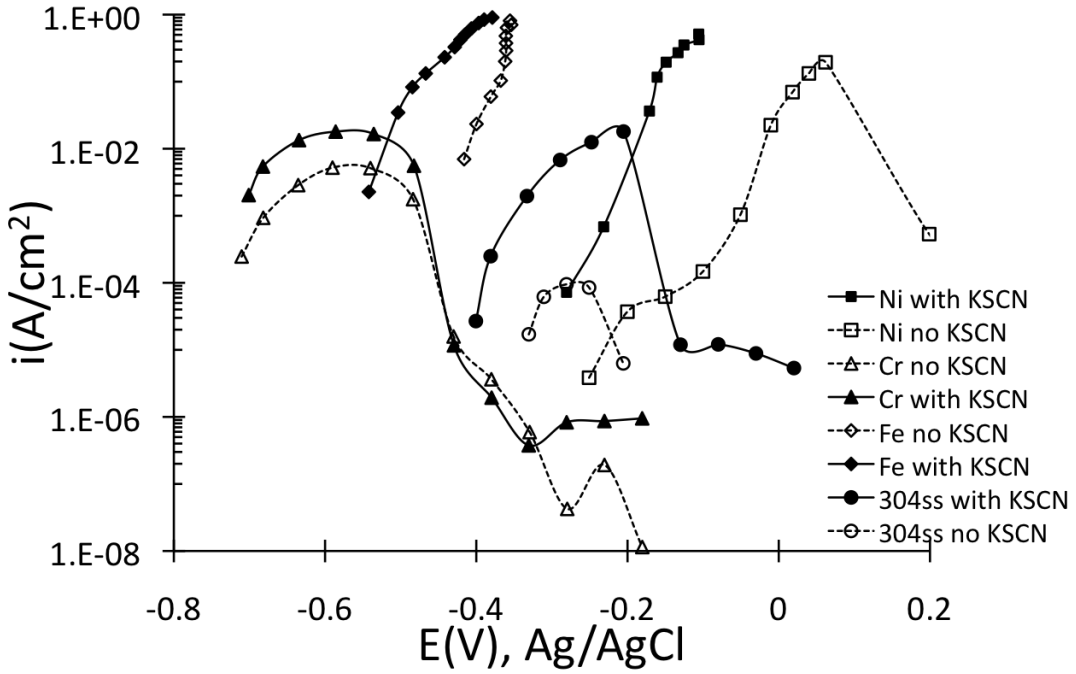

Figure 56. Potentiostatic polarization curves of pure Cr, pure Fe, pure Ni and Type 304 stainless steel in deaerated 1 M H_2SO_4 (pH=0) at 25°C. Open symbols: electrolyte without KSCN; filled symbols: electrolyte containing KSCN (0.14mM).

The potentiostatic polarization results for pure Fe, Cr, Ni and Type 304 stainless steel at *p*H=0 (Figure 56) show that the presence of KSCN increased the dissolution rate of Cr by 3-5 times, shifted the active dissolution curve of nickel and iron to more negative potentials, and had a strong catalytic effect on the dissolution rate of Type 304 stainless steel.

It is concluded that the effect of thiocyanate on the active dissolution rate of Type 304 stainless steel may be due to a similar reason to that proposed for Type 430 stainless steel, namely increased chromium dissolution rate counteracting the formation of a Cr-O-Cr passivating network at the ledges of the etched surface. Nickel, as a relatively noble element

which enriches on the electrode surface during dissolution, modifies this effect, but does not change the underlying mechanism. This conclusion is supported by surface composition analyses by XPS (reported in section **6.4**) and the morphology of corroded surfaces as studied by scanning electron microscopy (SEM) (reported later in section **6.3.2**). It is proposed that surface enrichment of nickel on the actively dissolving surface makes it easier for chromium atoms to link with oxygen (giving incipient passivation): the effect of nickel would hence be that the percolation limit for passivation by chromium would decrease, which means that nickel-containing Type 304 stainless steel tends to passivate more easily (at a lower critical current density) than Type 430 stainless steel. In the computer simulation of the percolation model for passivation of Fe-Cr alloy by Qian and his coworkers, different probabilities for dissolution of surface Fe and Cr (q_{Fe} and q_{Cr}) were tested to model the active-passive transition of the alloy[48][49]. For a fixed value of q_{Cr}, lower q_{Fe} results in a lower critical current density at the active-passive transition and a lower percolation limit of Cr is needed for the passivity of the alloy. Since Ni has much lower dissolution rate than Fe, the average dissolution probability for the elements which do not contribute to the passive layer in acid solution (Fe and Ni) is lower for 304 stainless steel than 430 stainless steel (where the base element is only Fe). This is a plausible reason why the critical current density for 304 stainless steel is lower than 430 stainless steel and why it is easier for 304 stainless steel to passivate. Although there is no nickel in the passive layer of stainless steel, nickel does promote passivation by retaining chromium on the surface of the steel.

6.3.2 Morphology of Corroded Surfaces

For chromium, grain boundary etching was observed after active dissolution in solutions with and without thiocyanate, but crystallographic etching (with steps on the surface) was more evident in the thiocyanate-containing solution (Figure 57). This supports the idea that sulfur adsorbs at the step edges or ledges on the chromium surface and that faster dissolution occurs at the edges than from terrace sites. The surface morphology of chromium after dissolution at *p*H=0 is similar to *p*H=2.5, but with less obvious differences between the thiocyanate-containing and thiocyanate-free solution for *p*H=0. This is consistent with the potentiostatic polarization results: the catalytic effect of thiocyanate on chromium dissolution is smaller at *p*H=0 than at *p*H=2.5 (see Figures 55 and 56).

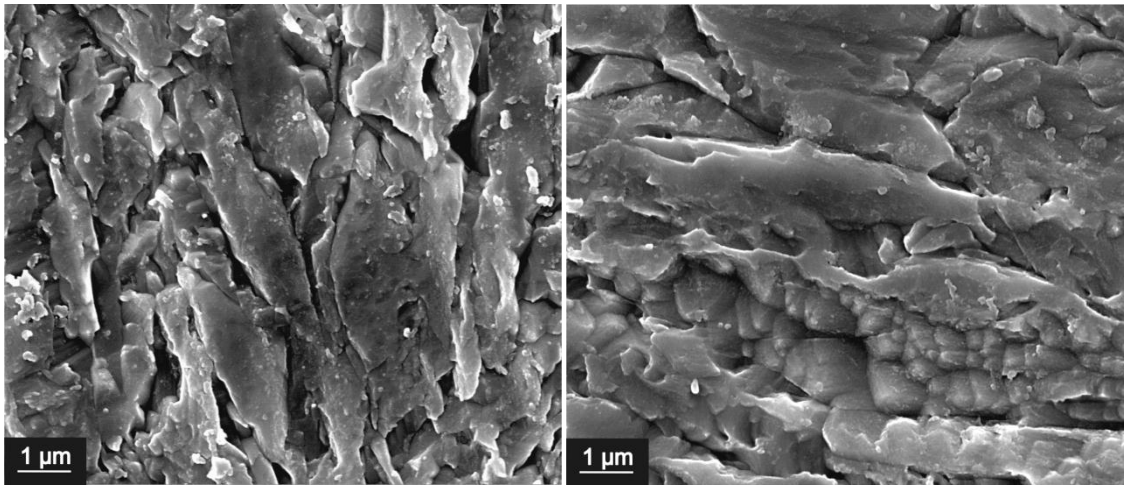

*Figure 57. Cr: etched electrode surfaces after potentiostatic polarization in deaerated 1 M H_2SO_4 (p*H=0) at 25°C, for solutions without (left) and with (right) KSCN (E=-0.63$V_{Ag/AgCl}$; anodic charge passed 1C/cm^2). Scanning electron micrographs (secondary electron images).*

For pure nickel, crystallographic etching (fine-scale steps) was much more obvious for the thiocyanate-containing solution (Figure 58), which may have contributed to a larger specific area after dissolution in the thiocyanate-containing solution (compared with the thiocyanate-free solution). However, as discussed later, the effect of surface morphology on double-layer

capacitance was small compared with that of growth of a porous, electronically conductive nickel sulfide product on the electrode surface.

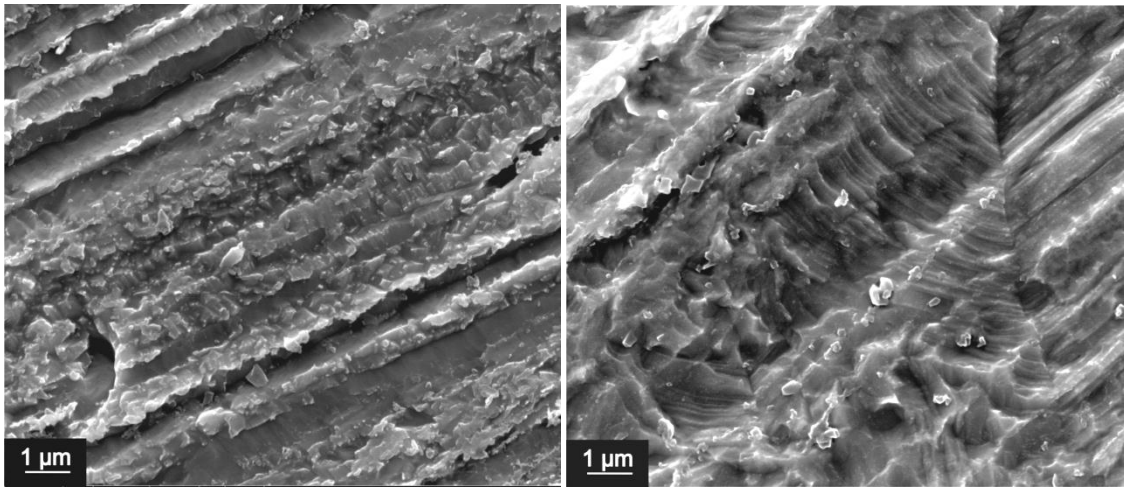

*Figure 58. Ni: etched electrode surfaces after potentiostatic polarization in deaerated 1 M H_2SO_4 (p*H=0) at 25°C, for solutions without (left) and with (right) KSCN (*E=-0.1$V_{Ag/AgCl}$; anodic charge passed 1C/cm^2). Scanning electron micrographs (secondary electron images).*

Similar to what was found for Type 430 stainless steel at *p*H=2.5, the difference in surface morphology is more evident for Type 304 stainless steel than any of the pure elements (Figure 59): clear etching of crystal facets occurred in thiocyanate-containing solution resulting in steps of various heights, with finer steps on larger steps appearing on the surface; in contrast, no obvious crystallographic etching occurred in the thiocyanate-free solution. As mentioned in the previous section, the strong crystallographic etching is consistent with the loss of Cr-O-Cr passivation of ledges when thiocyanate is present, as was also found for Type 430 stainless steel at *p*H=2.5.

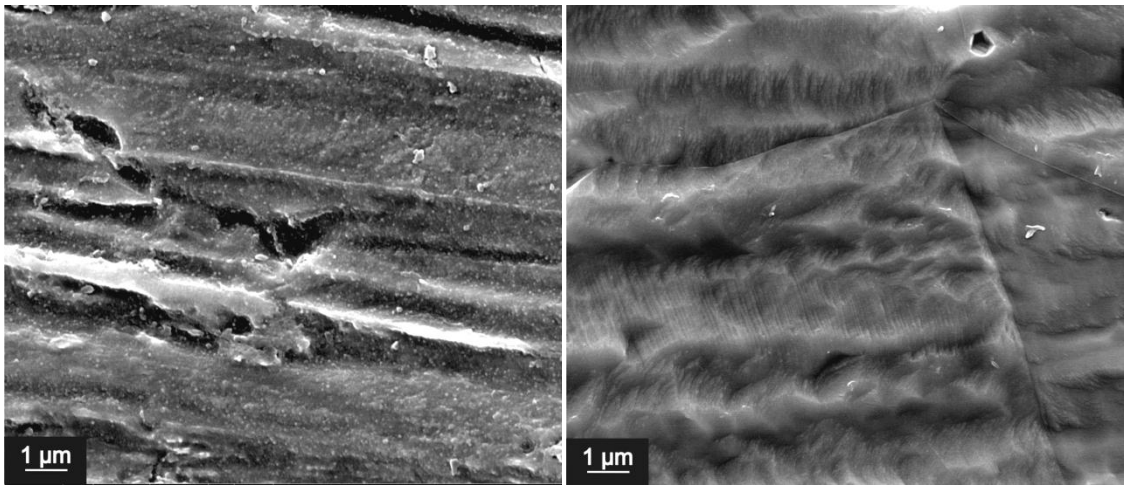

*Figure 59. 304: etched electrode surfaces after potentiostatic polarization in deaerated 1 M H_2SO_4 (pH=0) at 25°C, for solutions without (left) and with (right) KSCN (*E*=-0.28$V_{Ag/AgCl}$; anodic charge passed 4.7C/cm^2). Scanning electron micrographs (secondary electron images)*

6.3.3 Electrochemical Impedance Spectroscopy

6.3.3.1 Dissolution mechanism

The impedance results were fitted to the equivalent circuit shown in Figure 60, which is similar to that used to fit the impedance behavior of pure Fe, Cr and Type 430 stainless steel at *p*H=2.5, but with one extra series combination of resistance R_4 and a constant-phase element CPE_4. R_s is the solution resistance, R_1 is the charge transfer resistance and CPE_1 was associated with double-layer capacitance. R_2 and CPE_2 are associated with pseudo-inductive behavior and both R_3-CPE_3 and R_4-CPE_4 are associated with pseudo-capacitive behavior. The measured and fitted impedance results are shown in Figure 61-63 and the fitted parameters are summarized in Table 8.

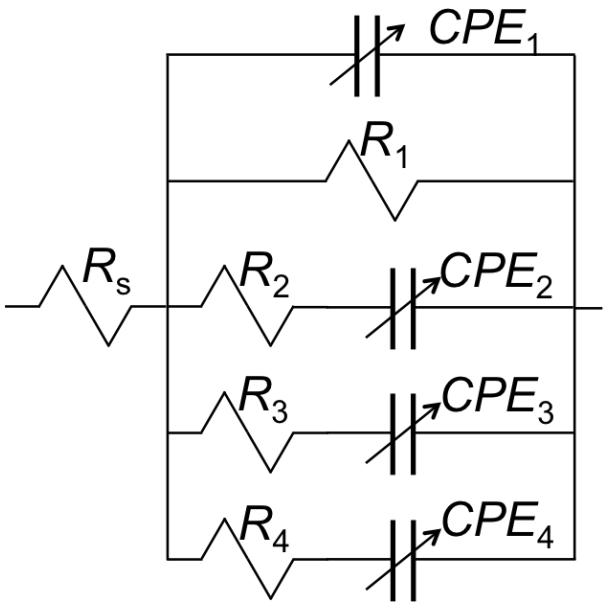

Figure 60. Equivalent circuit used when fitting impedance results. "CPE" indicates constant-phase elements, which could be either inductive or capacitive in nature.

As in the previous section for 430 stainless steel, the minimum number of circuit elements necessary to fit the measured impedance data was used. Blanks in Table 8 indicate that a particular branch of the circuit was not necessary to fit the data.

For pure chromium, the total real resistance at low frequency in the thiocyanate-containing solution is close to the resistance in thiocyanate-free solution, which is in line with the small difference in the steady-state polarization current (Figure 56). Nevertheless, in the presence of thiocyanate, the dissolution rate of the bare metal was significantly increased (smaller charge transfer resistance R_1, see Table 8). Despite this, the overall dissolution rate was similar (to that in the absence of thiocyanate), apparently because of two extra passivating intermediates formed on the surface, slowing down the dissolution rate. The occurrence of two extra pre-passivation steps is deduced from the presence of additional pseudo-capacitive elements in the thiocyanate-containing solution (Figure 61).

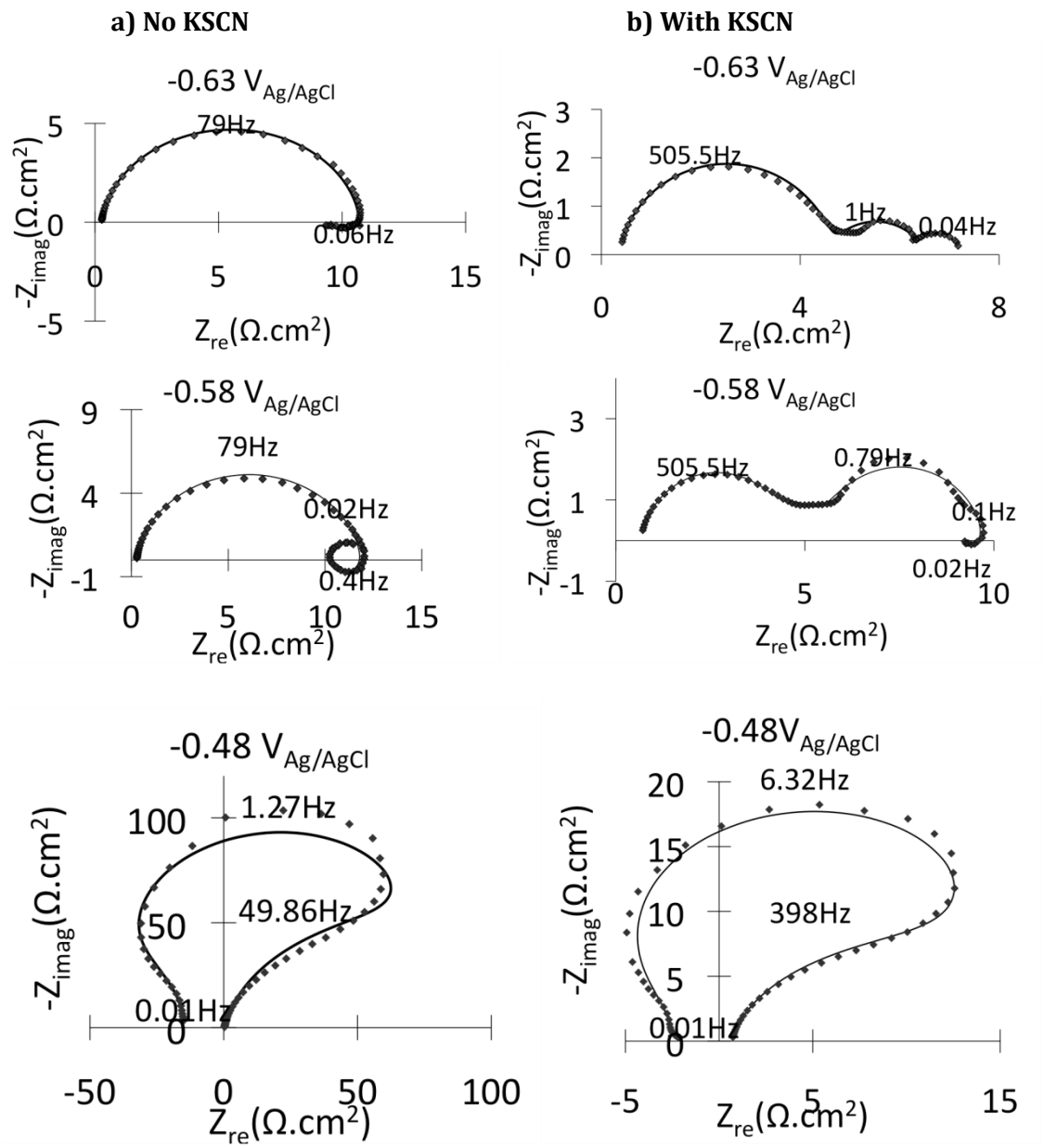

Figure 61. Cr: impedance results in deaerated 1M H_2SO_4 (pH=0) at 25°C, for solutions without (left) and with (right) KSCN; potentials as indicated on figures. Symbols: measured data; lines: fitted equivalent circuits.

Hence the differences in the shapes of the impedance plots between measurements in solutions with and without thiocyanate (for potentials more negative than the passivation potential) indicate a change in the dissolution mechanism of chromium in the thiocyanate-

containing solution. While the dissolution mechanism is different, there is no big difference in the dissolution rates. In the passive range (E=-0.48V), the shapes of the impedance plots are similar.

For pure nickel (Figure 62), the dissolution rate of the underlying metal was significantly increased by thiocyanate (with a much smaller charge transfer resistance, R_1), which also dominates the total dissolution rate even though one extra pseudo-capacitive loop appeared (indicative of an additional incipient passivation step). Similar to what was observed for pure chromium, differences in the shapes of impedance plots do suggest changes in the dissolution mechanism, namely one extra passivating intermediate involved in the dissolution of nickel in the presence of thiocyanate.

For Type 304 stainless steel, one extra pseudo-inductive loop was observed in the presence of thiocyanate (Figure 63) indicating involvement of a catalytic intermediate in the dissolution of this steel in the thiocyanate-containing solution. However, as for nickel the catalytic effect of thiocyanate is mainly due to the greatly increased dissolution rate of underlying metal (reflected in the much smaller charge transfer resistance R_1).

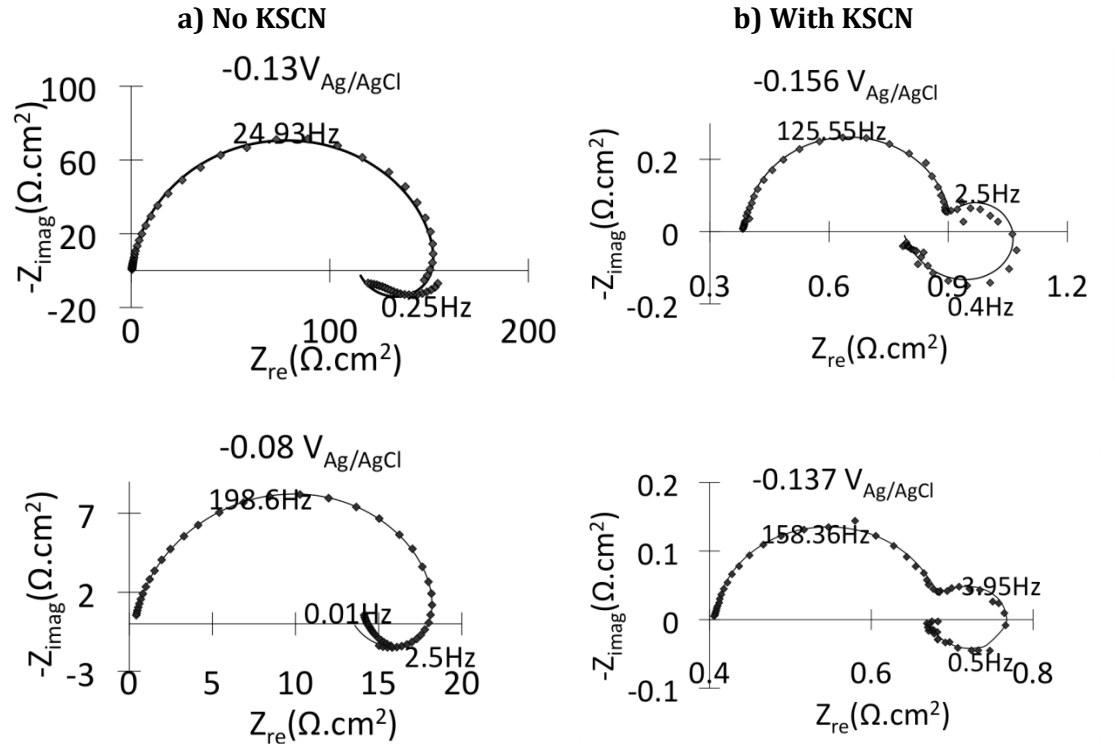

Figure 62. Ni: impedance results in deaerated 1M H_2SO_4 (pH=0) at 25°C, for solutions without (left) and with (right) KSCN; potentials as indicated on figures. Symbols: measured data; lines: fitted equivalent circuits.

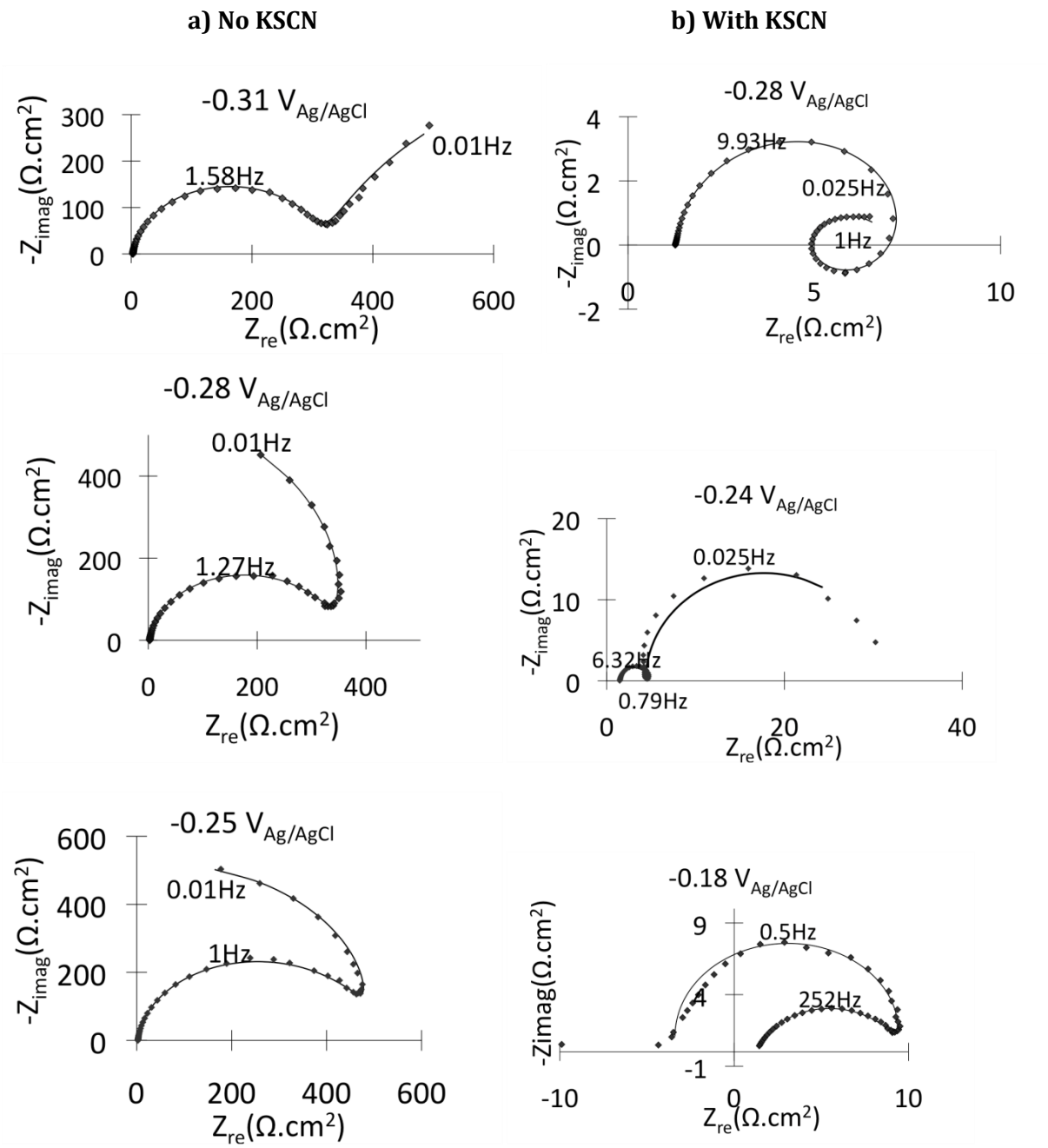

Figure 63. 304ss: impedance results in deaerated 1M H_2SO_4 (pH=0) at 25°C, for solutions without (left) and with (right) KSCN; potentials as indicated on figures. Symbols: measured data; lines: fitted equivalent circuits.

Table 8. Summary of experimental conditions for impedance testing, showing holding potential, holding time before start of testing, and values of fitted circuit elements.

Material	KSCN	$E(V_{Ag/AgCl})$	t_{hold}(s)	R_s	R_1	CPE_1		R_2	CPE_2		R_3	CPE_3		R_4	CPE_4	
						A	α		A	α		A	α		A	α
				($\Omega.cm^2$)	($\Omega.cm^2$)	$F/cm^2s^{1-\alpha}$	(–)	($\Omega.cm^2$)	$F/cm^2s^{1-\alpha}$	(–)	($\Omega.cm^2$)	$F/cm^2s^{1-\alpha}$	(–)	($\Omega.cm^2$)	$F/cm^2s^{1-\alpha}$	(–)
Ni	Absent	-0.13	7200	0.34	156	4.8E-05	0.94	421	2.6E-03	-0.80						
		-0.08	7200	0.35	19.4	5.8E-05	0.94	41.1	1.5E-01	-0.66	42.9	1.5E-05	0.85			
	Present	-0.137	300	0.39	33.7	2.5E-03	1	0.4	6.8E+00	-0.83	0.52	2.6E-01	0.95			
		-0.156	700	0.41		3.9E-03	0.99	0.26	1.9E+01	-0.82	0.28	3.2E-01	0.89			
Cr	Absent	-0.63	1200	0.26	11	2.7E-04	0.93	74	7.8E-03	-0.71						
		-0.58	1200	0.26	14.9	3.1E-04	0.92	61.9	3.6E-02	-1	53.1	1.3E-01	1			
		-0.48	1200	0.23	-15.0	1.9E-04	0.87				41.7	7.9E-03	0.80	19.36	2.2E-01	1
	Present	-0.63	1800	0.35	6.8	1.5E-04	0.91				55.0	7.6E-02	1	14.95	7.0E-03	0.8
		-0.58	1200	0.64	9.23	2.0E-04	0.89	133	1.2E-03	-1	9.9	1.3E-02	0.85	23.93	1.5E-04	1
		-0.48	1200	0.59	-3.0	3.2E-04	0.82				7.03	1.7E-02	0.80	4.122	1.9E-01	1
304ss	Absent	-0.31	1200	2.73	1398	3.3E-04	0.94				410	1.5E-02	1			
		-0.28	1200	2.73	-580	3.5E-04	0.94				216	5.5E-02	0.85			
		-0.25	1200	2.73	-400	3.6E-04	0.95				222	8.6E-02	1			
	Present	-0.28	600	1.28		3.1E-03	0.95	5.76	8.5E-01	-0.82543	7.5	3.8E-01	1			
		-0.24	600	1.45		6.6E-03	1	29.5	2.5E-01	-1	3.31	2.8E-01	1			
		-0.18	600	1.28	-4.58	3.2E-04	0.80				3.0	1.8E-01	1			

6.3.3.2 Effect of thiocyanate on double-layer capacitance

Less obvious than the change in (Nyquist) impedance curve shape is an effect of thiocyanate on the double layer capacitance (calculated as the effective capacitance of CPE_1); see Figure 64. The double layer capacitance of pure chromium was similar for the KSCN-containing and KSCN-free solutions, which is in line with the similar surface morphology and the absence of bulk sulfide formation (to be discussed in the next section). However, for pure nickel and Type 304 stainless steel, the double layer capacitances after dissolution in the thiocyanate-containing solution were 1-2 orders of magnitude higher than for the thiocyanate-free solution (except for Type 304 stainless steel at the passive potential). One factor which likely contributed somewhat to the increased double layer capacitance is the large surface roughness for the thiocyanate-containing solution, which can be seen from the SEM images of the corroded surfaces of nickel and Type 304 stainless steel after exposure to thiocyanate-containing solutions. While the fine steps and edges on the surface would have increased the true electrode surface areas, the main factor which contributed to the double-layer capacitance was electronically conductive sulfides which formed on the nickel and Type 304 stainless steel surfaces during active dissolution in the thiocyanate-containing solutions, as discussed below.

Evidence of sulfides formed on the Type 304 stainless steel in thiocyanate-containing solution was found by SEM/EDX and XPS analysis (shown in section **6.4**). Visually, the presence of sulfides was detected as a black deposit on the electrodes. To test the effect, the double-layer capacitance of Type 304 stainless steel in thiocyanate-containing solution was recorded during potentiostatic polarization (Figure 65); manual removal of sulfides from the surface by wet paper towel (Kimberly-Clark, Wypall L40) caused a sharp decrease in the double-layer capacitance (Figure 65). As shown in Figure 65, the double-layer capacitance of Type 304 stainless steel increased from 63 $\mu F/cm^2$ to 530 $\mu F/cm^2$ during the initial 1-2 minutes of polarization, perhaps caused by the surface roughening. Over the subsequent hour of

polarization the capacitance increased by almost another one order of magnitude, likely by sulfides developing on the surface; the capacitance dropped by almost one order of magnitude after removing the sulfides from the surface but there was no obvious change of the current density. Upon resumption of polarization, within approximately half an hour the capacitance recovered to the value which it had before removal of sulfides.

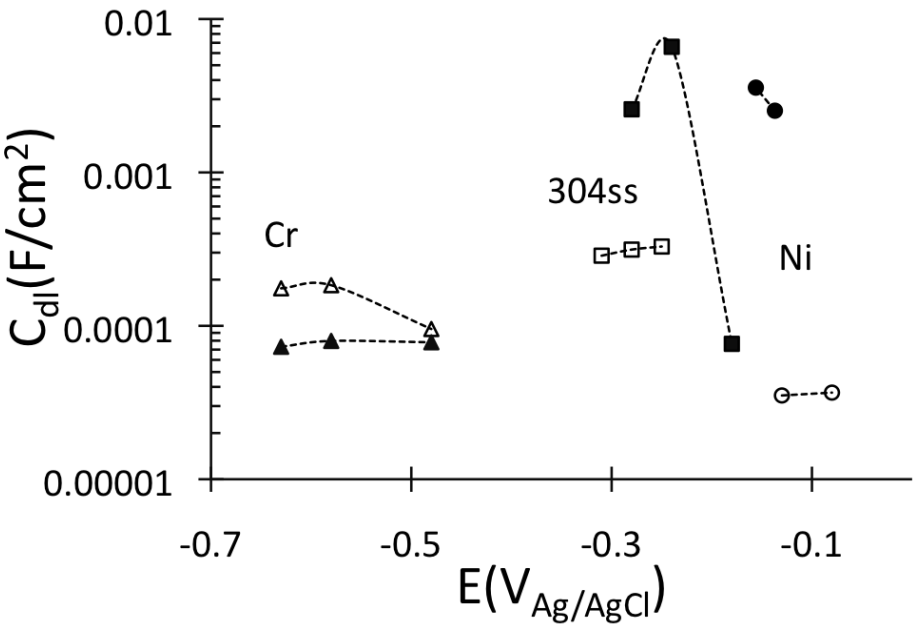

Figure 64. Double layer capacitance of pure Cr, pure Ni and 304 stainless steel at different potentials in deaerated 1M H_2SO_4 (pH=0) at 25°C (calculated from the fitted values given in Table II). Open symbols: electrolyte without KSCN; filled symbols: electrolyte containing KSCN (0.14mM)

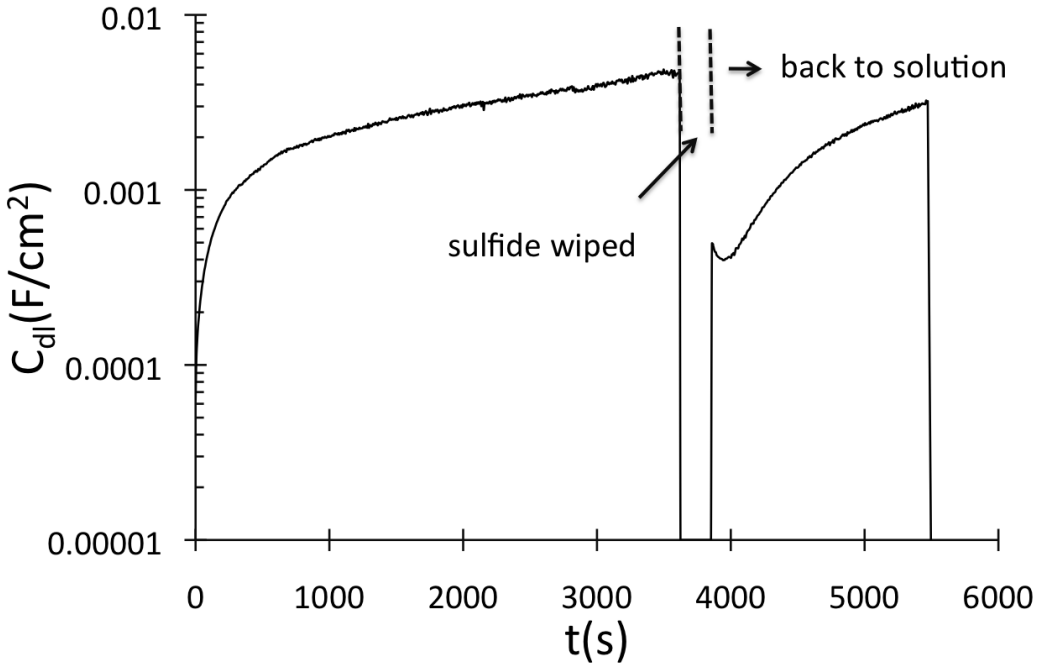

*Figure 65. Double layer capacitance of 304 stainless steel in 1M H_2SO_4 (*p*H=0) with 0.14mM KSCN at 25°C; E=-0.23V; f=1kHz;*

Development of sulfide product on the electrode surface was also evident in the results of surface analysis, and affected electrode behavior upon interruption of polarization, as discussed in section **6.4**.

6.3.3.3 Effect of thiocyanate on passivation

For Type 304 steel, the electrochemical impedance in solutions with and without thiocyanate showed one pesudocapacitive loop, which is generally taken to indicate early stages of passivation. To test whether thiocyanate affects passivation, the effective capacitance of CPE_3 (the pseudocapacitance from passivation) and total real part of the resistance of that branch of 304 stainless steel was calculated from the fitted values (using the same equation as before); the results are plotted in Figure 66. The results show the same trend for Type 304 stainless steel as for Fe, Cr and Type 430 stainless steel in the *p*H=2.5 solution, namely that in the presence of thiocyanate the pseudo-capacitance was larger and the associated series resistance

was smaller. This suggests that thiocyanate suppresses the passivation of Type 304 stainless steel (in the presence of thiocyanate, more charge needs to be passed for a given decrease in current density, than in the absence of thiocyanate) just like what was found for Fe, Cr and Type 430 stainless steel at *p*H=2.5.

a)

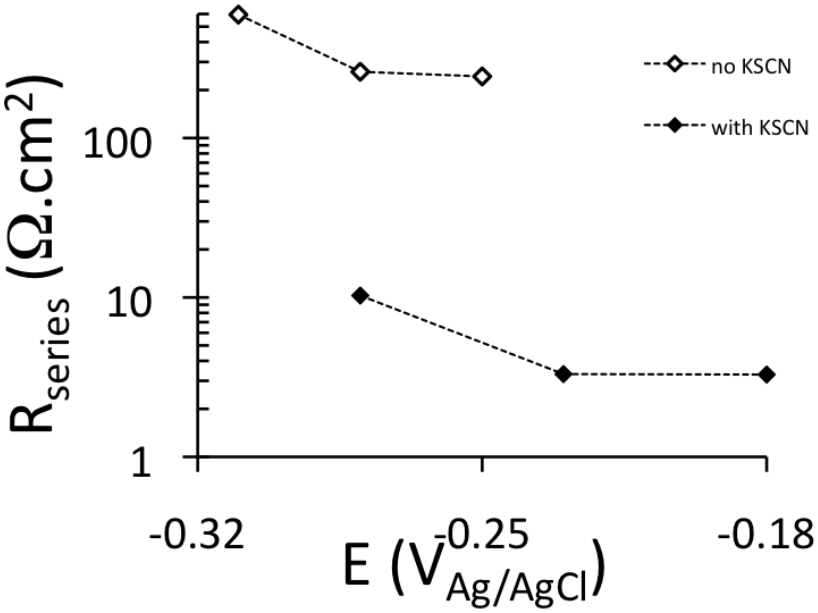

b)

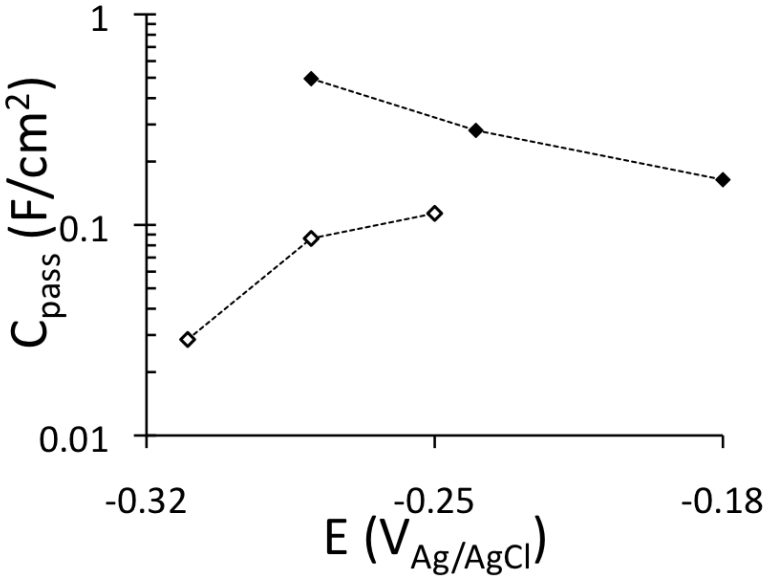

Figure 66. Fitted impedance values associated with pseudo-capacitive part of circuit (R_3*-*CPE_3 *combination), for Type 304. The effective series resistance a) and the effective pseudo-capacitance b) are shown, both evaluated at the frequency corresponding to the apex of the semicircle associated with pseudo-capacitive behavior.*

6.4 Surface analysis using X-ray photoelectron Spectroscopy

In this work, the accelerating effect of thiocyanate on active dissolution of stainless steel in acid sulfate solution has been proposed to occur by adsorption of sulfur on the steel surface, causing accelerated dissolution of chromium from the steel surface[73]. Accelerated dissolution of chromium would impede the early stages of passivation (which occur during active dissolution[52]) and so would cause the active dissolution rate to increase. This section presents the results of surface analysis (by X-ray photo electron spectroscopy; XPS) with associated electrochemical measurements, which tested the following main aspects of the proposed mechanism:

First, sulfur is proposed to adsorb – in the form of elemental sulfur or sulfide – on the steel surface in the presence of reduced sulfur compounds in solution. Upon transfer of electrodes from solutions containing reduced sulfur compounds, to solutions without these compounds, the coverage of sulfide or elemental sulfur is expected to decrease. Sulfur as sulfide or elemental sulfur would give a 2p XPS peak at a binding energy of around 162 eV, whereas adsorbed sulfate (the main form of sulfur in the test electrolytes) would give a peak around 169 eV[74]. (Because it was not possible to distinguish between adsorbed elemental sulfur and sulfide in this work, but bulk sulfide was found to form during prolonged anodic dissolution of nickel and nickel-bearing steels in the presence of reduced sulfur compounds, adsorbed sulfur – or sulfur in reaction product – with a 2p binding energy around 162 eV is here termed "sulfide".)

Second, accelerated dissolution of chromium in the presence of adsorbed sulfur would result in a lower Cr/Fe ratio on the surface of the steels. The proposed effect of adsorbed sulfur on the dissolution rate of chromium from the steel surface is based on the following: Dissolution of pure chromium is accelerated by the presence of thiocyanate[73]. The electrochemical signature of passivation – pseudo-capacitance – is present in the impedance of stainless-steel electrodes during active dissolution (at potentials more negative than the

passivation potential)[52], [73]. Increased pseudo-capacitance indicates that passivation is retarded in the presence of thiocyanate, as expected if passivation occurs by formation of chromium-oxygen-chromium networks on the steel surface[48]. The proposed mechanism hence implies that the surface concentration of chromium on stainless steels would be lower in the presence of thiocyanate; this prediction was tested by XPS.

Electrodes used for surface analysis were pure (electrolytic) chromium and nickel, a high-purity Fe-20wt% Cr alloy (prepared from electrolytic metals), and commercial cold-rolled Type 430 and Type 304 stainless steel.

The main method used to prepare samples for surface analysis was potentiostatic polarization to give active dissolution in an electrolyte containing a reduced sulfur compound (thiocyanate or tetrathionate), followed by removal of the electrode, rinsing with deionized water, and then resuming potentiostatic polarization (at the same potential) in electrolyte with no reduced sulfur compound. As anodic dissolution proceeds in the electrolyte without reduced sulfur compounds, sulfide is expected to be removed from the electrode surface, with an associated *decrease* in anodic current density[6]. This preparation procedure was found to result in a transient *increase* in anodic current density when polarization was restarted upon transferring Type 304 stainless steel and nickel electrodes to the electrolyte without reduced sulfur compounds. As shown below, this unexpected current increase had a pseudo-capacitive character (with exponentially decaying current density) and lasted for several tens of seconds. Possible origins of the transient current increase were tested by surface analysis and electrochemical tests.

6.4.1 Experimental

Static electrodes were used for electrochemical tests and subsequent surface analysis. Electrodes were suspended vertically in the electrolyte, establishing electronic contact above

the electrolyte surface with an alligator clip. Electrode were ground using 1200 grit silicon carbide paper. *IR* correction was applied to the potentials after the tests, using the solution resistance determined with a high-frequency (10 kHz) impedance measurement. The same reference electrode and counter electrode were used as used as mentioned before; potentials are given relative to the Ag/AgCl electrode filled with saturated KCl (E=0.20 V_{SHE}).

Conditions for X-ray photo-electron spectroscopy were as follows: Incident X-rays were Al K_α; spot size 200μm; beam power 50W; area analyzed 1400 μm×400 μm. Survey scans were performed (binding energy range 0-1100eV, 0.4eV step size, 25 ms per step, completing 16 repeat cycles for the survey scan; where sulfur and nitrogen peaks were small, 64 additional measurement cycles were completed over the sulfur 2p and nitrogen 1s peaks). At least one repeat measurement was performed on another part of the same electrode.

As before, the electrolyte used for Type 430 stainless steel, pure chromium and Fe20Cr alloy was 1M sodium sulfate, acidified to *p*H=2.5, containing zero or 0.14mM KSCN. The electrolyte was not deaerated and was kept at room temperature (25°C). Type 304 stainless steel was tested in 1M H_2SO_4 (*p*H≈0) containing zero or 0.14mM KSCN (using the *p*H≈0 solution because the active loop is small and little affected by thiocyanate in the *p*H=2.5 solution). Nickel was tested in 1M H_2SO_4 (*p*H≈0) containing 0.14mM KSCN or 0.035mM $Na_2S_4O_6$ (sodium tetrathionate). The tetrathionate-containing solution was used to test whether the transient accelerated anodic dissolution – which occurs upon transferring the nickel electrode from the thiocyanate-containing electrolyte to the electrolyte without thiocyanate – was related to the possible presence of adsorbed cyanide as an inhibiting species, in the thiocyanate-containing solution. No adsorbed cyanide would form in the tetrathionate solution. The concentration of tetrathionate was one-quarter that of thiocyanate, to give the same molar amount of reduced sulfur in solution; tetrathionate was used instead of thiosulfate, because thiosulfate disproportionates in acid solutions[75].

As noted above, samples for surface analysis were generally prepared by potentiostatic polarization in an electrolyte containing a reduced sulfur compound, polarizing for sufficiently long to allow the current to reach steady-state. In some cases, the electrode was subsequently also polarized in a second electrolyte, identical to the first except for the absence of the reduced sulfur compound. The duration of polarization in the second electrolyte was 1 minute to 10 minutes. For transfer, the electrode was rinsed with deionized water after removal from the first electrolyte; the transfer process was completed within 1 minute. The electrodes were exposed to laboratory air during transfer; to test whether oxidation of the electrode (especially of adsorbed sulfur) may have affected subsequent anodic dissolution, some electrodes were prepared in a glove box. The glove box was flushed with high-purity nitrogen for 16-20 hours beforehand. Measurement of the oxygen concentration inside the glove box using a portable gas monitor indicated that the decrease in oxygen concentration followed simple first-order kinetics with a time constant of 1-1.5 hours. The oxygen depletion curve in the glove box is shown in Figure 67.

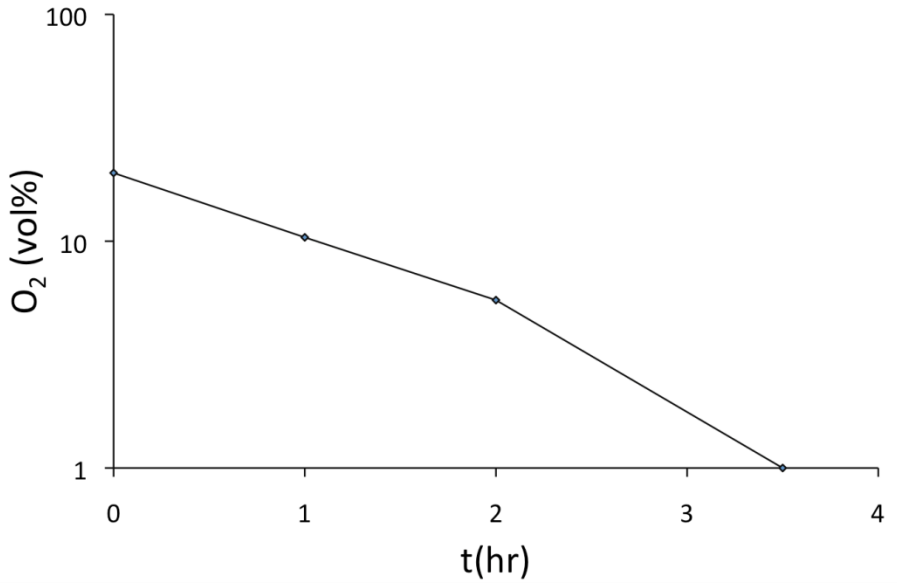

Figure 67. The oxygen depletion curve in the glove box during flushing with pure nitrogen gas.

In preparation for surface analysis, each electrode was removed from the electrolyte, rinsed with deionized water, dried in laboratory air (or nitrogen, in the case of glove box experiments), and stored in a desiccator. Surface analysis was completed within one to three days after removal from the electrolyte.

When interpreting the surface analysis results, it is necessary to recognize that all electrodes developed significant surface roughness during active dissolution. In general, the electrode surfaces were smoother after dissolution in the electrolyte without reduced sulfur compounds, compared with the electrode appearance after the first step of active dissolution in the electrolyte containing a reduced sulfur compound.

6.4.2 Mechanism test: Adsorbed sulfur and change in Cr/Fe ratio

With the exception of pure chromium (discussed below), all the tests confirmed that sulfide (or adsorbed sulfur) does form on the metal surfaces during exposure to electrolytes containing reduced sulfur compounds. As an example, the sulfide was observed on the Fe20Cr electrode after anodic dissolution in the KSCN-containing solution; the sulfide coverage diminished during subsequent dissolution in the KSCN-free solution (see Figure 68 and Figure 69). Clearly, low concentrations of reduced sulfur compounds in the electrolyte can cause sulfide (or adsorbed sulfur) to form on the metal surfaces.

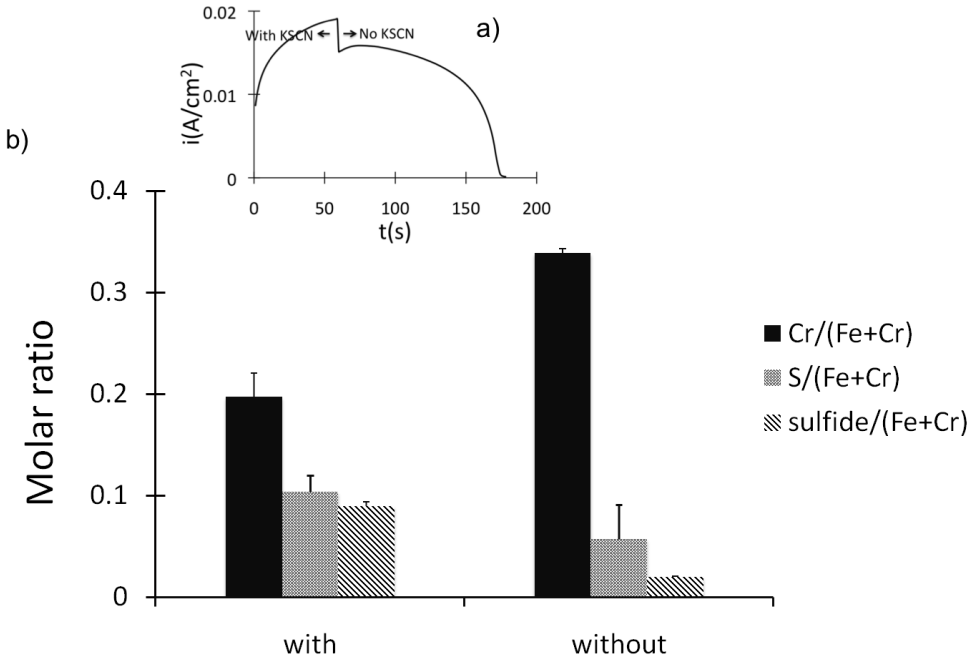

*Figure 68. a) Current-time curve and b) Surface compositions of Fe20Cr after anodic dissolution in 1 M Na_2SO_4, 0.01 M H_2SO_4 (*pH*=2.5) with 0.14mM KSCN, and after transfer to a KSCN-free solution; E=-0.41V$_{Ag/AgCl}$*

The format of Figure 68 is also used in several subsequent figures; the figures show the measured apparent current density during anodic polarization (first in the electrolyte with KSCN, and subsequently in the KSCN-free electrolyte), with the measured surface composition of electrodes exposed to just the KSCN-containing electrolyte, or to both electrolytes. The error bars give the range of values (of surface composition) found upon repeat measurements on different areas of the same electrode.

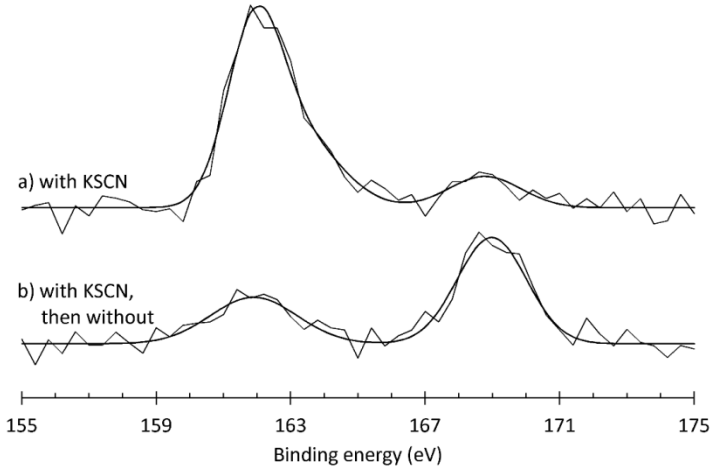

Figure 69. Sulfur 2p peak in XPS measurements on Fe20Cr alloy after dissolution in a) 1 M Na_2SO_4, 0.01 M H_2SO_4, 0.14mM KSCN, and b) KSCN-containing solution followed by transfer to KSCN-free solution; E=-0.41$V_{Ag/AgCl}$.The peak with a binding energy around 162 eV is characteristic of adsorbed sulfur or sulfide, and the peak at 169 eV corresponds to sulfate. (Smooth lines are fitted Gaussian peaks.)

The surface composition of the Fe20Cr alloy (Figure 68) confirmed the expected lower Cr concentration on the alloy surface after dissolution in the KSCN-containing solution; the Cr concentration was higher after subsequent dissolution in the KSCN-free solution. This supports the proposed mechanism for the effect of thiocyanate on stainless steels: the increased rate of chromium dissolution in the presence of adsorbed sulfur counteracts prepassivation (the formation of a Cr-O-Cr network).

6.4.3 Sulfur coverage on pure chromium

The current-time curve and associated surface compositions of pure chromium after anodic dissolution are shown in Figure 70. In contrast with the result for the Fe20Cr alloy, surface

analysis of pure chromium did not show a relationship between sulfide coverage and anodic activation. Anodic activation clearly occurred (as shown by the higher current density in the KSCN-containing electrolyte; see Figure 70 a), but there was no change in the sulfide coverage during subsequent (slower) dissolution in the KSCN-free electrolyte. (Note also that the sulfide coverage on chromium was small compared with that on the Fe20Cr alloy; Figure 68) The surface concentration of sulfate did increase with increased time that the electrode stayed in the solution.

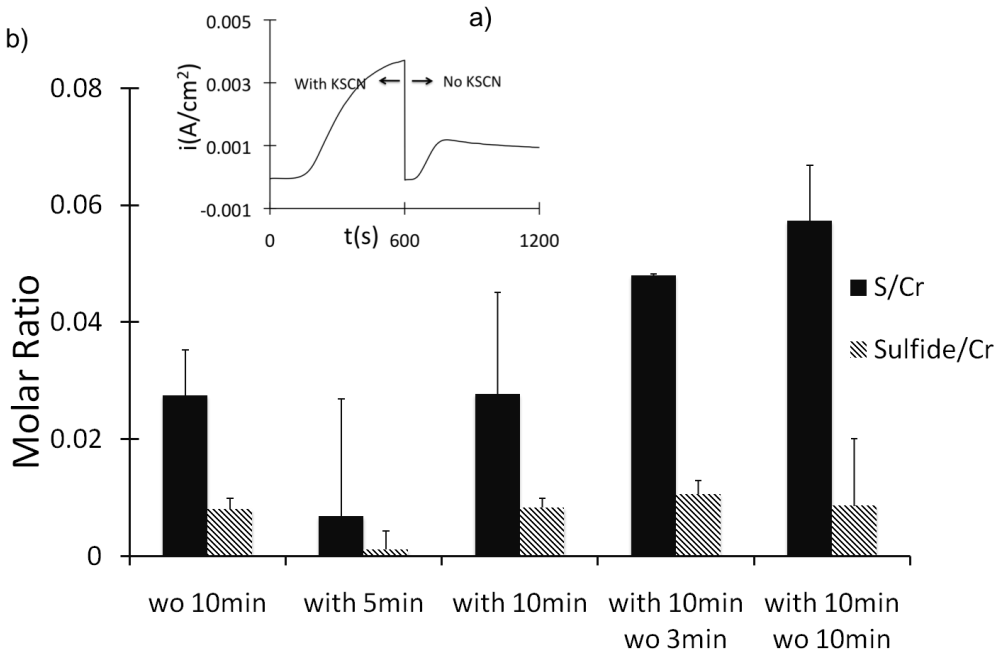

Figure 70. a) Current-time curve and b) Surface compositions of pure chromium after anodic dissolution in 1 M Na_2SO_4, 0.01 M H_2SO_4 (pH=2.5) with 0 or 0.14mM KSCN; E=-0.63$V_{Ag/AgCl}$

Clearly, it is not the total sulfur coverage as such which affects anodic activation of pure chromium. The morphology of the corroded surface indicates that the presence of adsorbed sulfur accelerates dissolution quite specifically, at crystallographic edges; the surface analysis method used here does not resolve adsorption sites of sulfur. It is hence possible that only a small portion of the adsorbed sulfur (that adsorbed at crystallographic edges) contributes to

accelerated dissolution, and that loss of this sulfur (upon transfer to the KSCN-free solution) would not cause a significant change in the total sulfide coverage.

6.4.4 Surface compositions of steels

The compositions of the commercial steels (Table 4) are much more complex than that of the pure Fe20Cr alloy. This affected both anodic behavior and surface composition. Comparison of Figure 68 (Fe20Cr alloy) and Figure 71 (Type 430 stainless steel) shows the much lower dissolution rate of the Type 430 steel (despite its lower chromium content); Type 304 stainless steel (with higher contents of Ni, Cu and Mo) has an even lower dissolution rate. While some intentionally added and residual alloying elements clearly have a beneficial effect in lowering the dissolution rate, the presence of nickel and copper affected interpretation of surface analyses: nickel and copper tended to form a bulk sulfide corrosion product.

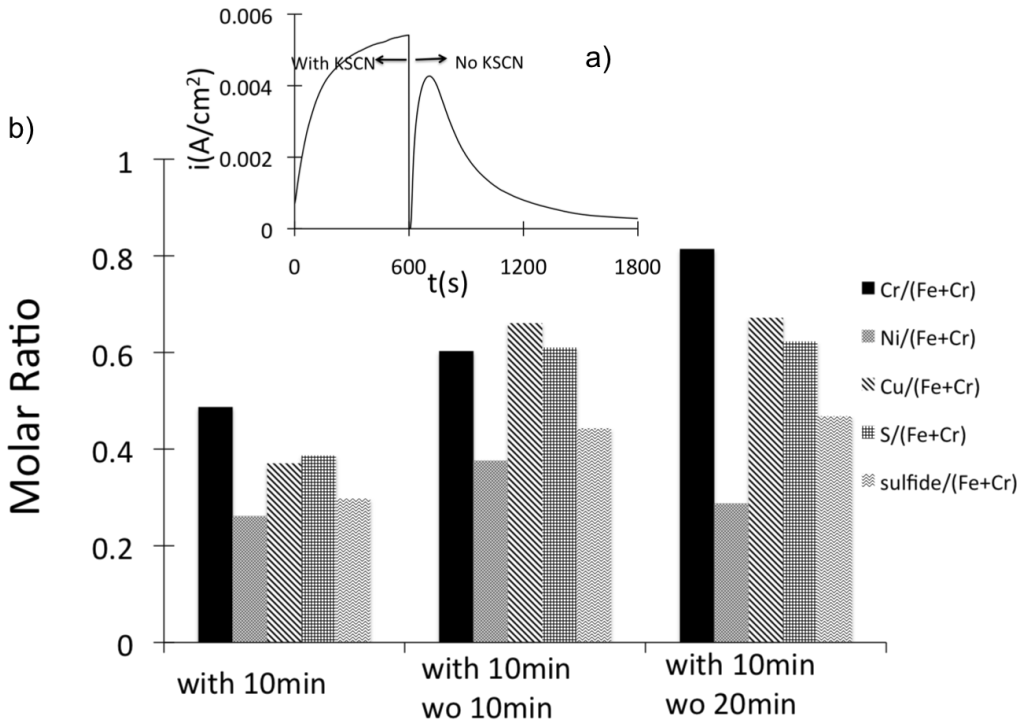

*Figure 71. a) Current-time curve and b) Surface compositions of Type 430 stainless steel after dissolution in 1 M Na_2SO_4, 0.01 M H_2SO_4 (*pH=2.5) with 0.14mM KSCN only, and in KSCN-containing solution followed by transfer to KSCN-free solution; E=-0.41$V_{Ag/AgCl}$.*

The equilibrium potentials (Table 9; values calculated with FactSage[76]) give an indication of the stability of the sulfides of Cr, Fe, Ni and Cu relative to that of their cations, in the presence of elemental sulfur. Based on the equilibrium potentials, the ranking of the tendency of these elements to form sulfides (rather than dissolving as cations) is as follows: Cr<<Fe<Ni<<Cu.

Table 9. Standard reduction potentials, 298K (FactSage)

Reaction	$E°$ (V_{SHE})
$Cr^{3+} + 3e^- + S = CrS$	-0.270
$2Cr^{3+} + 6e^- + 3S = Cr_2S_3$	-0.164
$Fe^{2+} + 2e^- + S = FeS$	0.135
$7Fe^{2+} + 14e^- + 8S = Fe_7S_8$	0.159
$7Ni^{2+} + 14e^- + 6S = Ni_7S_6$	0.180
$Ni^{2+} + 2e^- + S = NiS$	0.206
$2Cu^{2+} + 4e^- + S = Cu_2S$	0.595
$Cu^{2+} + 2e^- + S = CuS$	0.633

The strong tendency of Ni and Cu to form sulfides had the following effects in this investigation:

First, after dissolution in the KSCN-containing electrolyte, surface concentrations of nickel, copper and sulfur were high in the case of Type 430 stainless steel (Figure 71), despite the low concentrations of copper and nickel in the steel (Table 4). Coverages of nickel, copper and sulfur did not decrease upon transfer of the Type 430 stainless steel to the KSCN-free solution (Figure 71); in fact, the surface concentration of sulfide *increased*. This is the opposite of that found for the Fe20Cr alloy (Figure 68), and the opposite of what was expected, given that there was no clear source of additional sulfide in the KSCN-free solution. The apparent increase in sulfide coverage likely resulted from the large change in surface roughness which occurred when the Type 430 electrode was transferred to the KSCN-free solution: the electrode surface became much smoother during dissolution in the KSCN-free solution, and hence the surface concentration of sulfide could increase without any additional source of sulfide, simply because the true area of the electrode became smaller.

Second, the strong association between nickel, copper and sulfur prevented measurement of the nickel, copper and adsorbed sulfur content of the *metal surface* itself – whereas nickel, copper and sulfur were detected, the surface analyses did not allow distinction between nickel

and copper present as sulfide corrosion product, or as enriched or adsorbed elements on the metal surface itself. However, the analyses could be used to find the Cr/Fe ratio of the metal surface, because the sulfide corrosion product did not contain Cr or Fe, based on the following measurements:

The composition of bulk sulfide corrosion product was determined by recovering the black product which formed after extended anodic dissolution of Type 304 stainless steel in KSCN-containing solution (as mentioned in the previous section, formation of this black product was associated with a large increase in the double-layer capacitance). The product was analyzed by energy dispersive X-ray microanalysis in a scanning electron microscope; the results in Table 10 confirm that the product contained the elements Ni, Cu and S, and did not contain detectable Fe or Cr.

Table 10. Composition of metal sulfides on 304 stainless steel (mole fractions); 9 analyses were performed

Element	Ni	Cu	S	Fe	Cr
Average	0.237	0.321	0.442	0	0
Standard deviation	0.016	0.023	0.027	0	0

For both Type 430 and Type 304 stainless steels, Cr enriched on the steel surface during dissolution in the thiocyanate-free solution, and a lower Cr/Fe ratio was found on the steel surface after dissolution in the thiocyanate-containing solution (Figure 71 and Figure 72).

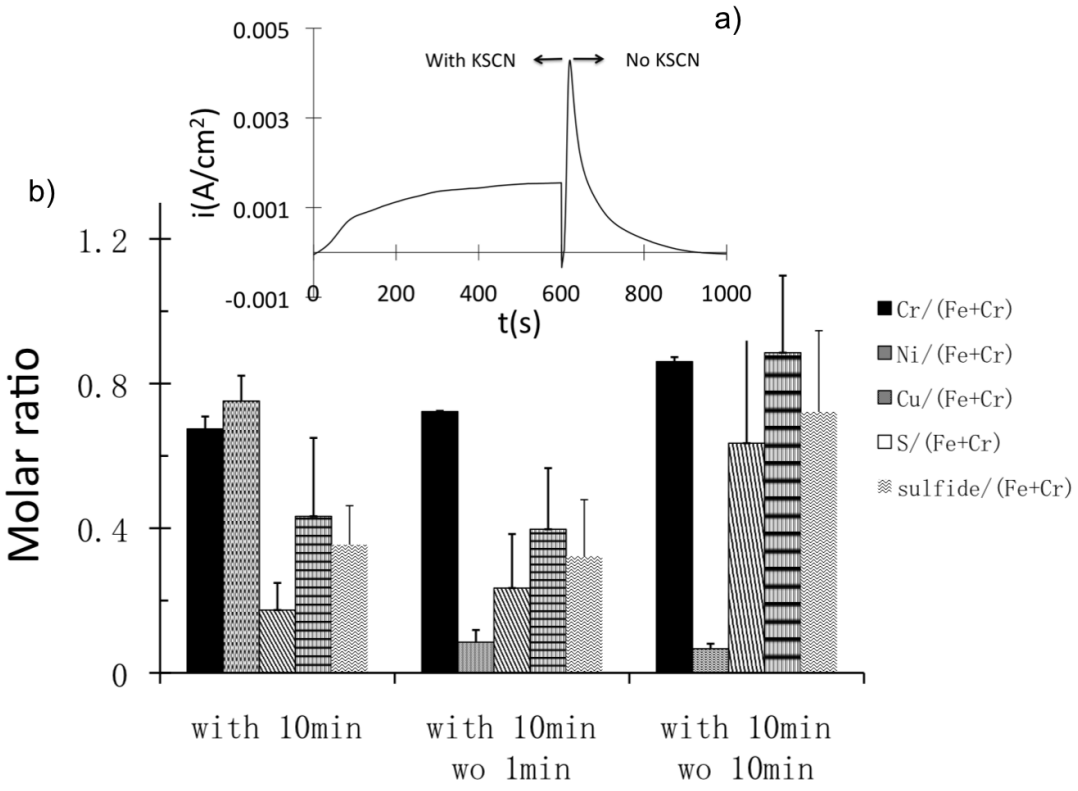

Figure 72. a) Current-time curve and b) Surface compositions of Type 304 stainless steel after anodic dissolution in 1M H_2SO_4 (pH=0) with 0.14mM KSCN only, and in KSCN-containing solution followed by transfer to KSCN-free solution; E=-0.28$V_{Ag/AgCl}$

However, the change in nickel content on the surface of Type 304 stainless was very different from Type 430 stainless steel: Figure 71 indicates that the nickel coverage on Type 430 stainless steel remained approximately unchanged when the electrode was transferred to the thiocyanate-free solution. In contrast, the Type 304 stainless steel showed an abrupt decrease in the nickel coverage within the first minute of transfer to the KSCN-free solution (with little change in the Cr, Cu or S coverage; Figure 72). The decrease in nickel appears to reflect dissolution of nickel from the nickel sulfide product: Scanning electron micrographs (Figure 73) of the Type 304 stainless steel samples used for XPS measurement show that the metal surface was covered by a porous layer (presumably the sulfide corrosion product) after corrosion in the KSCN-containing solution; the size of the pores increased greatly after

subsequent exposure to the KSCN-free solution (giving an appearance similar to that of materials which had undergone dealloying during corrosion) (Figure 73). The reason why similar dissolution of nickel sulfide was not seen in the case of Type 430 stainless steel may simply be the difference in *p*H: Type 304 stainless steel was tested at *p*H=0, whereas Type 430 stainless steel was tested at *p*H=2.5 (the higher *p*H was employed in the case of Type 430 to limit the anodic current densities). *p*H values of zero of less are expected to favor dissolution of nickel sulfide[77].

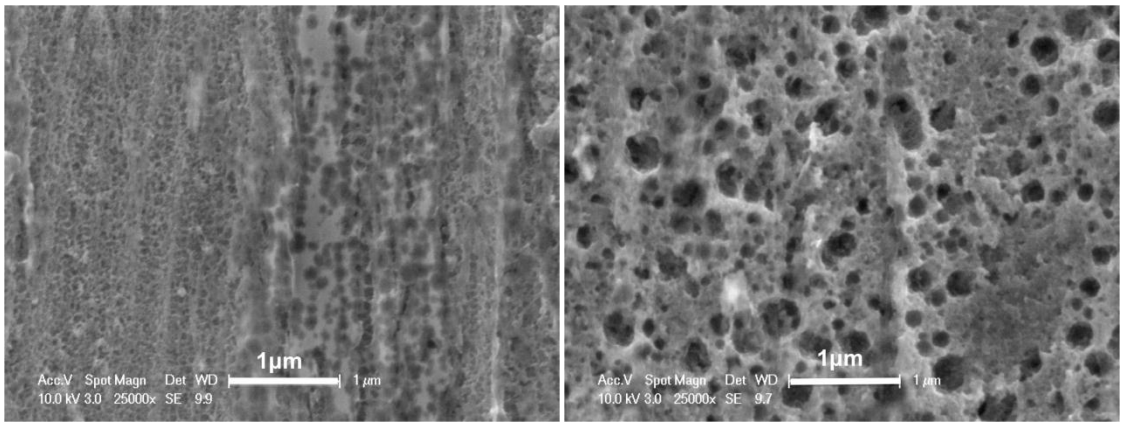

*Figure 73. Scanning electron micrographs (secondary electron images) of Type 304 stainless steel after anodic dissolution in a) 1M H_2SO_4 (*p*H=0) with 0.14mM KSCN for 10mins, b) 1M H_2SO_4 (*p*H=0) with 0.14mM KSCN for 10mins then 1M H_2SO_4 for another 3mins; E=-0.28$V_{Ag/AgCl}$*

The third effect ascribed to the sulfide corrosion product is the occurrence of unexpected faster dissolution upon transfer of Type 304 stainless steel electrodes from the KSCN-free electrolyte to the KSCN-containing electrolyte, visible as a current spike in Figure 72. A similar current increase was observed in the case of nickel (Figure 74). This effect was examined in greater detail, as discussed in the next section.

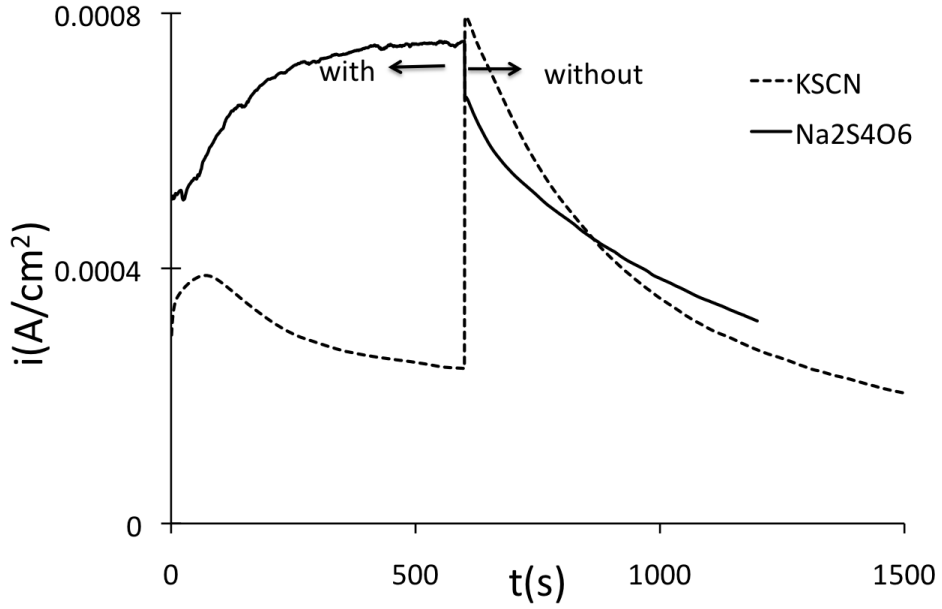

*Figure 74. Current-time curves for pure nickel in 1M H_2SO_4 (*pH*=0) with 0.14mM KSCN or 0.035mM $Na_2S_4O_6$, followed by transfer to 1M H_2SO_4; E=-0.25$V_{Ag/AgCl}$*

6.4.5 Increased anodic dissolution after interrupted polarization

Several different possible origins of the transient increased dissolution rate after transfer of nickel and Type 304 electrodes from KSCN-containing to KSCN-free solutions were examined. (It is worth noting that the current spike is not simply charging of the double-layer capacitance: while the double-layer capacitance of the Type 304 electrode did increase greatly due to sulfide formation, the charge associated with the current spike is orders of magnitude larger than that due to double-layer charging.) The possibilities were the following:

1. Dissolution of the sulfide corrosion product
2. Loss of inhibitive cyanide when the electrode is transferred into the KSCN-free solution.
3. Oxidation of sulfide to more-aggressive species (such as polythionic species) upon exposure of the electrode to air.

4. Surface restructuring of the sulfide leading to greater anodic activity.

Each of these is discussed in turn.

6.4.5.1 Dissolution of sulfide corrosion product

Surface analysis (Figure 72) and scanning electron micrographs (Figure 73) indicate that nickel sulfide dissolves from the electrode surface during the period of the current spike. To test whether large-scale dissolution of the sulfide product could account for the current spike, the double-layer capacitance was measured upon transfer of the electrode between electrolytes. As shown in the previous section, the double-layer capacitance of the Type 304 electrodes increases greatly when the (electronically conductive) sulfide product forms on the electrode surface; hence changes in the amount of sulfide on the electrode would be detectable as changes in the double-layer capacitance. Figure 75 confirms the large increase in double-layer capacitance as the sulfide product grows during anodic polarization in the tetrathionate-containing electrolyte. Upon transfer of the electrode to the tetrathionate-free electrolyte, the expected current spike was observed, but the double-layer capacitance did not decrease – the double-layer capacitance simply stopped increasing. This is as expected, since there is no source of sulfide in the tetrathionate-free electrolyte, and hence the sulfide stops growing.

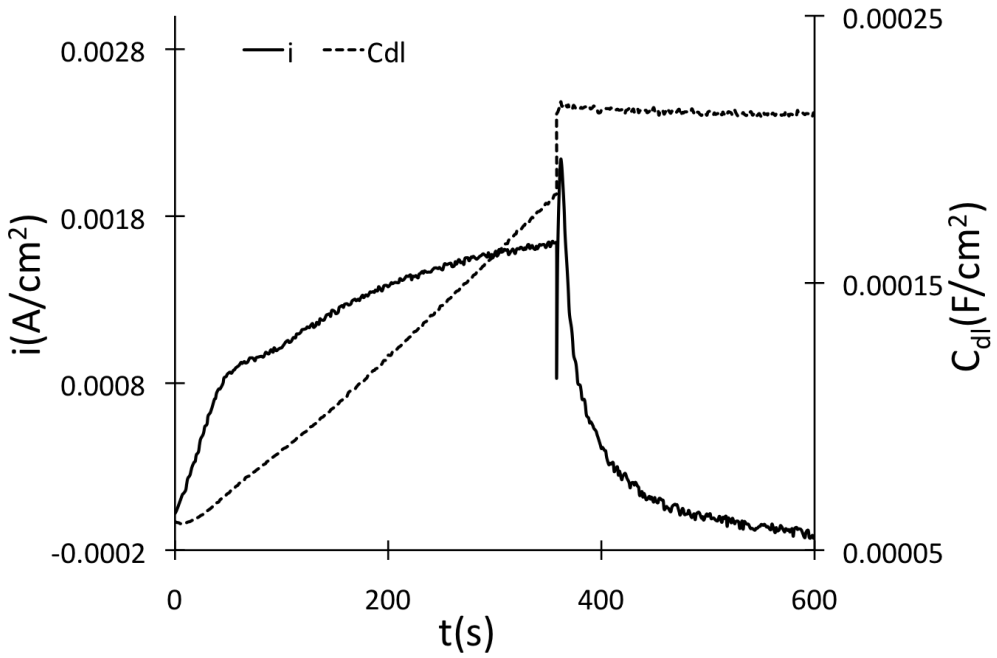

*Figure 75. Current density and double layer capacitance (measured at 1kHz) for Type 304 stainless steel in 1M H_2SO_4 (*pH*=0) with 0.035mM $Na_2S_4O_6$, transferred to 1M H_2SO_4; E=-0.28$V_{Ag/AgCl}$; measured in the glove box*

This effect was confirmed by experiments in which the Type 304 electrode was transferred from one tetrathionate-containing electrolyte to another container of nominally identical electrolyte: the current spike was observed (Figure 75) and the double-layer capacitance simply continued to increase as further dissolution occurred in the tetrathionate-containing electrolyte.

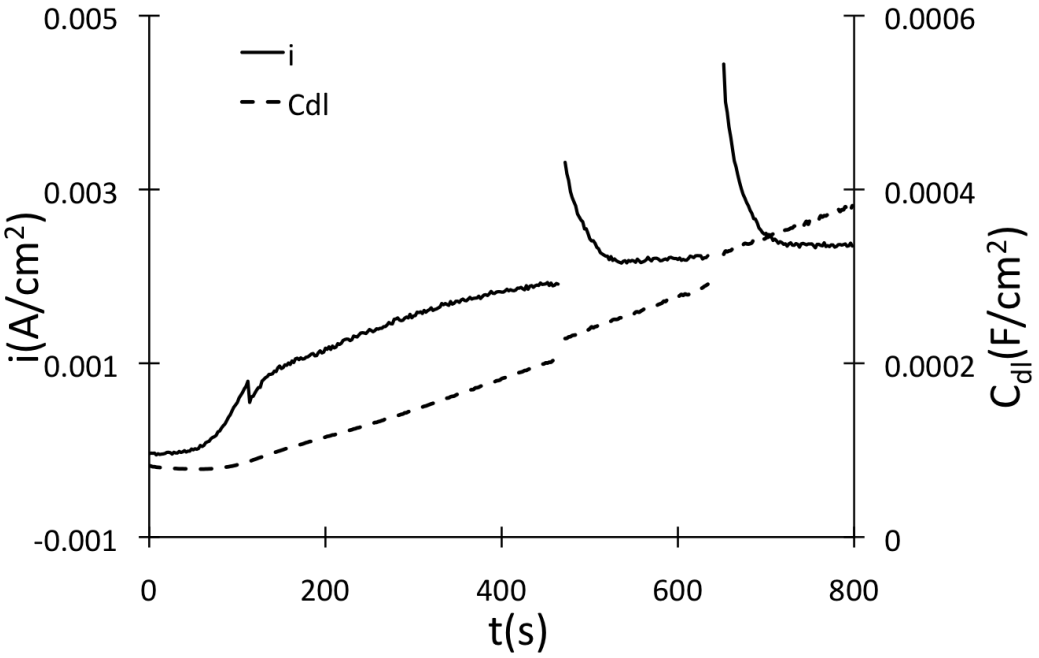

*Figure 76. Current density and double layer capacitance (measured at 1kHz) for Type 304 stainless steel during anodic dissolution in 1M H_2SO_4 (*pH*=0) with 0.035mM $Na_2S_4O_6$, transferred to another container of nominally identical solution; E=-0.28$V_{Ag/AgCl}$; measured in the glove box*

6.4.5.2 Possible inhibitive effect of cyanide

The expected products when thiocyanate disproportionates on the electrode surface are sulfur and cyanide[11]. Cyanide may itself adsorb on the electrode surface and can act as a corrosion inhibitor. Upon transfer of the electrode to the thiocyanate-free solution, the source of cyanide is eliminated (and cyanide may oxidize during exposure of the electrode to air during the transfer process). Loss of cyanide might then lead to more rapid dissolution. To test this suggestion, measurements were performed in electrolytes containing tetrathionate instead of thiocyanate (Figure 74 to Figure 77). Surface analysis of nickel (after dissolution in these two electrolytes) showed a small nitrogen concentration, which was slightly higher after dissolution in the thiocyanate-containing electrolyte (Table 11), and no current spike was found when

transferring nickel from the tetrathionate-containing solution to the tetrathionate-free solution (Figure 74). However, a current spike was found when transferring Type 304 stainless steel from tetrathionate-containing solution to tetrathionate-free solution (Figure 75, Figure 77), which ruled out a general role of adsorbed cyanide in the observation of the current spike.

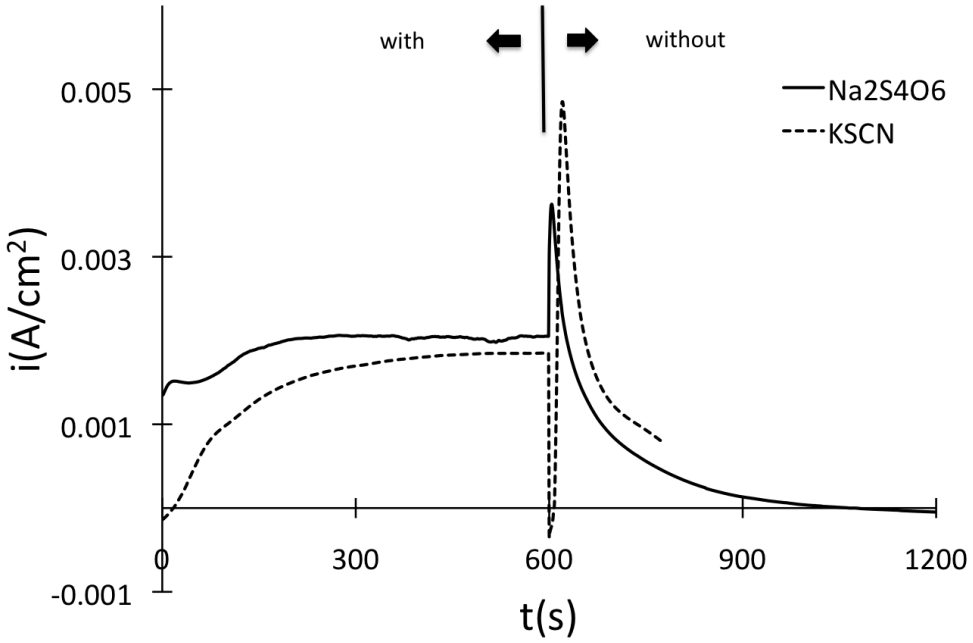

Figure 77. Current-time curves for Type 304 stainless steel polarized in 1M H_2SO_4 with 0.14mM KSCN or 0.035mM $Na_2S_4O_6$ followed by transfer to 1 MH_2SO_4; E=-0.28$V_{Ag/AgCl}$

Table 11. Nitrogen content on nickel surface after dissolution in 1 M H_2SO_4; i=1.5mA/cm^2; t=400s(results from two measurements in each case)

Electrolyte	N/Ni (molar ratios)
with KSCN	0.48; 0.32
with $Na_2S_4O_6$	0.24; 0.16

6.4.5.3 Possible oxidation of electrode to form aggressive species

Aggressive polythionic species are known to form when sulfide-covered steels are exposed to air and moisture[59]. To test the possibility that oxidation of the electrode surfaces (upon exposure to air when transferring the electrode from one electrolyte to another) contributed to anodic activation, the same polarization measurements on Type 304 stainless steel were performed in a glove box which had been flushed with high-purity nitrogen. The results (Figure 78) showed that the current spike persisted for measurements in a nitrogen atmosphere in the glove box. Figure 78 also shows that a similar current spike was observed when Type 304 stainless steel was transferred between two different containers, containing nominally identical thiocyanate-containing solutions. These results show that it is not oxidation of the electrode during transfer from one electrolyte to another, nor the identity of the second electrolyte, that is primarily responsible for the current spike. Rather, it is simply the interruption of anodic dissolution that causes subsequent more rapid dissolution.

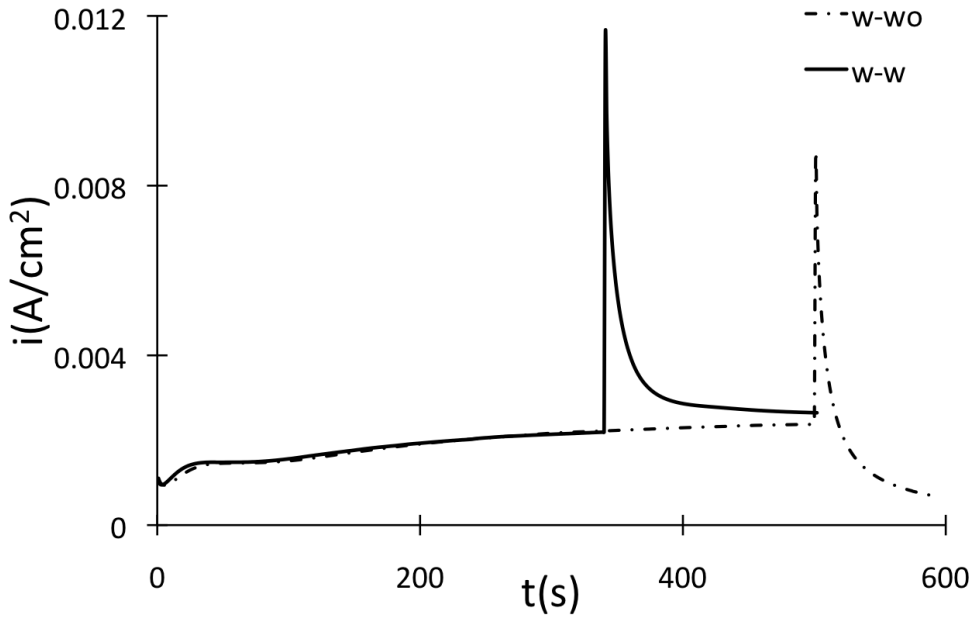

Figure 78. Current-time curves of Type 304 stainless steel polarized in 1M H_2SO_4 with 0.035mM $Na_2S_4O_6$, then transferred to 1 M H_2SO_4 (dashed line) or 1MH_2SO_4 with 0.035mM $Na_2S_4O_6$ (full line) (glove box measurements); E=-0.28$V_{Ag/AgCl}$

6.4.5.4 Interrupted anodic polarization and possible reconstruction of sulfide-covered electrode surface

The effect of interrupted anodic dissolution is illustrated in Figure 79, which gives the changes in anodic current density (for dissolution in the tetrathionate-containing solution, measured under nitrogen in the glove box) upon initial potentiostatic polarization, and following interruption of polarization for times ranging from 5s to 120s. The open-circuit potential was similar, in the range -0.39$V_{Ag/AgCl}$ to -0.41 $V_{Ag/AgCl}$ at the end of the open-circuit period, for the different durations of interruption tested here. The large differences in the current spike upon resumption of polarization hence do reflect fundamental changes in the electrode (rather than simply resulting from differences in the size of the potential change upon resumption of polarization).

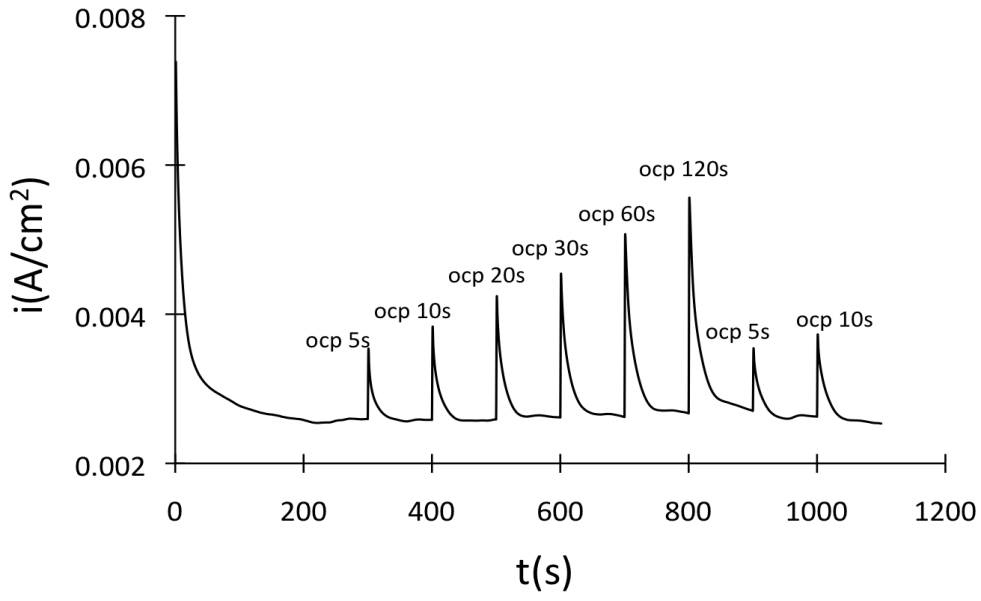

Figure 79. Current-time curves of Type 304 stainless steel polarized at -0.28$V_{Ag/AgCl}$ in 1M H_2SO_4 with 0.035mM $Na_2S_4O_6$, interrupted by periods at the open-circuit potential as indicated.

While there is no direct evidence for this, it appears possible that the change in anodic activity following interrupted dissolution may result from a surface relaxation process, perhaps related to adsorbate-induced restructuring. Adsorbate-induced restructuring has been observed for several metals and adsorbates[78][79][80][81], for example, by carbon and sulfur adsorbed on nickel, and sulfur adsorbed on Fe. Restructuring was found to occur at room temperature on time scales ranging from milliseconds to hours, giving large changes in the surface, such as changing the crystallographic orientation of the exposed metal surface[82][83]. It can be seen from Figure 79 that the peak value of the subsequent current spike increases with increased time at open circuit potential, which is as expected for a time-dependent restructuring process.

7. Conclusions

The results show that small concentrations of thiocyanate (in *p*H=2.5 sulfate solution) have little effect on the dissolution rate of pure iron, significantly accelerates dissolution of pure chromium, and has a far stronger effect on dissolution of Type 430 stainless steel. For the pure metals, thiocyanate appears to affect the rates of the dissolution reactions without any change in the dissolution steps. In contrast, the effect of thiocyanate on the alloy is different in several respects: the increase in current density is much larger, the morphology of the corroded surface is quite different, and – at the highest potential where the effect is strongest – there is an indication of an effect of thiocyanate on the actual dissolution mechanism (and not just the rate of dissolution). The origin of this effect is likely closely linked to the interaction between chromium and iron (and their oxidation products) on the surface of the corroding alloy.

These results for Type 430 stainless are broadly in agreement with the suggestions in the literature that initial signs of passivation of Fe-Cr alloys can be recognized in impedance results at potentials below the passivation potential[52], that passivation relies on inhibition – by Cr-O-Cr networks – of dissolution at ledges[68][48], and that an increase in the dissolution rate of chromium from the surface of the alloy would inhibit (or at least delay) passivation[48].

The steady-state polarization results in *p*H=0 solutions show that small concentrations of thiocyanate shifted the active-dissolution polarization curve of nickel to more negative potentials but had no obvious effect on the critical current density of nickel, increased the active dissolution rate of chromium by 3~5 times and had a significantly stronger catalytic effect on the dissolution of Type 304 stainless steel. The impedance results suggest that the catalytic effects of the dissolution rate on the electrodes are mainly due to the increased dissolution rate of the bare metal, although there are some mechanistic changes in the dissolution of chromium

and nickel. Nickel and Type 304 stainless steel develop electronically conductive sulfide corrosion products during active dissolution in the thiocyanate-containing solution.

As proposed for Type 430 stainless steel, the catalytic effect of thiocyanate on anodic dissolution of Type 304 stainless steel also appears to be primarily caused by the increased dissolution rate of chromium, counteracting the formation of the Cr-O-Cr passivating network at ledges. This is in line with the SEM results of corroded surfaces and surface composition analysis by XPS. Nickel, as a more slowly dissolving element than iron, does contribute to the corrosion resistance of Type 304 stainless steel[84], but its beneficial effect appears to be secondary to that of chromium: while the anodic polarization behavior of nickel in thiocyanate-containing solutions is similar for *p*H=2.5 and *p*H=0, the active corrosion behavior of Type 304 stainless steel differs greatly between these two solutions.

Surface analysis of a Fe20Cr alloy and stainless steels (Types 430 and 304) confirmed that chromium enriched on the metal surface during anodic dissolution in thiocyanate-free solution and that the surface enrichment of chromium was smaller in thiocyanate-containing solution. This is in line with the proposed fundamental effect of thiocyanate: thiocyanate increases the dissolution rate of chromium, counteracting the formation of the passivating Cr-O-Cr network. Surface analysis also confirmed the formation of sulfide or adsorbed sulfur on the Fe20Cr alloy, when thiocyanate was present in the solution.

Due to the strong affinity of nickel and copper for sulfur, sulfides of these metals formed on the Type 304 and Type 430 steel surfaces during anodic dissolution in thiocyanate-containing electrolytes. The resulting sulfide product had several effects on these measurements. One of these was the observation of increased anodic current density ("spike") lasting several tens of seconds (for Type 304 stainless steel, and nickel); the spike occurred whenever polarization was interrupted, even for only 5 seconds. The likely origin of the increased current density is relaxation (restructuring) of the sulfide-covered metal surface when dissolution ceased.

8. Possible Future work

Percolation Theory

As mentioned previously, nickel contributes significantly to the corrosion resistance of Type 304 stainless steel (with regards to active corrosion); the proposed mechanism is that nickel lowers the percolation limit of chromium needed to passivate the steel. The proposed effect of nickel on the percolation limit of chromium is just a conjecture at this stage. Also not known is how the early stages of passivation - occurring during active dissolution - are affected by the presence of nickel, and whether the same percolation ideas can be used to understand the strong effect of nickel on the critical current density of stainless steels. This appears to be a potentially fruitful area of study, which could be approached through a combination of simulation and experimental work. Copper, as another relatively noble element, is expected to have a similar effect to nickel. The dissolution of steel with different contents of nickel, copper and chromium could be simulated using a percolation model.

Experimentally, dissolution behavior of steels with specific compositions (varying the content of chromium, nickel or copper) could be investigated to test the simulation results. The fundamental importance of such an investigation would be to understand how the active (or pre-passive) corrosion of stainless steel is changed by alloying and by environmental effects (such as temperature, and the presence of aggressive species such as reduced sulfur compounds).

9. Appendix

9.1 Discussion of Keddam's model for anodic dissolution of binary Fe-Cr alloys

9.1.1 Model description

Keddam and his coworkers[52] proposed a model for active dissolution of binary Fe-Cr alloys, as already shown in Figure 19.

The individual reaction steps of the model are as follows:

$$Fe \xrightarrow{k_1} Fe(I)_{ad} + e^- \quad \text{..... (1)}$$

$$Fe(I)_{ad} \xrightarrow{k_2} Fe(II)_{soln} + e^- \quad \text{..... (2)}$$

$$Fe(I)_{ad} \xleftrightarrow{k_3} Fe^*(I)_{ad} \quad \text{..... (3)}$$

$$Fe^*(II)_{ad} + Fe \xrightarrow{k_4} Fe^*(II)_{ad} + Fe(II)_{soln} + 2e^- \quad \text{..... (4)}$$

$$Fe^*(I)_{ad} \xleftrightarrow{k_5} Fe^*(II)_{ad} + e^- \quad \text{..... (5)}$$

$$Cr \xrightarrow{q_1} Cr(I)_{ad} + e^- \quad \text{..... (Cr-1)}$$

$$Cr(I)_{ad} \xrightarrow{q_2} Cr(II)_{soln} + e^- \quad \text{..... (Cr-2)}$$

$$Cr(I)_{ad} + Cr \xleftrightarrow{q_3} Cr(I)_{ad} + Cr(II)_{ad} + 2e^- \quad \text{..... (Cr-3)}$$

At steady state, surface coverages of adsorbed intermediates (θ_1 to θ_5) are constant. The dissolution rate of Fe is equal to the sum of the rates of reaction (1) and (4) and the dissolution rate of Cr is equal to rate of reaction (Cr-1). At steady state, the ratio in which the elements go into solution must equal the elemental ratio in the bulk alloy, which gives the following equation:

$$\frac{rate_1 + rate_4}{rate_{\text{Cr-1}}} = \frac{\gamma}{1-\gamma} \quad \text{(A)}$$

where γ is the mole fraction of Fe in the bulk alloy. The rates of these reactions are given by:

$$rate_1 = k_1\gamma_0\left[1-(\theta_1+\theta_2+\theta_3+\theta_4+\theta_5)\right] \quad \text{(B)}$$

$$rate_4 = k_4\theta_3\left(1-\sqrt{\theta_5}\right) \quad \text{(C)}$$

$$rate_{Cr^{3+}} = q_1(1-\gamma_0)\left[1-(\theta_1+\theta_2+\theta_3+\theta_4+\theta_5)\right] \quad \text{(D)}$$

where γ_0 is the mole fraction of Fe at the surface of the dissolving alloy; $[1-(\theta_1+\theta_2+\theta_3+\theta_4+\theta_5)]$ gives the fraction of bare metal surface.

9.1.2 Model testing

This model was tested using steels with 2 different compositions (Fe-22%Cr and Fe-17% Cr). The rate constants for Fe-22% Cr were given by Keddam et al. and rate constants for Fe-17%Cr were estimated by interpolation; estimated values are given in Table 12.

Table 12. Estimated rate constants for 17% Cr alloy

i	1	2	3	-3	5	-5	4	**i**	1	2	3	-3
$\mathbf{k_{0i}}$	8.08E7	2E-3	8.08E-9	5.2E-20	2.73E+5	1.78E-11	5.22E-8	$\mathbf{q_{0i}}$	2.32E11	3E-3	2.42E-2	6.12E-15
$\mathbf{b_i}$	38.4	7	0	30	35.4	3	2	$\mathbf{l_i}$	38.4	10	19.2	19.2

Calculated steady state results are shown in Figure 80a and the results obtained by Keddam are shown in Figure 80b. The calculated result for Fe-22%Cr agrees with the result reported by Keddam, and the calculated result for Fe-17% shows the right trend of a higher critical current density and more positive passive potential at a lower Cr content.

a) b)

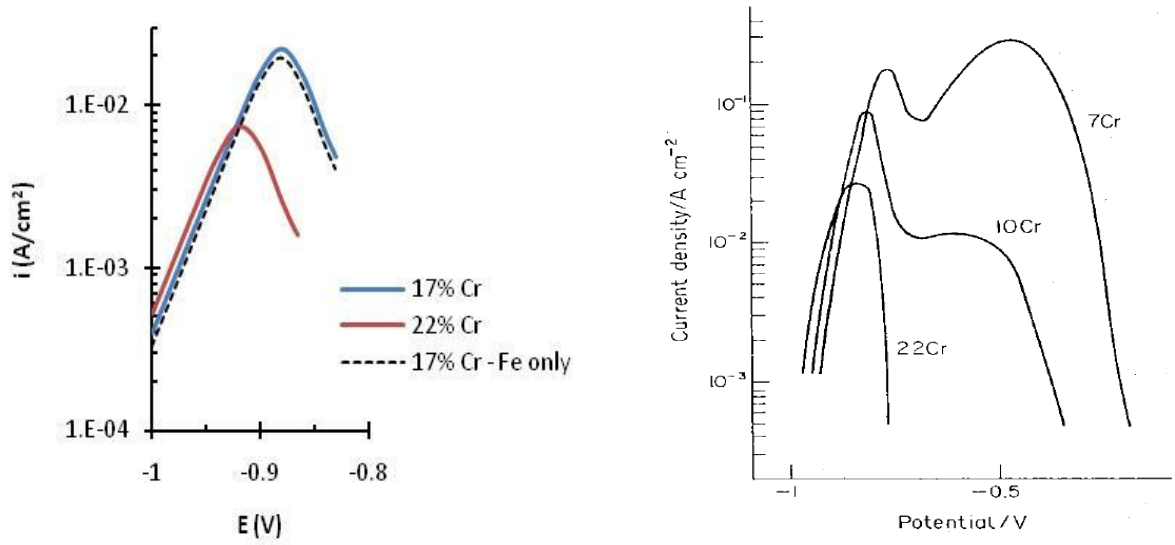

Figure 80. a) Calculated steady-stated current density for dissolution in pH=0 sulfuric acid, compared with b) the simulated curves reported by Keddam et al.

Although this model gives reasonable steady state current density results, some of the model predictions indicate some serious difficulties with the model: the prediction of the surface concentration of iron (γ_0) is larger than 0.9999 over most of the active potential range. This means the surface is nearly pure Fe, which contradicts the experimental data reported by Knote et al.[54], which indicated that Cr enriched on the surface because of the preferential dissolution of Fe.

To confirm the calculated surface composition, a simplified method was used to estimate the surface composition. Calculation results show that the rate of reaction (4) is very small compared with the rate of reaction (1) over the most of the potential range and the surface coverages of adsorbed species are much smaller than 1 over most of the potential range upon the passivation, as shown in Figure 81.

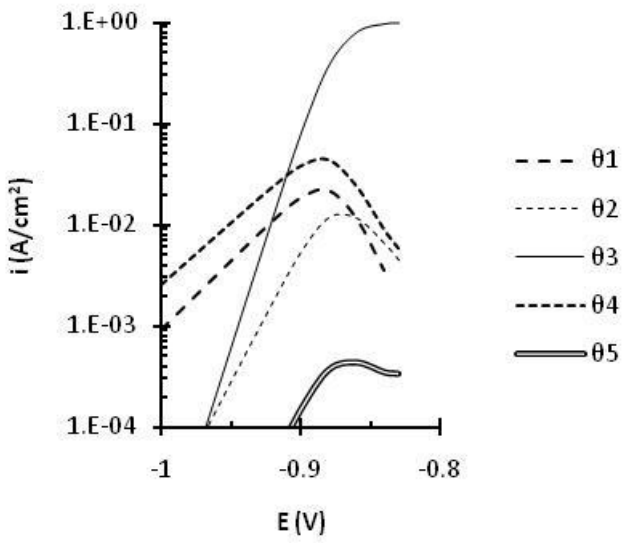

Figure 81. Calculated potential dependence of the surface coverage by adsorbed species, for the Fe-17% Cr alloy.

For the case where reaction (4) is negligible compared with reaction (1), equation (A) can be simplified as follows:

$$\frac{rate_1 + rate_4}{rate_{Cr^{+3}}} = \frac{\gamma}{1-\gamma} \approx \frac{rate_1}{rate_{Cr^{+3}}} = \frac{k_1\gamma_0}{q_1(1-\gamma_0)} \quad \Rightarrow \gamma_0 \approx \frac{1}{\frac{k_1}{q_1}\left(\frac{1-\gamma}{\gamma}\right)+1}$$

According to Table 6, q_1 is much larger than k_1 and for Fe-17%Cr $(1-\gamma)/\gamma=0.2$. Based on these simplifications, the result for γ_0 is approximately 1. Both the calculations based on the full model and the simplified method give the same result: the surface of the dissolving alloy is predicted to be essentially pure Fe.

The predicted near-zero Cr surface concentration is caused by the inherent features of the model formulation and it also leads to the inevitable (wrong) conclusion that Cr could have no effect on the dissolution of iron. To test the conclusion, the model-predicted current densities of the alloy were calculated using only Fe reactions (reaction (1) to (5)) without

involving Cr. The polarization curve is shown in Figure 80a, which is very close to the curve calculated with all the reaction steps in the model.

Although the model can successfully describe the effect of Cr on the steady state polarization behavior, it does not necessarily mean that it models the interactions between Cr and Fe correctly. On the contrary, by allowing the reaction constant of Fe dissolution to depend on Cr content, the model manages to model the right effect of Cr on the polarization behavior (polarization curve is shifted to more negative potentials with larger Cr content). In this case, the model needs different reaction constants of Fe dissolution for alloys with different contents of Cr, which does not successfully indicate the nature of Fe-Cr interaction. The prediction of the model contradicts its premise: it is assumed that Fe dissolution rate depends on Cr content even thought the model predicts that there is no Cr on the alloy surface during active dissolution (shown in Figure 82).

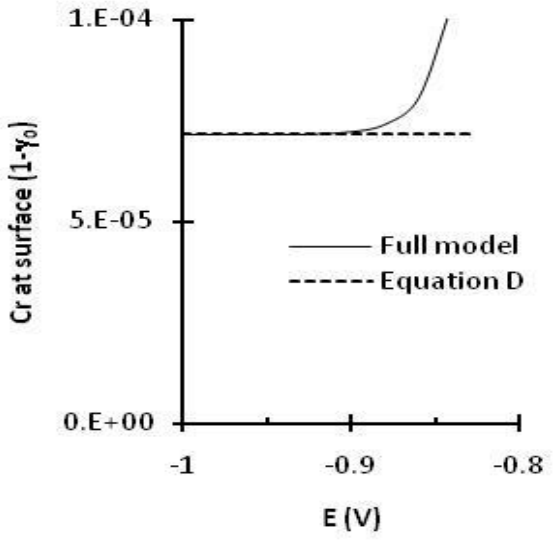

Figure 82. Comparison of the predicted steady-state Cr concentration at the surface of the alloy, as calculated with the full model, and with the approximate expression ("Equation D").

9.2 Mercury Contact

The mercury contact was used to lower the noise in the impedance tests caused by using a rotating electrode with a sliding silver-carbon contact. The sketch of the system is shown in Figure 83. The mercury contact is connected to the shaft by the shaft connector and the working electrode attached to the other end of the shaft. The motor of the standard electrode rotator was used to rotate the electrode; a drive roller (placed where the rotating electrode would normally be placed, at the end of the rotator), was used to transmit the rotation speed to another drive roller immediately below the mercury contact. The mercury contact system was attached with a Nylon bearing block to a specially manufactured aluminum holder. A photograph of the system is shown in Figure 84.

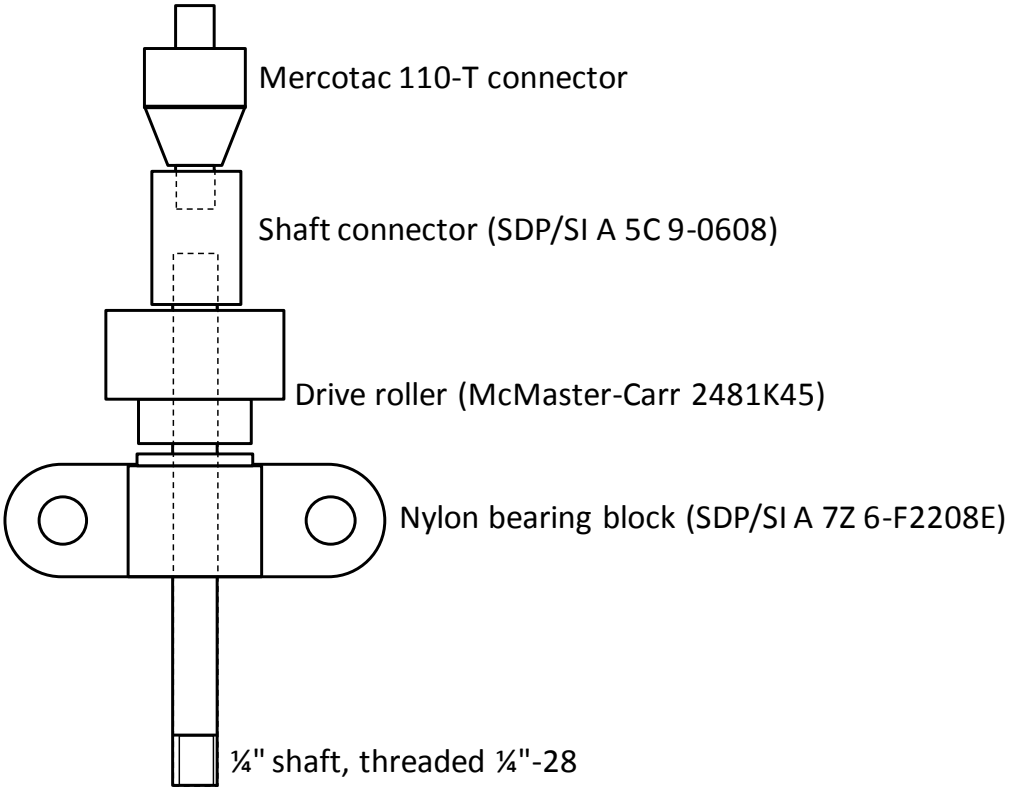

Figure 83. Sketch of parts of the mercury contact system of rotating electrode.

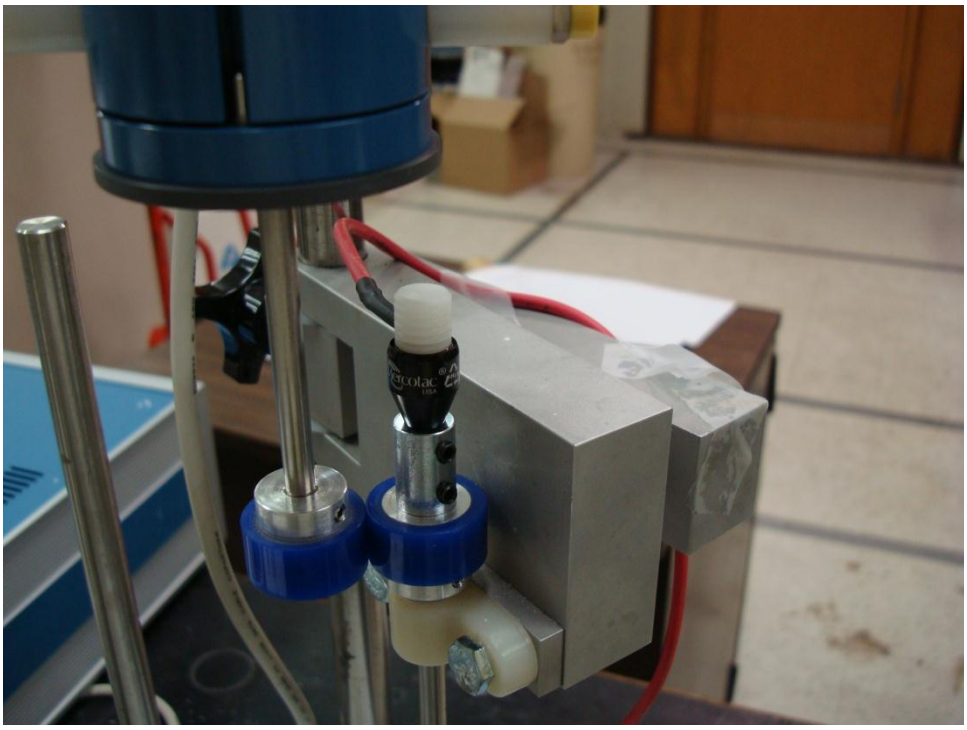

Figure 84. Photograph of rotating electrode with mercury contact.

9.3 Current - time curves of the potentiostatic measurements of Fe, Cr and type 430ss in sulfuric acid at pH2.5

The potentiostatic polarization curves of Fe, Cr and Type 430ss are shown in Figure 39; the corresponding current-time curves are shown in Figure 85, 86 and 87.

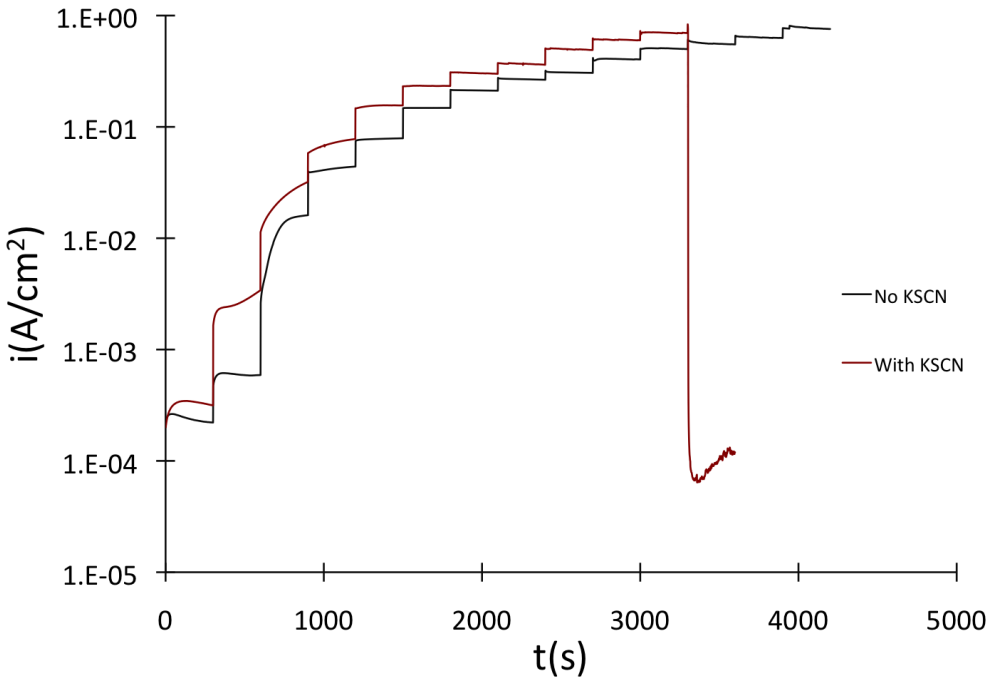

Figure 85. The current-time curves of pure Fe in sulfate solution with/without thiocyanate at pH=2.5.

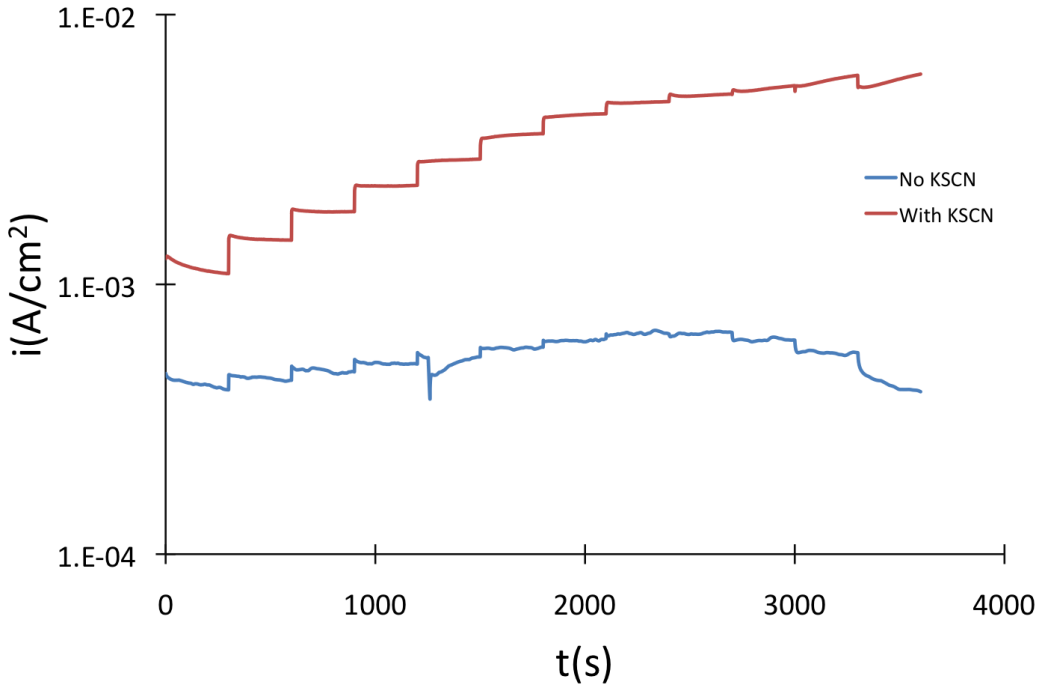

Figure 86. The current-time curves of pure Cr in sulfate solution with/without thiocyanate at pH=2.5.

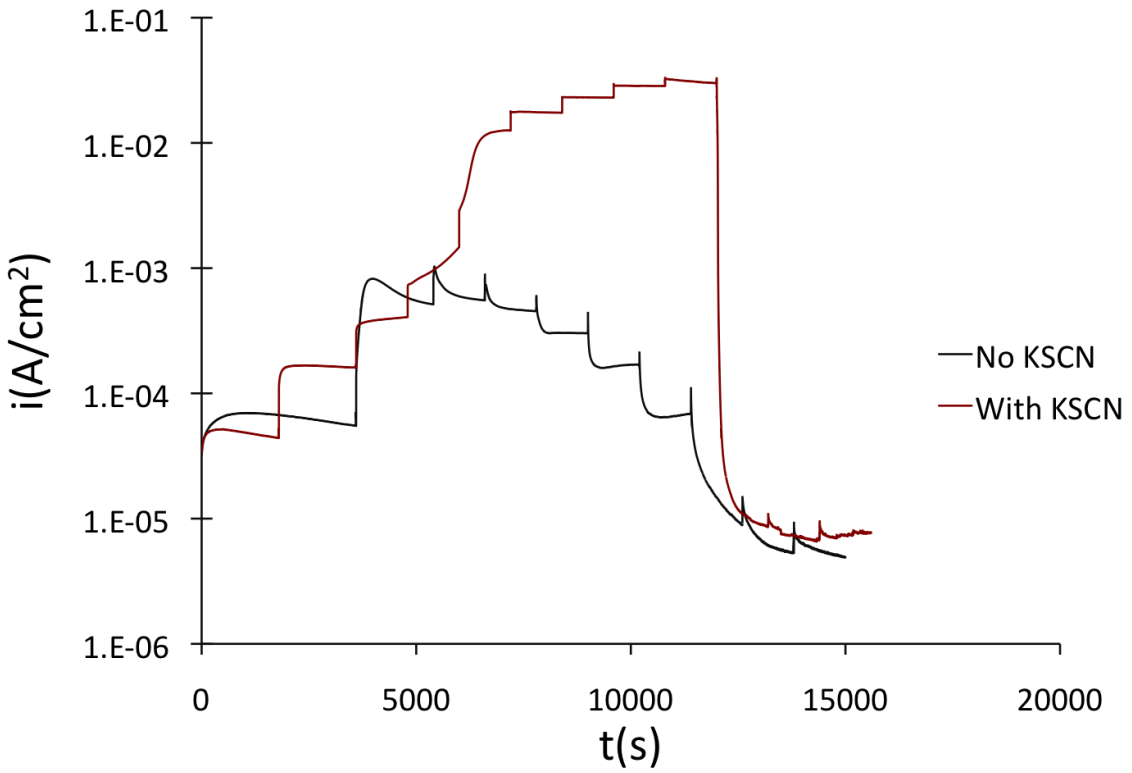

Figure 87. The current-time curves of type 430ss in sulfate solution with/without thiocyanate at pH=2.5.

9.4 The effect of thiocyanate on pure Fe at pH5

When pH=5, effect of thiocyanate on the dissolution of Fe is similar to the effect of thiocyanate on the dissolution of Fe in the solution of pH2.5. Thiocyanate inhibited dissolution of Fe at more negative potentials and promoted dissolution at less negative potentials. The dissolution rate of Fe at potentials close to the peak was controlled by a salt film on the surface and effect of thiocyanate was masked by the salt film. However, it can be seen that Fe dissolves faster at higher pH in the low potential range (below -0.5V).

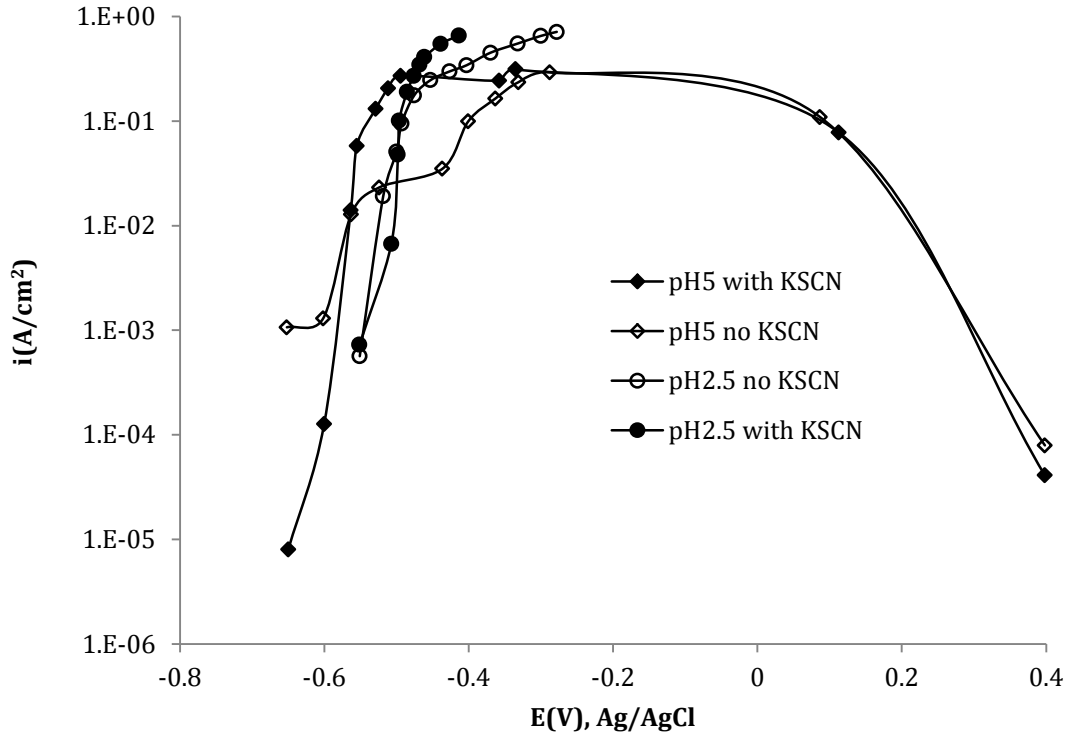

Figure 88. Potentiostatic polarization curves of Fe in Na_2SO_4 + H_2SO_4 with different concentrations of thiocyanate (0, 0.14mM) at different pH values (1M SO_4^{2-} in all cases).

9.5 XPS spectrum of electrodes

Examples of XPS spectra (survey scans and detail of sulfur 2p peak) of corroded electrodes are shown in the following figures.

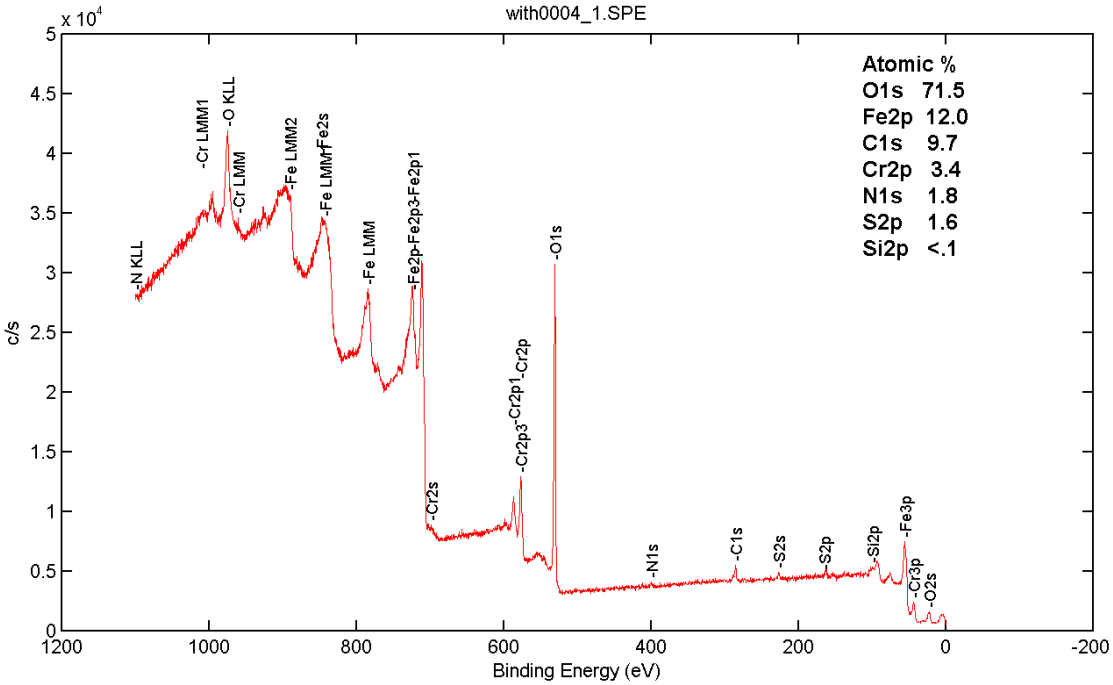

Figure 89. XPS spectrum of Fe20Cr after anodic dissolution in 1 M Na_2SO_4, 0.01 M H_2SO_4 (pH=2.5) with 0.14mM KSCN; E=-0.41$V_{Ag/AgCl}$

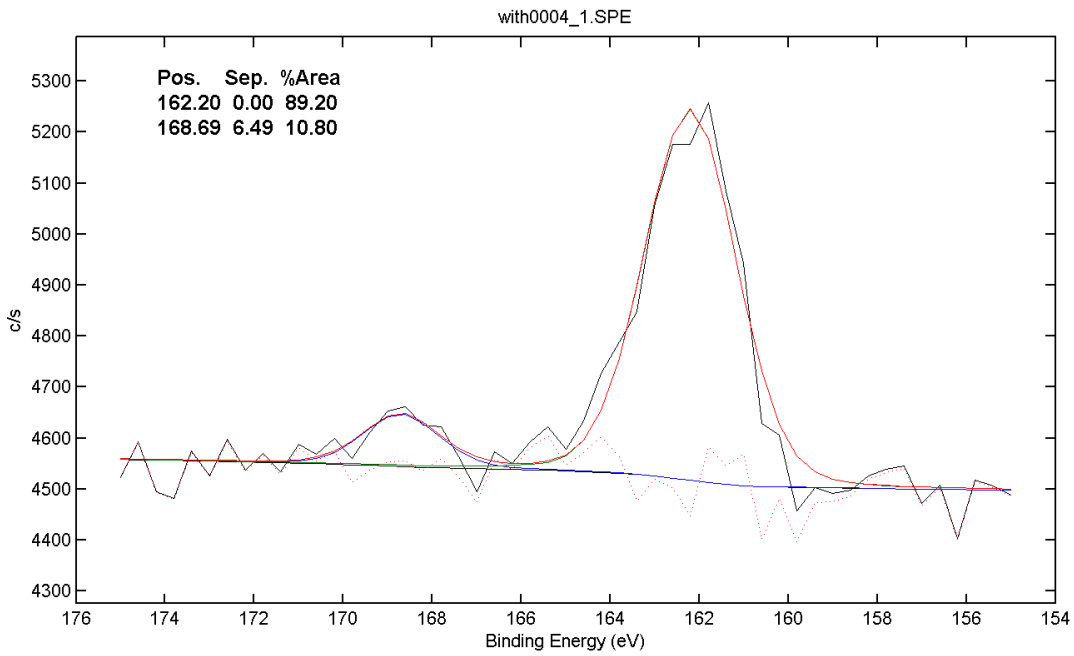

Figure 90. XPS spectrum of sulfur peak of Fe20Cr after anodic dissolution in 1 M Na_2SO_4, 0.01 M H_2SO_4 (pH=2.5) with 0.14mM KSCN; E=-0.41$V_{Ag/Ag}$

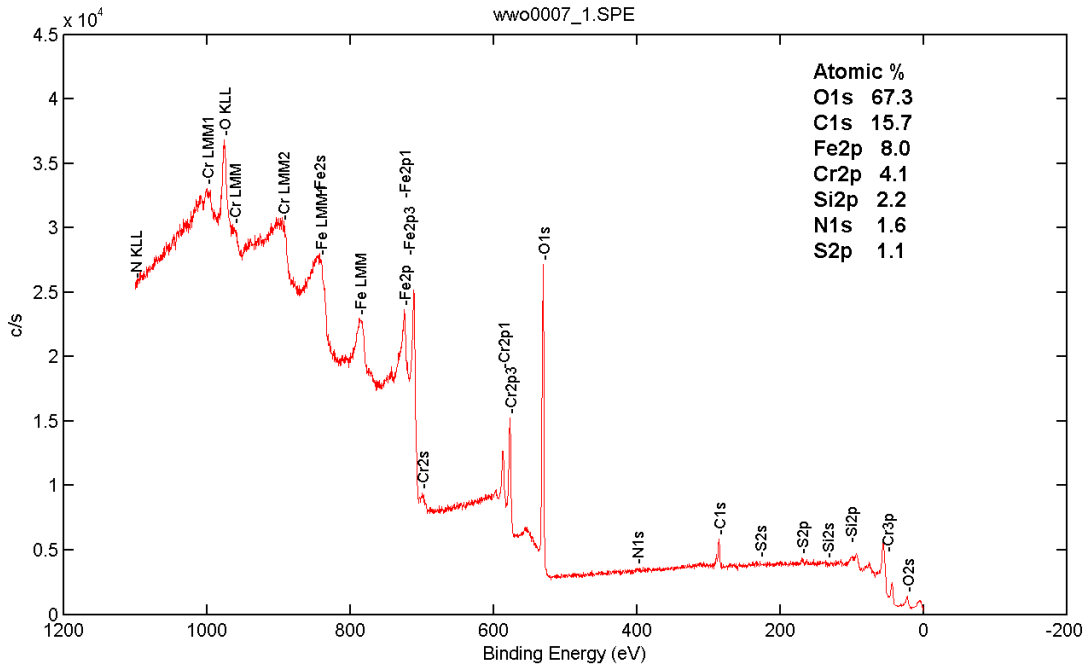

Figure 91. XPS spectrum of Fe20Cr after anodic dissolution in 1 M Na_2SO_4, 0.01 M H_2SO_4 (pH=2.5) with 0.14mM KSCN followed by transfer to KSCN-free solution; E=-0.41$V_{Ag/AgC}$

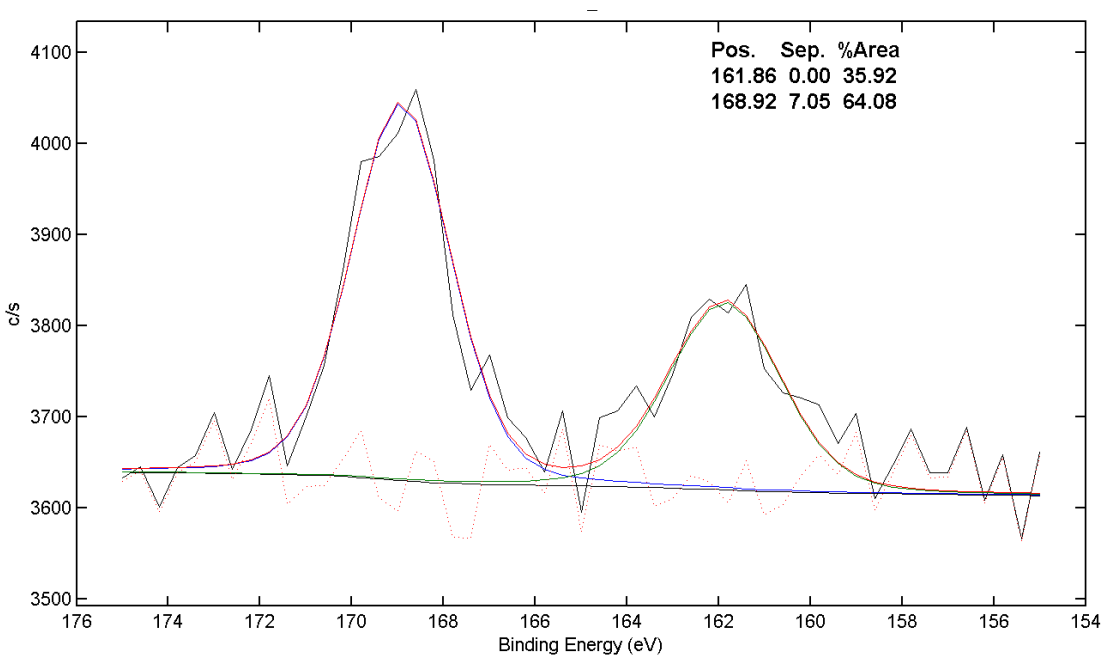

Figure 92. Sulfur peaks of Fe20Cr after anodic dissolution in 1 M Na_2SO_4, 0.01 M H_2SO_4 (pH=2.5) with 0.14mM KSCN followed by transfer to KSCN-free solution; E=-0.41$V_{Ag/AgCl}$

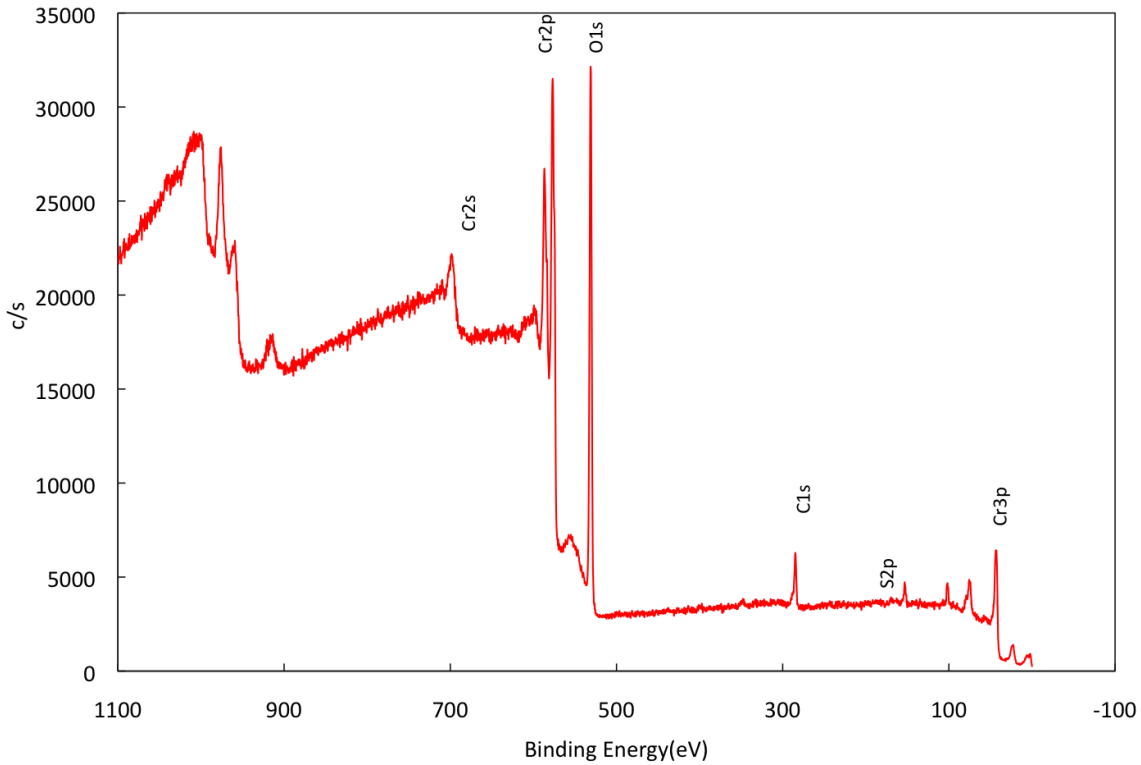

Figure 93. XPS spectrum of Cr after anodic dissolution in 1 M Na_2SO_4, 0.01 M H_2SO_4 (pH=2.5) with 0.14mM KSCN; E=-0.7 $V_{Ag/AgCl}$

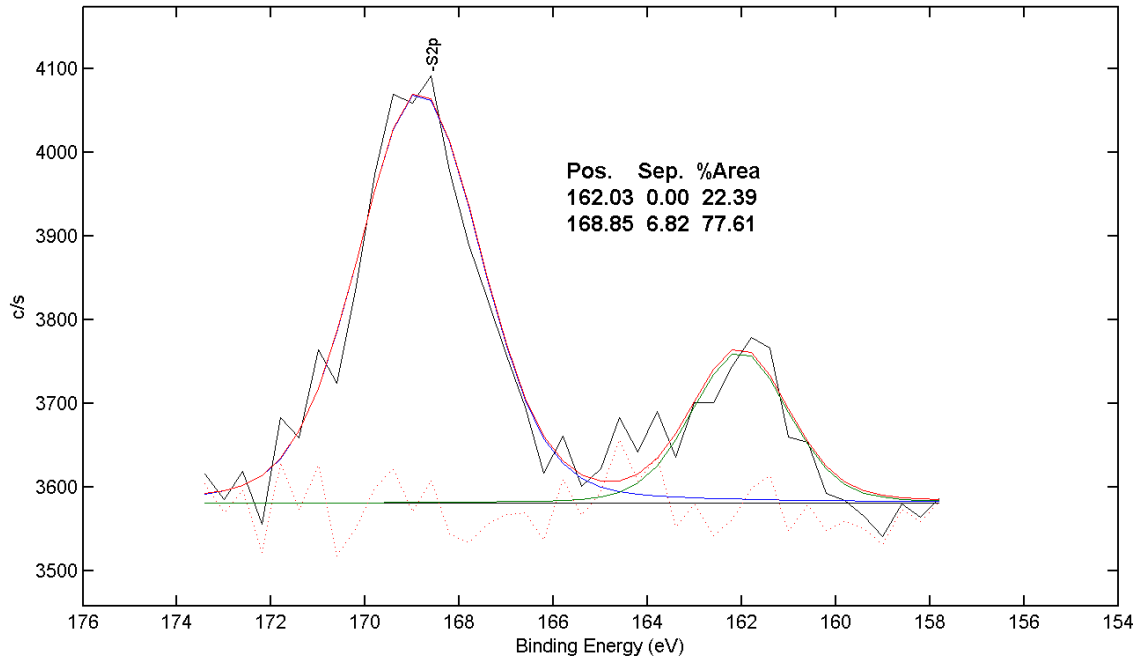

Figure 94. Sulfur peaks of Cr after anodic dissolution in 1 M Na_2SO_4, 0.01 M H_2SO_4 (pH=2.5) with 0.14mM KSCN; E=-0.7 $V_{Ag/AgCl}$

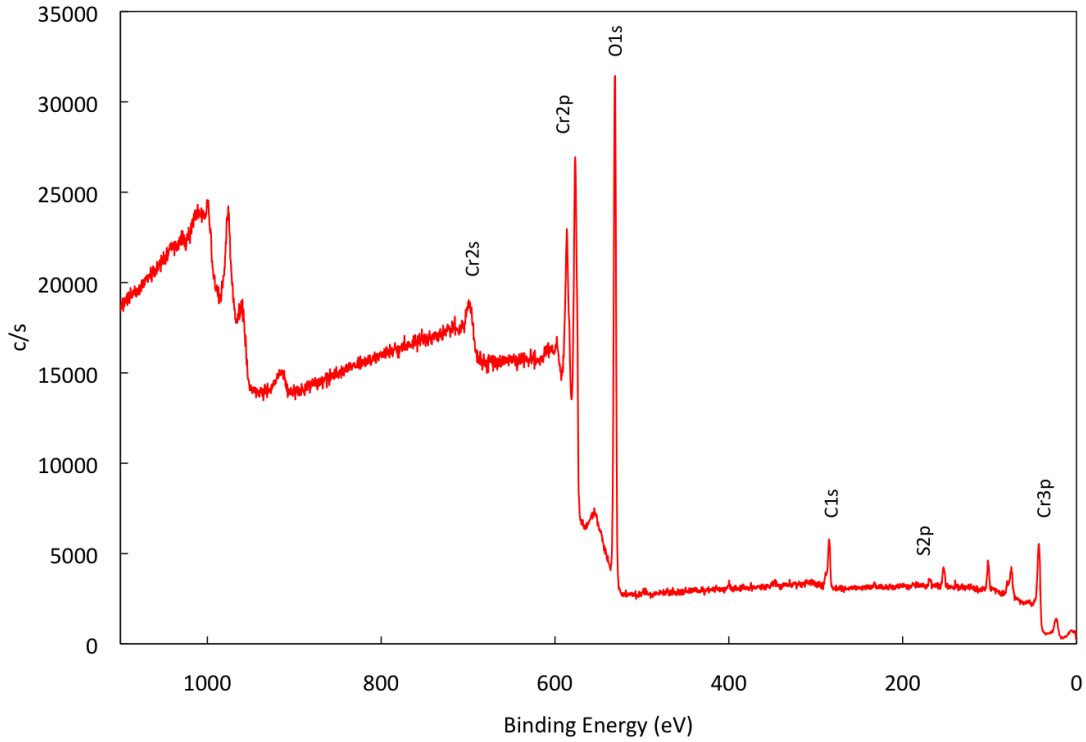

Figure 95. XPS spectrum of Cr after anodic dissolution in 1 M Na_2SO_4, 0.01 M H_2SO_4 (pH=2.5) with 0.14mM KSCN followed by transfer to KSCN-free solution; E=-0.7$V_{Ag/AgCl}$

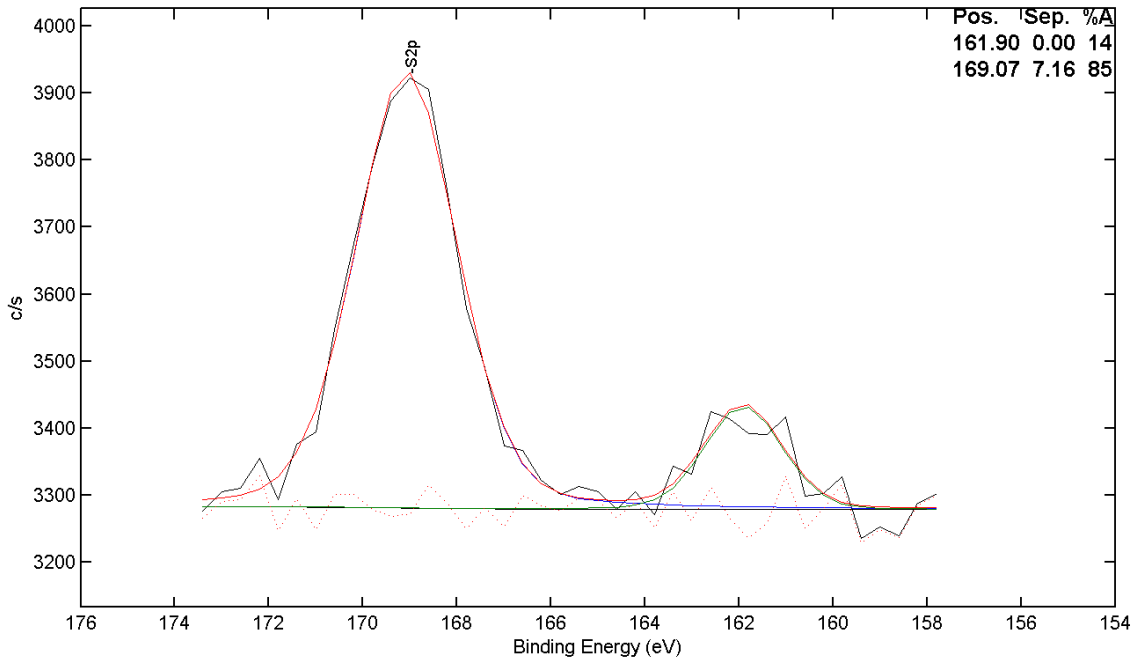

Figure 96. Sulfur peaks of Cr after anodic dissolution in 1 M Na_2SO_4, 0.01 M H_2SO_4 (pH=2.5) with 0.14mM KSCN followed by transfer to KSCN-free solution; E=-0.7$V_{Ag/AgCl}$

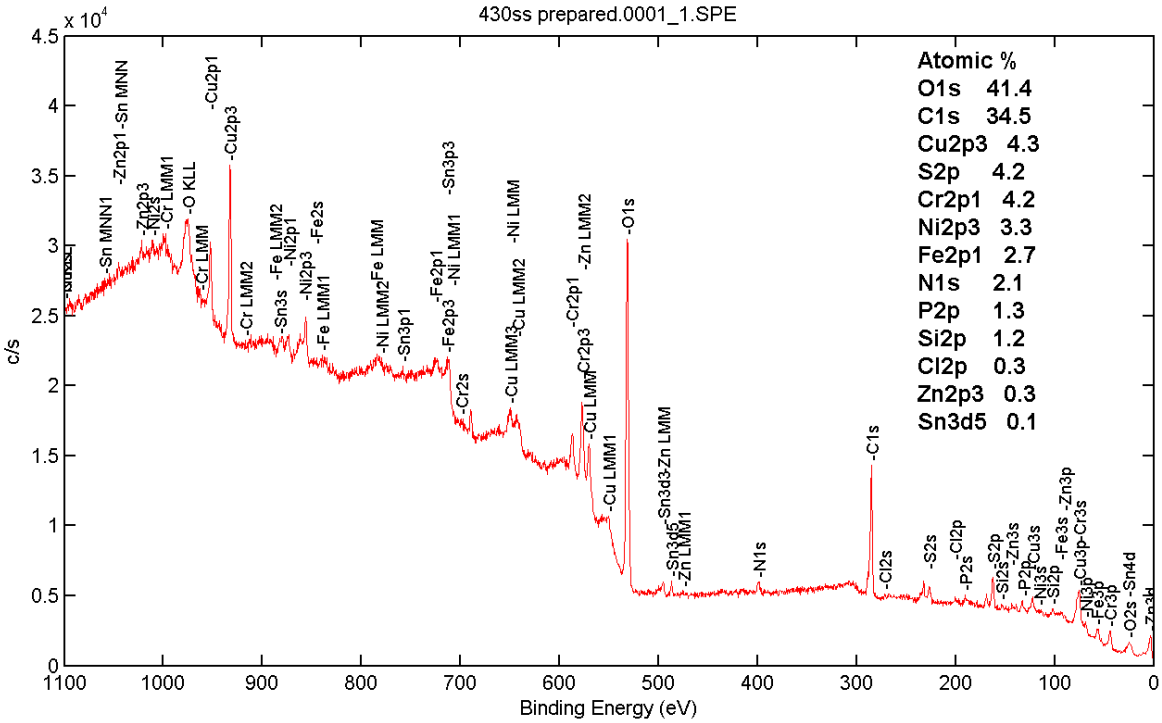

Figure 97. XPS spectrum of Type 430 stainless steel after dissolution in 1 M Na_2SO_4, 0.01 M H_2SO_4 (pH=2.5) with 0.14mM KSCN-containing solution followed by transfer to KSCN-free solution; E=-0.41$V_{Ag/AgCl}$.

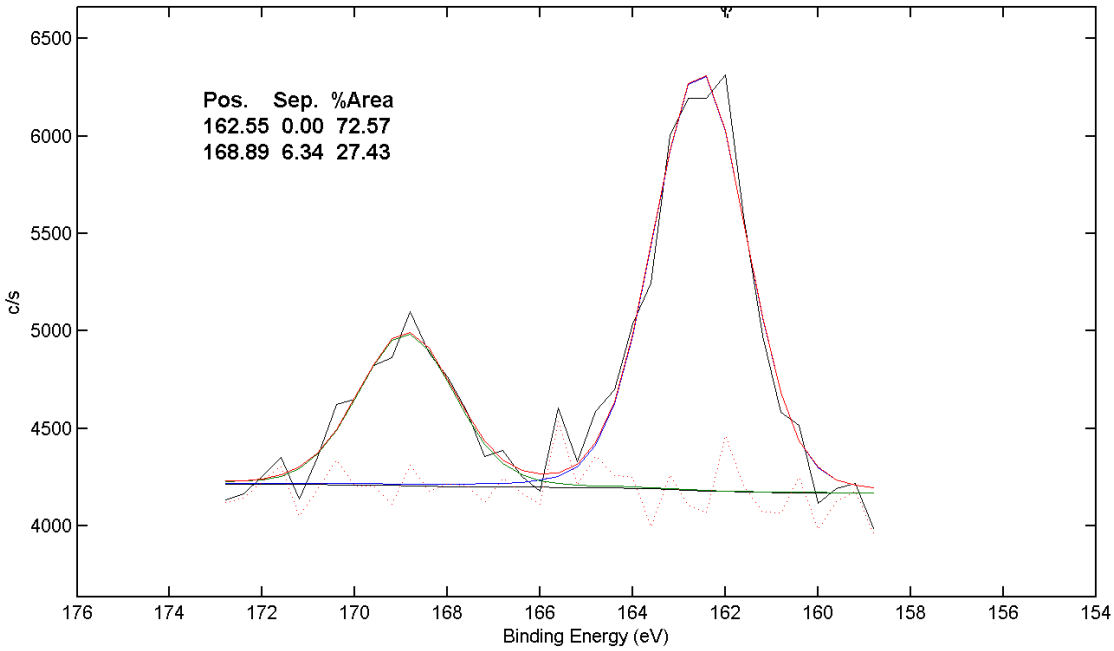

Figure 98. Sulfur peaks of Type 430 stainless steel after dissolution in 1 M Na_2SO_4, 0.01 M H_2SO_4 (pH=2.5) with 0.14mM KSCN-containing solution followed by transfer to KSCN-free solution; E=-0.41$V_{Ag/AgCl.}$

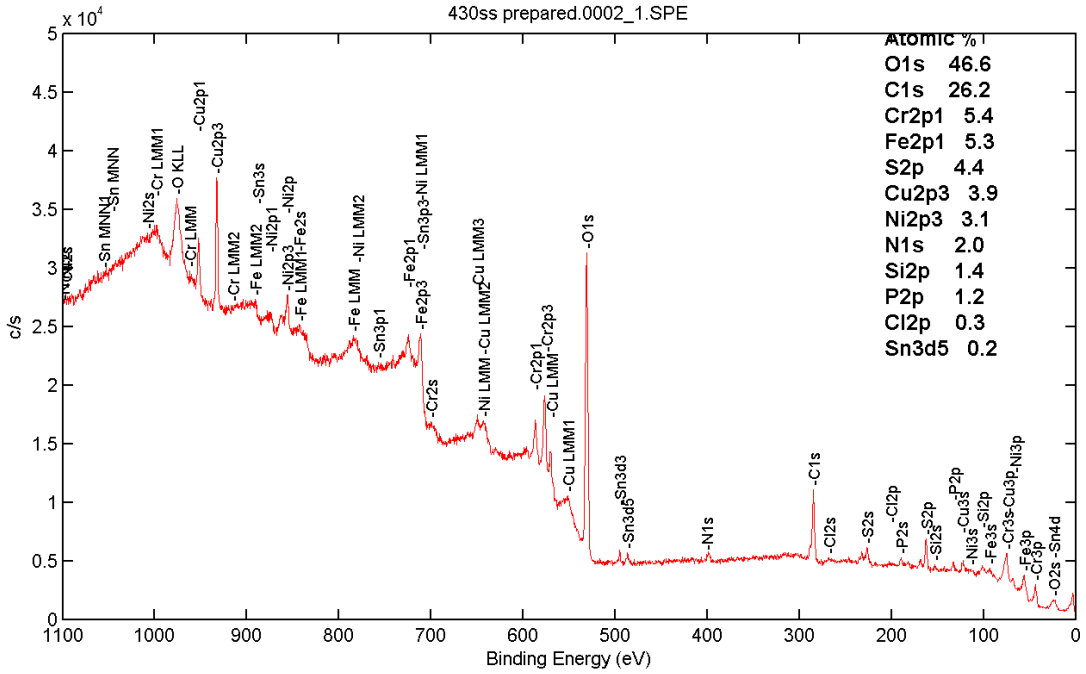

Figure 99. XPS of Type 430 stainless steel after dissolution in 1 M Na_2SO_4, 0.01 M H_2SO_4 (pH=2.5) with 0.14mM KSCN only; E=-0.41$V_{Ag/AgCl}$

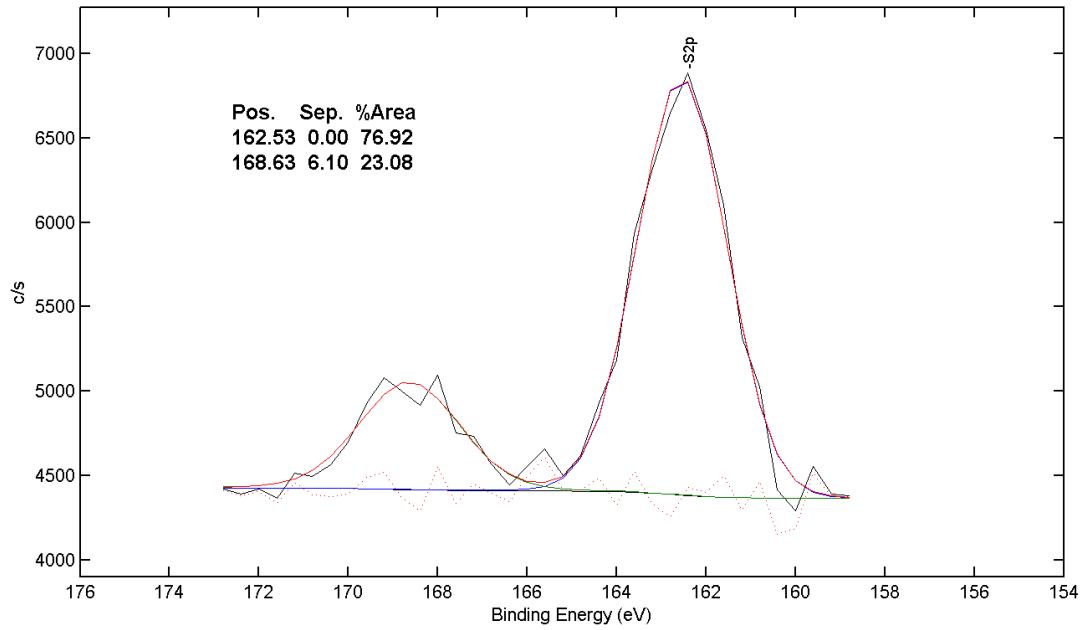

Figure 100. Sulfur Peaks of Type 430 stainless steel after dissolution in 1 M Na_2SO_4, 0.01 M H_2SO_4 (pH=2.5) with 0.14mM KSCN only; E=-0.41$V_{Ag/AgCl}$

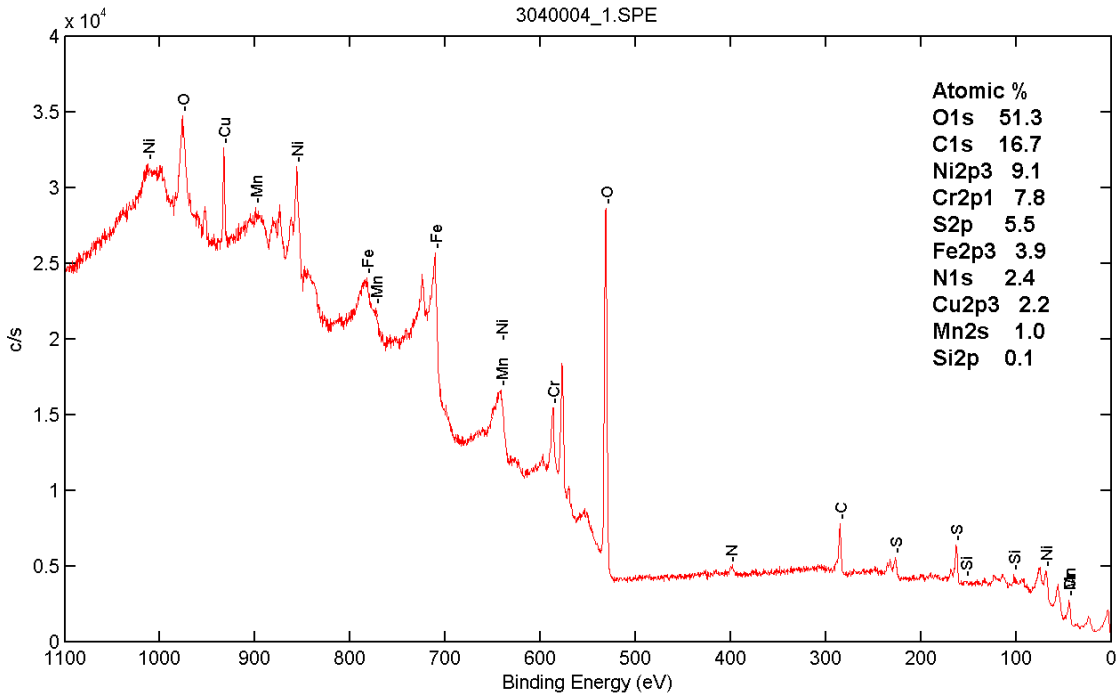

Figure 101. XPS spectrum of Type 304 stainless steel after anodic dissolution in 1M H_2SO_4 (pH=0) with 0.14mM KSCN only; E=-0.28$V_{Ag/AgCl}$

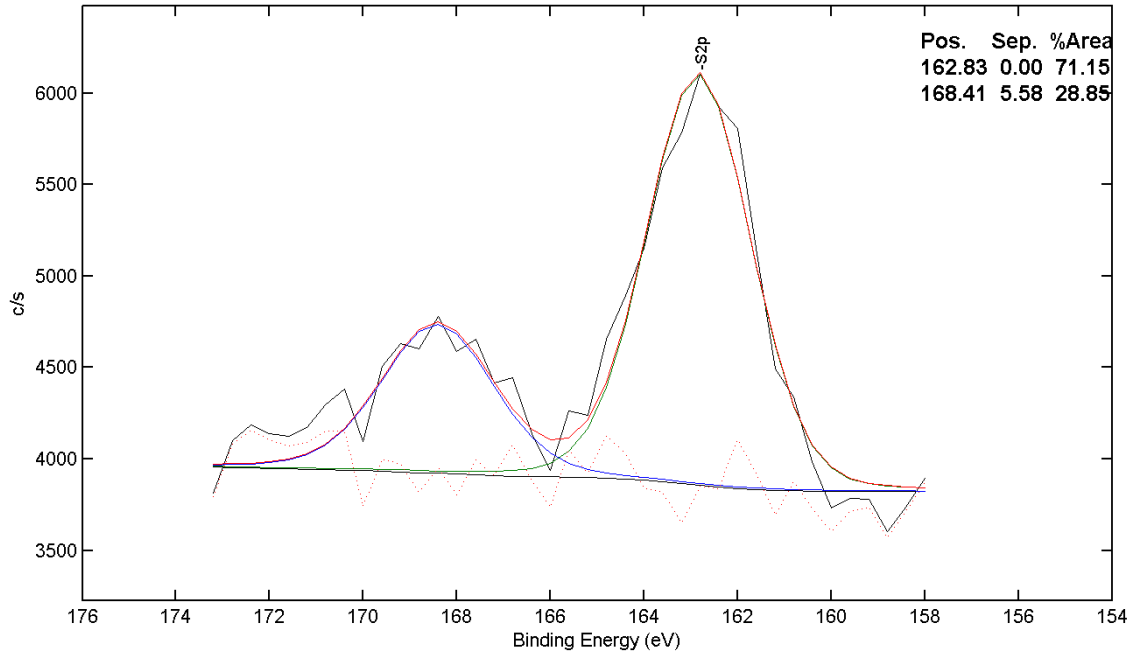

Figure 102. Sulfur peaks of Type 304 stainless steel after anodic dissolution in 1M H_2SO_4 (pH=0) with 0.14mM KSCN only; E=-0.28$V_{Ag/AgCl}$

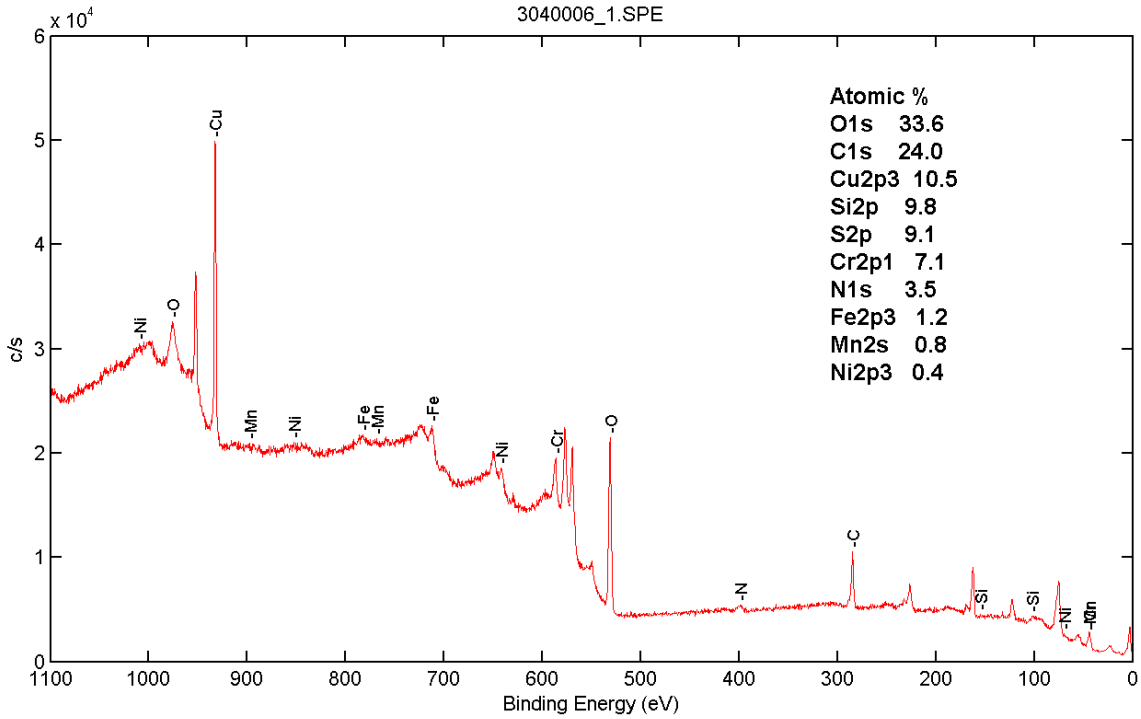

Figure 103. XPS spectrum of Type 304 stainless steel after anodic dissolution in 1M H_2SO_4 (pH=0) with 0.14mM KSCN solution followed by transfer to KSCN-free solution; E=-0.28$V_{Ag/AgCl}$

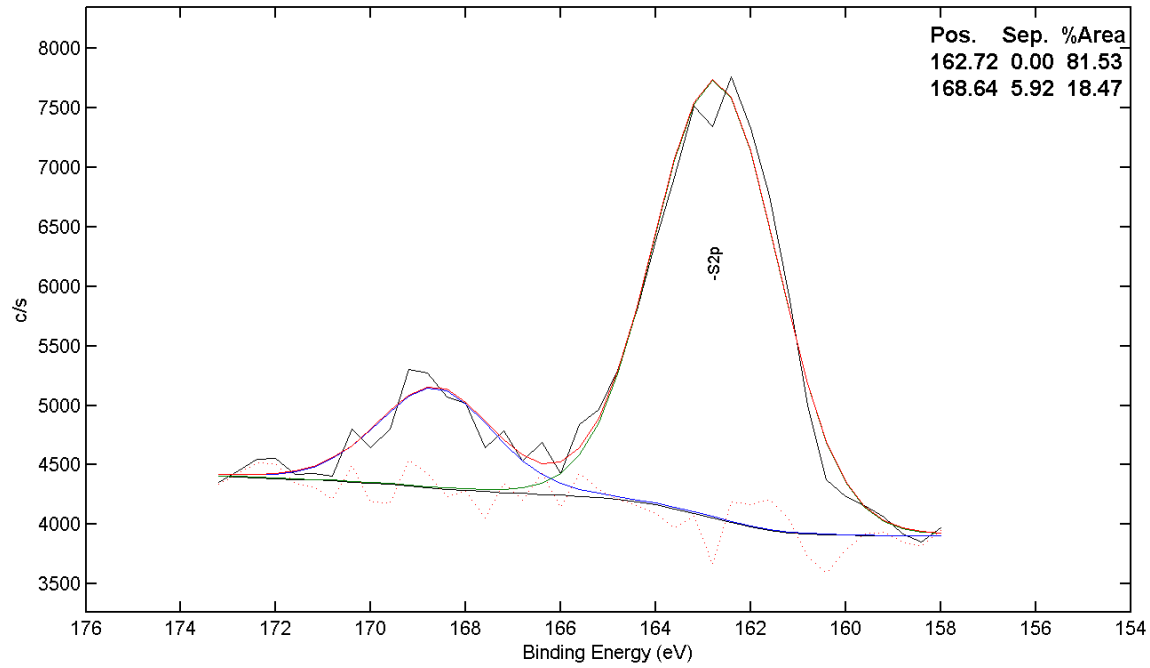

Figure 104. Sulfur peaks of Type 304 stainless steel after anodic dissolution in 1M H_2SO_4 (pH=0) with 0.14mM KSCN solution followed by transfer to KSCN-free solution; E=-0.28$V_{Ag/AgCl}$

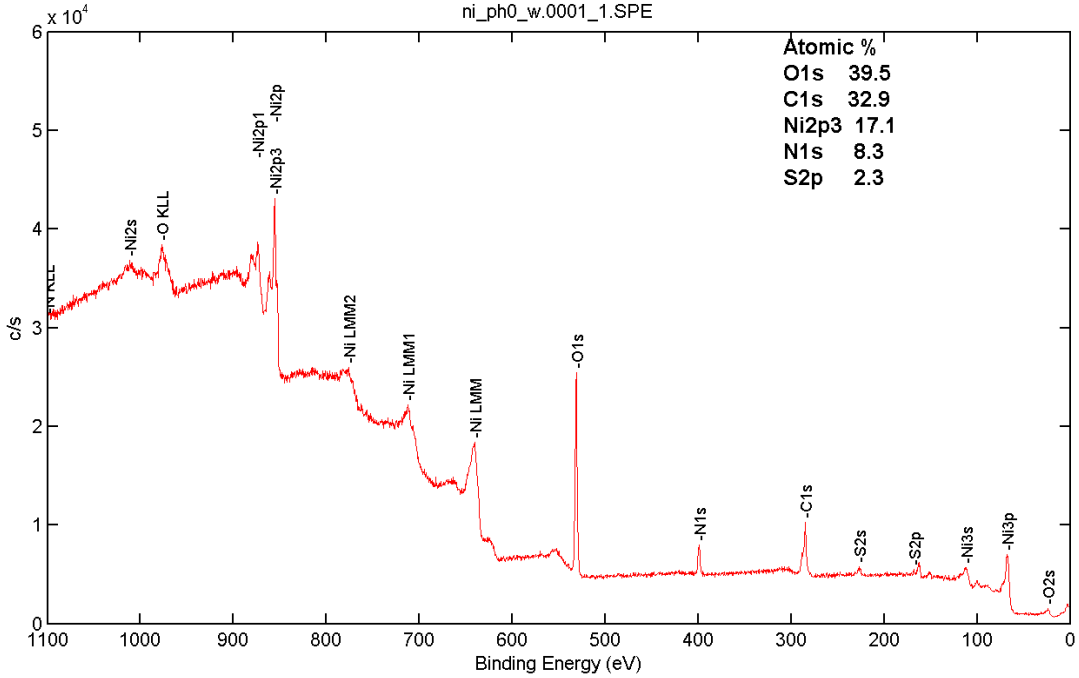

Figure 105. XPS spectrum of nickel surface after dissolution in 1 M H_2SO_4 with 0.14mM KSCN; i=1.5mA/cm²; t=400s

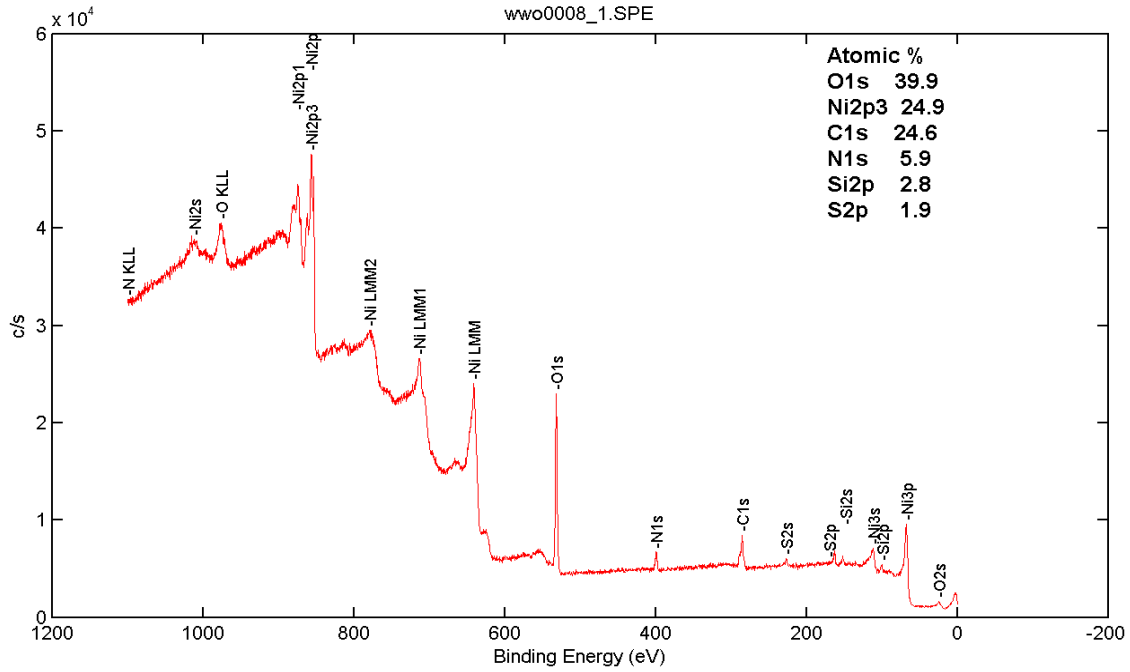

Figure 106. XPS spectrum of nickel surface after dissolution in 1 M H_2SO_4 with 0.035mM $Na_2S_4O_6$; i=1.5mA/cm²; t=400s

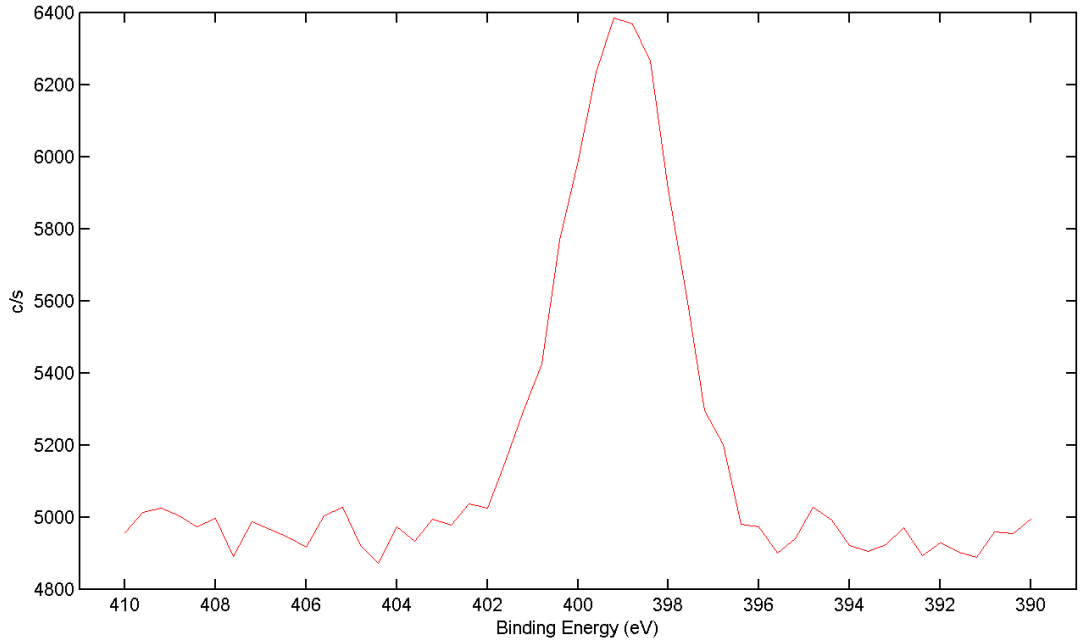

Figure 107. Nitrogen peak of nickel surface after dissolution in 1 M H_2SO_4 with 0.035mM $Na_2S_4O_6$; i=1.5mA/cm²; t=400s

10. References

[1] P.C. Pistorius And H. Möller, "Effect of Solution Composition on Anodic Behaviour of Type 316 Stainless Steel In Synthetic Eluate," *Unpublished Consultation Report*, 2006.

[2] H. Ma, X. Cheng, S. Chen, C. Wang, J. Zhang And H. Yang, "An Ac Impedance Study of The Anodic Dissolution of Iron In Sulfuric Acid Solutions Containing Hydrogen Sulfide," *Journal of Electroanalytical Chemistry*, Vol. 451, No. 1–2, Pp. 11–17, Jul. 1998.

[3] S. Ando, T. Suzuki And K. Itaya, "Layer-By-Layer Anodic Dissolution Of Sulfur-Modified Ni (100) Electrodes: In Situ Scanning Tunneling Microscopy," *Journal of Electroanalytical Chemistry*, Vol. 412, No. 1–2, Pp. 139–146, Aug. 1996.

[4] X. Cheng, H. Ma, S. Chen, L. Niu, S. Lei, R. Yu And Z. Yao, "Electrochemical Behaviour Of Chromium In Acid Solutions With H_2S," *Corrosion Science*, Vol. 41, No. 4, Pp. 773–788, Apr. 1999.

[5] P. Marcus, I. Olefjord And J. Oudar, "The Influence of Sulfur On The Dissolution And The Passivation Of A Nickel-Iron Alloy 2. Surface-Analysis By Esca," *Corrosion Science*, Vol. 24, No. 4, Pp. 269–278, 1984.

[6] A. Elbiache And P. Marcus, "The Role of Molybdenum In The Dissolution And The Passivation Of Stainless Steels With Adsorbed Sulphur," *Corrosion Science*, Vol. 33, No. 2, Pp. 261–269, 1992.

[7] P. Marcus And E. Protopopoff, "Potential pH Diagrams for Sulfur And Oxygen Adsorbed On Nickel In Water At 25°C And 300°C," *Journal of The Electrochemical Society*, Vol. 140, No. 6, Pp. 1571–1575, Jun. 1993.

[8] P. Marcus And E. Protopopoff, "Potential-pH Diagrams for Adsorbed Species," *Journal of The Electrochemical Society*, Vol. 137, No. 9, Pp. 2709–2712, 1990.

[9] P. Marcus And E. Protopopoff, "Potential-pH Diagrams for Sulfur And Oxygen Adsorbed On Chromium In Water," *Journal of Electrochemical Society*, Vol. 144, No. 5, Pp. 1586–1590, May 1997.

[10] P. Marcus And E. Protopopoff, “Thermodynamics of Thiosulfate Reduction On Surfaces of Iron, Nickel And Chromium In Water At 25 And 300 °C,” *Corrosion Science*, Vol. 39, No. 9, Pp. 1741–1752, Sep. 1997.

[11] T. Loucka And P. Janos, “Adsorption And Oxidation Of Thiocyanate On A Platinum Electrode,” *Electrochimica Acta*, Vol. 41, No. 3, Pp. 405–410, Feb. 1996.

[12] A. Majidi And M. Streicher, “The Double Loop Reactivation Method For Detecting Sensitization In AISI-304 Stainless Steels,” *Corrosion*, Vol. 40, No. 11, Pp. 584–593, 1984.

[13] ASTM G108-94, “Standard Test Method For Electrochemical Reactivation (EPR) For Detecting Sensitization of AISI Type 304 And 304L Stainless Steels.”

[14] C. Duretthual, D. Costa, W. Yang And P. Marcus, “The Role Of Thiosulfates In The Pitting Corrosion of Fe-17cr Alloys In Neutral Chloride Solution: Electrochemical And Xps Study,” *Corrosion Science*, Vol. 39, No. 5, Pp. 913–933, May 1997.

[15] G. Fierro, G. M. Ingo, F. Mancia, L. Scoppio And N. Zacchetti, “Xps Investigation On AISI-420 Stainless-Steel Corrosion In Oil And Gas-Well Environments,” *Journal Of Materials Science*, Vol. 25, No. 2b, Pp. 1407–1415, Feb. 1990.

[16] J. A. Rodriguez And J. Hrbek, “Interaction Of Sulfur With Well-Defined Metal And Oxide Surfaces: Unraveling The Mysteries Behind Catalyst Poisoning And Desulfurization,” *Accounts of Chemical Research*, Vol. 32, No. 9, Pp. 719–728, Oct. 2011.

[17] A. Taboada, L. Frank, “‘Intergranular Corrosion In Nuclear Systems’, Intergranular Corrosion Of Stainless Alloys,” *ASTM STP 656*, Pp. 85–98, 1978.

[18] V. Číhal, R. Štefec, T. Shoji, Y. Watanabe, And V. Kain, “Electrochemical Potentiodynamic Reactivation: Development And Applications of The EPR Test,” *Key Engineering Materials*, Vol. 261–263, Pp. 855–864, 2004.

[19] A. Majidi And M. Streicher, “Potentiodynamic Reactivation Method For Detecting Sensitization In AISI 304 And 304L Stainless Steels,” *Corrosion*, Vol. 40, No. 8, Pp. 393–408, 1984.

[20] V. Kain, R. Prasad And P. De, “Testing Sensitization And Predicting Susceptibility To Intergranular Corrosion And Intergranular Stress Corrosion Cracking In Austenitic Stainless Steels,” *Corrosion*, Vol. 58, No. 1, Pp. 15–37, Jan. 2002.

[21] K. I. Shutko And V. N. Belous, “Comparative Study: Sensitization Development In Hot-Isostatic-Pressed Cast And Wrought Structures Type 316l(N)-IG Stainless Steel Under Isothermal Heat Treatment,” *Journal Of Nuclear Materials*, Vol. 307, Pp. 1016–1020, Dec. 2002.

[22] V. Kain And Y. Watanabe, “Development Of A Single Loop EPR Test Method And Its Relation To Grain Boundary Microchemistry For Alloy 600,” *Journal Of Nuclear Materials*, Vol. 302, No. 1, Pp. 49–59, Apr. 2002.

[23] D. F. Bowers, “Localized Corrosion Of Stainless Steels In Paper Machine White Water,” IPC Technical Paper Series No. 74, The Institute of Paper Chemistry, Appleton, Wisconsin, Feb-1979.

[24] R. C. Newman, W. P. Wong, H. Ezuber And A. Garner, “Pitting of Stainless-Steels by Thiosulfate Ions,” *Corrosion*, Vol. 45, No. 4, Pp. 282–287, Apr. 1989.

[25] R. C. Newman, H. Isaacs And B. Alman, “Effects of Sulfur-Compounds On The Pitting Behavior Of Type-304 Stainless Steel In Near-Neutral Chloride Solutions,” *Corrosion*, Vol. 38, No. 5, Pp. 261–265, 1982.

[26] S. W. Dhawale, “Thiosulfate: An Interesting Sulfur Oxoanion That is Useful In Both Medicine And Industry-But is Implicated In Corrosion,” *Journal Of Chemical Education*, Vol. 70, No. 1, P. 12, Jan. 1993.

[27] R. C. Newman, K. Sieradzki, And H. Isaacs, “Stress-Corrosion Cracking Of Sensitized Type-304 Stainless-Steel In Thiosulfate Solutions,” *Metallurgical Transactions A-Physical Metallurgy And Materials Science*, Vol. 13, No. 11, Pp. 2015–2026, 1982.

[28] H. Isaacs, B. Vyas And M. Kendig, “The Stress-Corrosion Cracking Of Sensitized Stainless Steel In Thiosulfate Solutions,” *Corrosion*, Vol. 38, No. 3, Pp. 130–136, 1982.

[29] R. C. Newman, K. Sieradzki And H. S. Isaacs, “Stress-Corrosion Cracking Of Sensitized Type 304 Stainless Steel In Thiosulfate Solutions,” *Metallurgical Transaction*, Vol. 13, No. 11, Pp. 2015–2026, Nov. 1982.

[30] Z. Iofa, “Mechanism of The Effect of Hydrogen-Sulfide And Inhibitors On Iron Corrosion In Acid-Solutions,” *Protection Of Metals*, Vol. 16, No. 3, Pp. 220–225, 1980.

[31] Z. A. Iofa, V. V. Batrakov And Cho-Ngok-Ba, “Influence Of Anion Adsorption On The Action Of Inhibitors On The Acid Corrosion Of Iron And Cobalt,” *Electrochimica Acta*, Vol. 9, No. 12, Pp. 1645–1653, Dec. 1964.

[32] P. Süry, “Similarities In The Corrosion Behaviour Of Iron, Cobalt And Nickel In Acid Solutions. A Review With Special Reference To The Sulphide Adsorption,” *Corrosion Science*, Vol. 16, No. 12, Pp. 879–901, 1976.

[33] H. Ma, X. Cheng, G. Li, S. Chen, Z. Quan, S. Zhao And L. Niu, “The Influence Of Hydrogen Sulfide On Corrosion Of Iron Under Different Conditions,” *Corrosion Science*, Vol. 42, No. 10, Pp. 1669–1683, Oct. 2000.

[34] J. Oudar And P. Marcus, “Role Of Adsorbed Sulfur In The Dissolution And Passivation Of Nickel And Nickel-Sulfur Alloys,” *Applied Surface Science*, Vol. 3, No. 1, Pp. 48–67, 1979.

[35] P. Marcus, A. Teissier And J. Oudar, “The Influence Of Sulfur On The Dissolution And The Passivation Of A Nickel-Iron Alloy 1. Electrochemical And Radiotracer Measurements,” *Corrosion Science*, Vol. 24, No. 4, Pp. 259–268, 1984.

[36] P. Marcus And I. Olefjord, “The Dissolution And Passivation Of A Single-Crystal Ni50fe50 Alloy And The Influence Of Sulfur Studied By Electron-Spectroscopy For Chemical-Analysis,” *Corrosion*, Vol. 42, No. 2, Pp. 91–98, Feb. 1986.

[37] M. Keddam, O. Mattos And H. Takenouti, “Reaction Model For Iron Dissolution Studied By Electrode Impedance. 1. Experimental Results And Reaction Model - Reply,” *Journal of The Electrochemical Society*, Vol. 128, No. 12, Pp. 2606–2606, 1981.

[38] M. Keddam, O. Mattos And H. Takenouti, “Reaction Model For Iron Dissolution Studied By Electrode Impedance. 2. Determination Of The Reaction Model,” *Journal of The Electrochemical Society*, Vol. 128, No. 2, Pp. 266–274, 1981.

[39] H. Gerisher And W. Mehl, “Zum Mechanismus Der Kathodischen Wasserstoffabscheidung An Quecksilber, Silber Und Kupfer,” *Z. Elektrochem.*, Vol. 59, Pp. 1049–1060, 1955.

[40] J. Dobbelaar And J. Dewit, “Impedance Measurements And Analysis of The Corrosion of Chromium,” *Journal of The Electrochemical Society*, Vol. 137, No. 7, Pp. 2038–2046, Jul. 1990.

[41] J. Dobbelaar And J. Dewit, “The Corrosion Behavior of Polycrystalline And Single-Crystal Chromium - A Revised Model,” *Journal of The Electrochemical Society*, Vol. 139, No. 3, Pp. 716–724, Mar. 1992.

[42] A. Jouanneau, M. Keddam And M. C. Petit, “A General Model of The Anodic Behaviour Of Nickel In Acidic Media,” *Electrochimica Acta*, Vol. 21, No. 4, Pp. 287–292, Apr. 1976.

[43] J. Gregori, J. J. Garcia-Jareno, D. Gimenez-Romero And F. Vicente, “Kinetic Calculations Of The Ni Anodic Dissolution From EIS,” *Journal of Solid State Electrochemistry*, Vol. 9, No. 2, Pp. 83–90, Jul. 2004.

[44] N. Sato And G. Okamoto, “Kinetics of The Anodic Dissolution of Nickel In Sulfuric Acid Solutions,” *Journal of Electrochemical Society*, Vol. 111, No. 8, Pp. 897–903, 1964.

[45] M. Streicher, “Stainless Steels: Past, Present And Future,” *Stainless Steel ’77*, Pp. 1–34, Sep. 1977.

[46] R. C. Newman, F. Meng And K. Sieradzki, “Validation Of A Percolation Model For Passivation Of Fe-Cr Alloys. 1. Current Efficiency In The Incompletely Passivated State,” *Corrosion Science*, Vol. 28, No. 5, Pp. 523–527, 1988.

[47] R. C. Newman, "2001 W.R. Whitney Award Lecture: Understanding The Corrosion Of Stainless Steel," *Corrosion*, Vol. 57, Pp. 1030–1041, Dec. 2001.

[48] S. Qian, R. Newman, R. Cottis, And K. Sieradzki, "Validation Of A Percolation Model For Passivation Of Fe-Cr Alloys - 2-Dimensional Computer-Simulations," *Journal of The Electrochemical Society*, Vol. 137, No. 2, Pp. 435–439, Feb. 1990.

[49] S. Qian, R. Newman, R. Cottis And K. Sieradzki, "Computer-Simulation Of Alloy Passivation And Activation," *Corrosion Science*, Vol. 31, Pp. 621–626, 1990.

[50] A. Davenport, M. Ryan, M. Simmonds, P. Ernst, R. Newman, S. Sutton And J. Colligon, "In Situ Synchrotron X-Ray Microprobe Studies of Passivation Thresholds In Fe-Cr Alloys," *Journal of The Electrochemical Society*, Vol. 148, No. 6, Pp. B217–B221, Jun. 2001.

[51] R. Kirchheim, B. Heine, H. Fischmeister, S. Hofmann, H. Knote And U. Stolz, "The Passivity Of Iron-Chromium Alloys," *Corrosion Science*, Vol. 29, No. 7, Pp. 899–917, 1989.

[52] M. Keddam, O. Mattos, And H. Takenouti, "Mechanism of Anodic-Dissolution of Iron Chromium-Alloys Investigated By Electrode Impedances. 1. Experimental Results And Reaction Model," *Electrochimica Acta*, Vol. 31, No. 9, Pp. 1147–1158, Sep. 1986.

[53] M. Keddam, O. Mattos And H. Takenouti, "Mechanism of Anodic-Dissolution Of Iron Chromium-Alloys Investigated By Electrode Impedances. 2. Elaboration of The Reaction Model," *Electrochimica Acta*, Vol. 31, No. 9, Pp. 1159–1165, Sep. 1986.

[54] H. Knote, S. Hofmann And H. Fischmeister, "AES- und XPS-Untersuchungen zum Einfluß von Chrom, Nickel und Molybdän auf das Korrosionsverhalten von rostfreien Stählen in Säuren," *Fresenius' Journal of Analytical Chemistry*, Vol. 329, Pp. 292–297, 1987.

[55] P. Marcus, "Advances In Localized Corrosion," *NACE, Houston*, P. 289, 1990

[56] E04 Committee, "Practice for Microetching Metals and Alloys," ASTM International E407-07, 2007.

[57] C. C. Herrmann, G. G. Perrault And A. A. Pilla, "Dual Reference Electrode For Electrochemical Pulse Studies," *Analytical. Chemistry*, Vol. 40, No. 7, Pp. 1173–1174, 1968.

[58] M. R. Shoar Abouzari, F. Berkemeier, G. Schmitz And D. Wilmer, "On The Physical Interpretation of Constant Phase Elements," *Solid State Ionics*, Vol. 180, No. 14–16, Pp. 922–927, Jun. 2009.

[59] H. Hugh H., "Chemical Studies of Polythionic Acid Stress-Corrosion Cracking," *Corrosion Science*, Vol. 23, No. 4, Pp. 353–362, 1983.

[60] A. J. Betts And R. C. Newman, "The Effect of Alloyed Molybdenum On The Activation of Anodic Dissolution By Reduced Sulphur Compounds," *Corrosion Science*, Vol. 34, No. 9, Pp. 1551–1555, Sep. 1993.

[61] K. Akselvoll And P. Moin, "Large-Eddy Simulation of Turbulent Confined Coannular Jets," *Journal of Fluid Mechanics*, Vol. 315, Pp. 387–411, 1996.

[62] X. H. Wu And K. D. Squires, "Prediction And Investigation of The Turbulent Flow Over A Rotating Disk," *Journal of Fluid Mechanics*, Vol. 418, Pp. 231–264, Sep. 2000.

[63] P. Bryan, "Electrochemical Measurements In Flowing Solutions," *Corrosion Science*, Vol. 23, No. 4, Pp. 391–430, 1983.

[64] R. C. Newman, "The Dissolution And Passivation Kinetics Of Stainless Alloys Containing Molybdenum—1. Coulometric Studies Of Fe-Cr And Fe-Cr-Mo Alloys," *Corrosion Science*, Vol. 25, No. 5, Pp. 331–339, 1985.

[65] R. C. Newman and M. A. A. Ajjawi, "A Micro-electrode Study Of the Nitrate Effect on Pitting of Stainless Steels," *Corrosion Science*, Vol. 26, No. 12, Pp. 1057–1063, 1986.

[66] T. R. Beck, "Formation of Salt Films during Passivation of Iron," *Journal of The Electrochemical Society*, Vol. 129, No. 11, Pp. 2412–2418, Nov. 1982.

[67] W. F. Linke, Solubilities : Inorganic And Metal-Organic Compounds *: A Compilation Of Solubility Data From The Periodical Literature*, Vol. 1. 1958.

[68] R. P. Frankenthal, "On The Passivity of Iron-Chromium Alloys," *Journal of The Electrochemical Society*, Vol. 116, No. 5, Pp. 580–585, May 1969.

[69] J. A. L. Dobbelaar, E. C. M. Herman, And J.H.W. De Wit, "The Corrosion Behavior of Iron-Chromium Alloys In 0.5m Sulphuric Acid," *Corrosion Science*, Vol. 33, No. 5, Pp. 765–778, 1992.

[70] S. Fujimoto, R. C. Newman, G. S. Smith, S. P. Kaye, H. Kheyrandish And J. S. Colligon, "Passivation Thresholds In Iron-Chromium Alloys Prepared By Ion-Beam Sputtering," *Corrosion Science*, Vol. 35, No. 1–4, Pp. 51–55, 1993.

[71] P. Marcus, *Corrosion Mechanisms In Theory And Practice*. CRC Press, 2002.

[72] D. M. Drazic, J. P. Popic, B. Jegdic And D. Vasiljevic-Radovic, "Electrochemistry Of Active Chromium. Part IV. Dissolution of Chromium In Deaerated Sulfuric Acid," *Journal of Serbian Chemical Society*, Vol. 69, No. 12, Pp. 1099–1110, 2004.

[73] W. Li And P. C. Pistorius, "Effects of Thiocyanate On Anodic Dissolution of Iron, Chromium And Type 430 Stainless Steel," *Journal of The Electrochemical Society*, Vol. 159, No. 3, C114-C122, 2012

[74] J. F. Moulder, W. F. Stickle, P. E. Sobol And K. D. Bomben, *Handbook of X-Ray Photoelectron Spectroscopy: A Reference Book of Standard Spectra For Identification And Interpretation of Xps Data*. Physical Electronics, 1995.

[75] R. H. Dinegar, R. H. Smellie, And V. K. L. Mer, "Kinetics of The Acid Decomposition Of Sodium Thiosulfate In Dilute Solutions," *Journal of the American Chemical Society*, Vol. 73, No. 5, Pp. 2050–2054, 1951.

[76] C. W. Bale, P. Chartrand, S. A. Degterov, G. Eriksson, K. Hack, R. Ben Mahfoud, J. Melançon, A. D. Pelton, And S. Petersen, "Factsage Thermochemical Software And Databases," *Calphad*, Vol. 26, No. 2, Pp. 189–228, Jun. 2002.

[77] E. Peters, "Direct Leaching of Sulfides: Chemistry And Applications," *Metallurgical And Materials Transactions B*, Vol. 7, No. 4, Pp. 505–517, 1976.

[78] J. Onuferko, D. Woodruff And B. Holland, “Leed Structure-Analysis of The Ni (100) (2x2)C(P4g) Structure - Case Of Adsorbate-Induced Substrate Distortion,” *Surface Science,* Vol. 87, No. 2, Pp. 357–374, 1979.

[79] W. Oed, H. Lindner, U. Starke, K. Heinz And K. Müller, “Adsorbate-Induced Relaxation And Reconstruction of C(2 × 2)O/Ni(100): A Reinvestigation By Leed Structure Analysis,” *Surface Science*, Vol. 224, No. 1–3, Pp. 179–194, Dec. 1989.

[80] W. Oed, U. Starke, F. Bothe And K. Heinz, “Leed Structure Analysis Of P(2 × 2)S/Ni(100),” *Surface Science*, Vol. 234, No. 1–2, Pp. 72–78, Aug. 1990.

[81] H. D. Shih, F. Jona, D. W. Jepsen And P. M. Marcus, “Metal-Surface Reconstruction Induced By Adsorbate: Fe(110) P(2×2)-S,” *Physical Review Letter*, Vol. 46, No. 11, Pp. 731–734, Mar. 1981.

[82] D. R. Strongin, S. R. Bare And G. A. Somorjai, “The Effects of Aluminum Oxide In Restructuring Iron Single Crystal Surfaces For Ammonia Synthesis,” *Journal Of Catalysis*, Vol. 103, No. 2, Pp. 289–301, Feb. 1987.

[83] G. A. Somorjai, “Surface Reconstruction And Catalysis,” *Annual Review of Physical Chemistry*, Vol. 45, No. 1, Pp. 721–751, 1994.

[84] R. C. Scarberry, D. Graver And C. Stephens, “Alloying For Corrosion Control - Properties And Benefits of Alloy Materials,” *Materials Protection*, Vol. 6, No. 6, Pp. 54–&, 1967.